Enabling Oxygen-dependent Biocatalysis Under Fine Bubble Aeration in a Rotating Bed Reactor

Dissertation (monograph) approved by the
Doctoral Degree Committee of
Hamburg University of Technology

in pursuit of the academic degree of

Doktor-Ingenieurin (Dr.-Ing.)

written by
M.Sc. Zeynep Perçin

from
Istanbul, Türkiye

2025

https://doi.org/10.15480/882.14932

Orcid iD
https://orcid.org/0000-0002-1291-7380

1st Supervisor: Prof. Dr. Andreas Liese
2nd Supervisor: Prof. Dr. Michael Schlüter
Date of oral examination: 17th of February 2025

Acknowledgements

I would like to thank the German Research Foundation (DFG) - [501131738] for providing a research grant for this project.

I would like to express my sincere thanks to Prof. Dr. Andreas Liese and Prof. Dr. Michael Schlüter for supervising this work and for their guidance throughout this journey, as well as for creating the conditions for a pleasant working atmosphere. I would also like to extend my thanks to Prof Dr. Stefan Heinrich, who chaired the examination committee.

Special thanks to Dr. Paul Bubenheim and the team of the Institute of Technical Biocatalysis for all the unforgettable memories. I would like to thank the project members M.Sc. Lotta Kursula, Dr Felix Kexel, M.Sc. Erik Löfgren and Dr Emil Byström for the informative scientific discussions.

A special thanks goes to B.Sc. Mona Brecht, B.Sc. Mansi Alevi, B.Sc. Madhava Madhusoodhanan, B.Sc. Sara Mansouri Mashhadi and B.Sc. Isa Badhalov as well as to the laboratory trainees Vincent Heineke and Lea Port for their great work in the laboratory of the Institute of Technical Biocatalysis.

Last but not least, I would like to thank my family for their support.

Summary

Oxidation of low-value chemical compounds to higher-value products is of interest in many biocatalytic applications. Oxidases are used in biotransformations as a powerful enzyme utilizing molecular oxygen, whose availability is limited by its low solubility in gas-liquid multiphase systems. A continuous supply of oxygen to the reaction medium during the course of the reaction is the common approach in many biotechnological applications such as fermentation, animal breeding, and biocatalytic oxidation reactions to overcome this bottleneck, which causes significant gas and energy consumption.

This study extends the application of fine bubble aeration to a rotating packed bed reactor. In addition to the improvement in the surface-to-volume ratio using fine bubble aeration, biocatalyst reuse in a rotating packed bed reactor was enabled through covalent immobilization of glucose oxidase on epoxy-functionalized supports. An immobilization activity yield of 98% was achieved, and the volumetric mass transfer coefficient is three times higher (67.3 h^{-1}) compared to macrobubble (22.5 h^{-1}) aeration, while the volume-specific aeration rate remains constant. This setup was shown to reduce oxygen consumption by 87.5% while maintaining the comparable glucose oxidase-specific activity at similar volumetric mass transfer coefficients. With the advantage of an enhanced oxygen mass transfer rate and reduced gas consumption, the performance of biocatalysts (activity and stability) was investigated in repetitive batches in a rotating packed bed reactor. The glucose oxidase-specific activity increased with higher substrate concentrations, and the stability of the biocatalyst was maintained at lower substrate concentrations, whereas it decreased at higher substrate concentrations. This finding raises the question of the severity of internal diffusion limitations in the carriers, where the deactivation of glucose oxidase was caused by the by-product hydrogen peroxide produced within the carriers during the reaction.

To mathematically express the influence of the diffusion limitation, kinetic parameters were measured for free and immobilized glucose oxidase in a rotating packed bed reactor. The maximum achievable glucose oxidase-specific activity was lower for the coupled enzyme system (immobilized glucose oxidase-free catalase) than for the free forms of the enzyme, thereby demonstrating the presence of internal diffusion limitations. The glucose oxidase-specific activity was not influenced by catalase co-immobilization. Considering the effect of biocatalyst deactivation and diffusion limitations on the reaction rate, the reaction rate equation was modified and modeled using the measured kinetic parameters to estimate the reactor performance.

The substrate concentration was identified as the key parameter for the reaction rate. The glucose oxidase-specific activity was improved by a factor of 12.9 for the fine bubble aeration compared to macrobubble aeration at the substrate concentration, at which the maximum reaction rate was achieved under the given experimental conditions. Compared to macrobubble aeration, productivity for glucose oxidase increased by a factor of 3.5 for the equal operating time. With the identical established

productivity for glucose oxidase, the process time was reduced by 3.9-fold to produce the same amount of product utilizing fine bubble aeration.

Validation of repetitive batches was accomplished by achieving a similar glucose oxidase-specific activity for the subsequent series of batches (Batch 1 and Batch 2) at reduced substrate concentrations, utilizing the same immobilized glucose oxidase. The repetitive batches enabled the reuse of cost-driven biocatalyst (glucose oxidase), and the product amount was doubled with fine bubble aeration at the identical process time when compared to macrobubble aeration. Based on the results of the laboratory-scale techno-economic performance for immobilized glucose oxidase using a rotating packed bed reactor, the total cost was reduced by half when using repetitive batches under fine bubble aeration. With the advantage of doubled production rate and productivity for glucose oxidase, the fine bubble aeration resulted in a 7.8 techno-economic performance improvement of the rotating packed bed reactor. The outcome of this thesis demonstrates the potential use of fine bubble technology for the efficient utilization of oxygen-limited oxidases by addressing the sustainability of biotransformation processes.

Table of contents

1. Introduction

This chapter gives an overview of the role of biotechnology in biocatalysis, the use of oxidases in biocatalytic applications, the limitations of oxidative biotransformation processes, and alternative reactor concepts. The focus of the thesis as the application of oxidases in a rotating packed bed reactor under fine bubble aeration is described at the end of the next section.

1.1. The role of biotechnology in biocatalysis

To understand the role of biotechnology in biocatalytic applications, the potential of enzyme technology on the global market was recently reviewed in the Global Opportunity Analysis and Industry Forecast report in 2022 [1], considering the enzyme classes, the origin of enzymes, the application areas as well as the regions. The enzyme market is estimated to be worth 10.2 billion Dollars by 2031 and the companies (Novozymes A/S, Koninklijke DSM N.V., DuPont de Nemours, Inc., BASF SE, Advanced Enzyme Technologies Ltd., AB Enzymes GmbH, Codexis, Inc., Amano Enzyme, Inc., F. Hoffmann-La Roche Ltd., Thermo Fisher Scientific Inc.) are reported as the major players [1].

More than 1000 reports have been written in the period 2012-2028 in the research areas for industrial biocatalysis [2, 3], as the use of enzymes in industrial applications is increasingly favored [4] due to the major advantages of chemo-regioselectivity, the ability to carry out the reactions in mild conditions, reducing by-products, and their origin from renewable resources [2,5,6]. They can catalyze a wide range of reactions by being engineered for the specific reaction [5], overcoming the disadvantages of being subject to inhibition by other compounds in the reaction medium. In view of these benefits, biocatalysis is considered a worthwhile alternative as it has the potential to provide solutions for minimizing energy use with alternative biocatalytic synthetic routes and leading to cleaner products while offering the advantage of regioselectivity [5,6].

The first application of biocatalysis in chemical synthesis was in the 1930s, when the bacterium Acetobacter suboxydans was used in the Reichstein-Grüssner synthesis for the production of vitamin C (L-ascorbic acid) in 1934 [7,8]. In the 1950s, the use of biocatalysis in the pharmaceutical industry was demonstrated for the synthesis of cortisone [7]. The approach of immobilization was first described by Nelson and Griffin [9] in 1916 to enable the technical use of enzymes. To improve enzyme half-life and enzyme recovery, the approach of enzyme immobilization is used, and the first application of immobilized enzymes was reported by (Grubhofer and Schleith) [10] in 1953. An integrated approach of protein engineering and enzyme immobilization, called immobilized biocatalyst engineering, has been reported as an alternative strategy for integrating biocatalyst improvement strategies [11].

The immobilized enzymes are available on the world market for practical applications, such as Novozym® 435 from Novozymes S/A for ester synthesis, Plexazyme® AC from

Röhm GmbH & Co. KG for the synthesis of chiral amino acids, Lentikats® - β-Galactosidase from LentiKat's Biotechnologies for the synthesis of galactooligosaccharides [7]. Immobilization is the scope of this thesis and is discussed in sections 2, 3 and 4.

S. Wu [4] published in 2021 a review of various industrial enzymatic reactions, i.e. the synthesis of chiral compounds for pharmaceuticals. The main sectors applying industrial biocatalysis are reported to be food, chemicals, and pharmaceuticals, as shown in Figure 1.

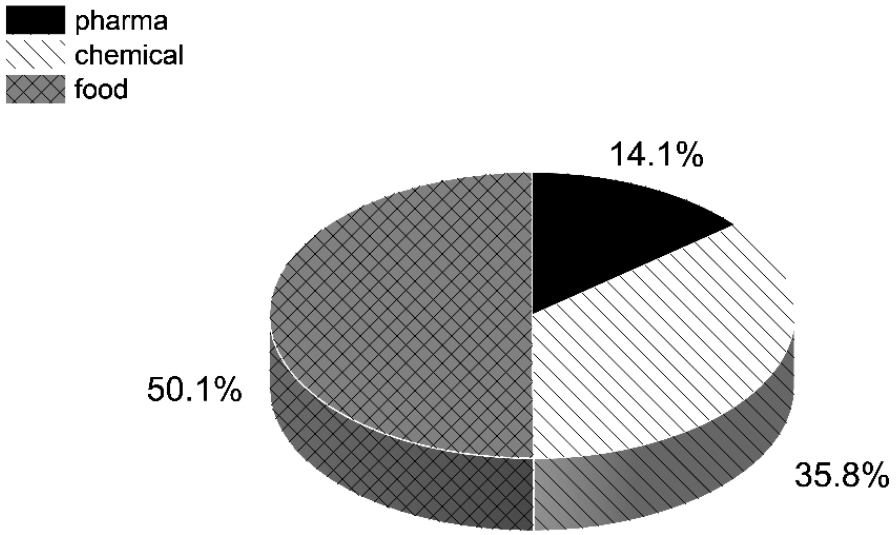

Figure 1. The main sectors involved in the application of industrial biotechnology. The pie chart was plotted using the data in the literature [2] summarizing the percentage of the number of reports between the years 2016-2020.

S. P. France [12] in 2023 has reported an overview for the evaluation of biocatalysis, including enzyme discovery, their use in pharmaceutical development, and the scale-up of manufacturing processes. The use of enzymes in the asymmetric synthesis of chiral intermediates is becoming more prominent, as reported in the work of S. P. France, where the limitations of biocatalytic applications are listed and oxidases are reported as one of the key enzymes catalyzing the synthesis of chiral intermediates [12]. F. Gallou [13] reported in 2023 on a study summarizing the potential for merging bio- and chemo-catalysis and concluded that there is potential for industrial integration of bio- and chemo-catalysis, although there are concerns about the strategic and technical areas.

According to the Global Opportunity Analysis and Industry Forecast report, the enzymes derived from microorganisms have the largest market share when compared to the ones derived from animals and plants [1]. Hydrolases and oxidoreductases are the enzyme classes that generated the highest profit [1,14] in the global market in 2021 and are expected to continue to do so until 2031 [1]. Oxidases (E.C.1 class) are reported as an emerging potential for sustainable chemistry [15], and the following section summarizes biocatalytic oxidation reactions supported with practical

applications, highlighting the class of enzymes, which were the subject of investigation in this thesis.

1.2. Application of biocatalytic oxidation reactions

Many oxidation reactions are used in synthetic chemistry, such as alcohol oxidases to oxidize alcohols, amine oxidases to synthesize (chiral) α-substituted amines, and lytic polysaccharide monooxygenases to cleave glycosidic bonds in polysaccharides [16]. The oxidoreductases are used in the asymmetric synthesis of amino acids, steroids, and value-added compounds in the pharmaceutical industry [14].

From a process chemist's perspective, biocatalytic oxidation reactions are divided into two categories: oxyfunctionalization and dehydrogenation reactions. In the oxyfunctionalization reactions, the enzymes monooxygenases, peroxygenases, halogenases and dioxygenases are biocatalysts for the biotransformation reaction by means of electrophilic insertion of oxygen atoms in the substrate in the presence of molecular oxygen as a second substrate. The dehydrogenation reactions are catalyzed by four types of enzymes [16]:

- Laccases and peroxidases are used for the removal of the hydrogen atom from the phenolic substrates.
- Dehydrogenases and oxidases are catalysts for the removal of hydride from alcohols and amines, respectively [16].

In the case of laccases and oxidases, the molecular oxygen is used for the removal of the hydrogen atom from the substrate [16]. Oxidases such as cytochrome P450 monooxygenases (CYPs), xanthine oxidoreductases (XORs), and flavin monooxygenases (FMOs) are involved in the biocatalytic synthesis of drug metabolites [17]. NADH oxidases are used to generate cofactors during the synthesis of an intermediate for inhibitor synthesis developed by researchers at Merck & Co [12,18]. A further example from Merck & Co. is the biocatalytic synthesis of an inhibitor used in the treatment of HIV, in which galactose oxidase catalyzes the desymmetrizing oxidation to yield an aldehyde intermediate [12,19]. An engineered pyruvate oxidase was used in the production of Molnupiravir as another pharmaceutical application [12,20].

In many biotransformation reactions used in industry, oxidases require molecular oxygen as a substrate to oxidize the low-value compound into a high-value compound or an intermediate molecule. From a process-engineering perspective, however, the use of oxygen is the limiting step in these biotransformation reactions, resulting from the insufficient oxygen solubility (0.254 mM [21] in water at 1 atm and 25°C), in comparison to the solubility of the second substrate for two-substrate enzymatic systems. To enable the application of oxidases in biocatalytic applications, the challenges and limitations of oxidative processes, as well as the identification of cost drivers in biocatalysis with optimal reactor concepts, are discussed in the following section.

1.3. Major challenges in oxidative biocatalytic reactions

The main limiting factors [22] in the oxidative biocatalytic reactions are the mass transfer and solubility of oxygen, as well as the loss of enzyme stability in multiphase systems when the biocatalyst is in contact with the hydrophobic gas-liquid interface [23,24]. For an effective reactor design, it is not only necessary to consider the approaches to overcome these limitations, but also the possible drawbacks in the implementation of the biocatalyst [23].

For oxidative biocatalytic reactions using molecular oxygen as a second substrate, the reaction rate is limited by the insufficient oxygen mass transfer rate and its solubility in the reaction medium. The oxygen mass transfer rate can be enhanced by improving the reactor design [25], as the oxygen mass transfer rate depends on the reactor geometry.

1.4. Reactor concepts: Improving biocatalyst performance

A large number of studies have been carried out to improve biocatalytic processes using a variety of engineering solutions, including reactor concepts enhanced with continuous flow biocatalysis operating under atmospheric and high-pressure conditions, where gas solubility has been increased [26-29]. The key factor in intensifying oxygen-dependent biotransformation reactions is reactor selection, as reactor geometry and process parameters affect its mass transfer performance.

A. Lorente-Arevalo [25] reported alternative approaches for oxygen-dependent reactions that included stirred tank reactors, flow tube reactors, tube-in-tube configurations, multi-injection microchannel reactors, and pressurized liquid phase reactors. The conclusion is that the improvement in the productivity for immobilized glucose oxidase, as well as stability and the space-time yield, are necessary to increase the biocatalytic performance [25]. A. T. Pedersen [30] published an example of the flow biocatalysis concept, where the performance of two reactor concepts, a continuous agitated cell reactor, and a batch reactor, was compared at similar reaction volumes for the oxidation of glucose to D-glucono-1,5-lactone by the enzyme glucose oxidase. The oxidative biotransformation process was intensified with this continuous reactor concept by improving the oxygen mass transfer rate from 104 h^{-1} to 344 h^{-1}, however, the application is not optimal for upscaling.

A comprehensive review of flow biocatalysis in the years 2020-2022 was written by M. Crotti [27], where it was reported that the widely used reactor configuration is the stirred tank reactors in continuous and discontinuous mode and the packed bed reactors. Mechanical agitation [31] in the stirred tank reactor applies shear forces through the impeller, which causes the inactivation of biocatalysts [20]. The negative effect of shear forces on the biocatalyst performance is solved by the packed bed reactors without the need for mixing, where no impeller is used [32]. Compared to the stirred tank reactors, the packed bed bioreactors showed a higher conversion as the reactor volume was largely occupied by the enzymes immobilized on carriers [27].

Membrane reactors are another alternative reactor concept to efficiently separate the product from the enzymes. The membrane biocatalytic reactor design is divided into two groups [33]. The reaction is catalyzed by the enzyme in the stirred tank reactor, and the product is removed by a membrane, or the biocatalytic reaction is performed in the membrane module of the stirred tank reactor with immobilized biocatalyst. Packed microreactors are the alternative reactor concept to intensify biocatalytic reactions with immobilized biocatalysts [34]. The reactor selection decision depends mainly on its mass transfer performance as well as kinetic studies to characterize substrate/product inhibitions of the reaction system. When product inhibition is high, the plug flow reactor model is the appropriate option because high product concentrations are only found at the end of the PFR, where the immobilized enzyme is exposed to that high concentration [35, 36]. The continuous stirred tank reactor, on the other hand, is an option for reactions with strong substrate inhibition because the substrate is diluted in the reaction volume. However, high conversions per unit volume are not feasible in stirred tank reactors, where the biocatalyst occupies only 10% of the reaction volume [27]. Packed bed bioreactors have the advantage of achieving a high conversion to free volume ratio since the reactor volume is mostly filled with enzymes immobilized on carriers.

A reactor concept, namely a rotating bed reactor (Figure 2), has been introduced to the market by SpinChem AB of Sweden. It was developed as an inspiration of the basket reactors and the annular spinning basket reactors, the first results of which were published in 1964 and 1978, respectively [37-39].

Figure 2. The rotating bed basket from SpinChem AB. The predicted flow pattern (top, left) around a SpinChem® rotating bed reactor S2 in vessel V2, simulated using Ansys Fluent, SpinChem AB [44]. The inside of the rotating bed basket was filled with solid particles (top, right, SpinChem AB [45]). The elements of the rotating packed bed reactor S2 assembled to form a basket with a stainless steel (SS316L, EN2348) filter inside (down, SpinChem AB [46]).

In a comprehensive review, it was reported that the SpinChem® rotating packed bed reactor reduces the mechanical friction [40] on the solid catalysts and allows the catalyst to be used again [40,41]. As of today, SpinChem® vessels with a rotating bed reactor have been used in many biocatalytic applications [42,43], either with immobilized enzymes or whole-cell biocatalysis, such as the asymmetric hydrogenation of C=C bonds and the synthesis of perillyl alcohol.

This concept represents an alternative to conventional packed bed reactors. The advantage is not only that the enzymes are immobilized on carriers and retained in the packed bed basket, but also that the rotation introduces high convection forces into the liquid medium, thereby facilitating efficient mixing performance. The SpinChem® rotating packed bed reactor acts as an impeller (diameter 45 mm), and the reactants are dispersed in the liquid medium. The reaction medium is circulated through the rotating packed bed basket and is recirculated back to the vessel. The approach for the application of oxidases is described in the following section.

1.5. The use of immobilized oxidases in a rotating packed bed reactor

Enzyme retention/immobilization is a successful strategy to contribute to the reuse of cost-intensive biocatalysts. The most common enzyme immobilization techniques are reported as physical adsorption, entrapment, encapsulation, ionic bonding, and cross-linking/covalent bonding. There is no standard immobilization method that can be applied to all biocatalysts as immobilization methods depend on several parameters such as temperature, pH, salt concentration, functional groups on the supports, and the amino acids of the protein [47,48].

The advantage of the adsorption method, which is a cheap and rapid technique, is its wide range of applicability to different enzymes, however, it has the disadvantage of enzyme leakage and low enzyme stability [49]. The encapsulation method brings strong diffusion limitations, and the cross-linking method requires a linker to promote immobilization [48]. The technique of ionic bonding is reversible [48], and high levels of charges can cause changes in the enzyme structure. The entrapment method is a method of irreversible immobilization, but the technique is limited by the low loading capacity of enzymes [48].

The approach of covalent bonding allows for the strong fixation of enzymes to the carriers [50]. The functional group of the carrier forms a chemical bond with the amino group of the protein, resulting in irreversible immobilization (Figure 3). Sepabeads® EC-HFA carriers and ReliZyme™ HFA M grade carriers improve enzyme reuse [41] and do not require prior activation for covalent immobilization [41, 52], assuming irreversible immobilization [53] and allowing multipoint attachment [54-56]. Sepabeads® EC-HFA carriers and ReliZyme™ HFA M grade carriers have the identical chemical structure with the same functional and epoxy groups [53] and are used in many biocatalytic immobilization [41, 57-59].

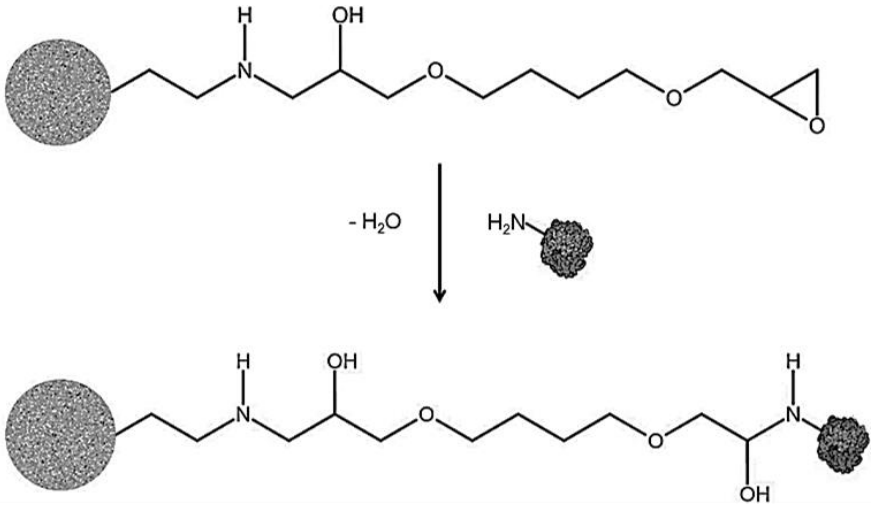

Figure 3. ReliZyme^{TM} HFA 403 M grade carrier (with a methacrylic polymer matrix) with functional groups. A chemical bonding between the epoxy group of the carrier and the amino group of the protein occurs, which results in irreversible immobilization. The figure was drawn according to the product information sheet [53] of Resindion S.r.l. with the online software Chemical Sketch Tool from RCSB PDB Core Operations.

In a rotating packed bed reactor, the oxidative biotransformation of D-glucose to D-glucono-1,5-lactone (Scheme 1) is catalyzed by covalently immobilized glucose oxidase on epoxy-functionalized carriers in the presence of molecular oxygen and catalase (free) [41]. The approach of covalent bonding is the favored method for the enzyme glucose oxidase, according to M.Y. Arica [51].

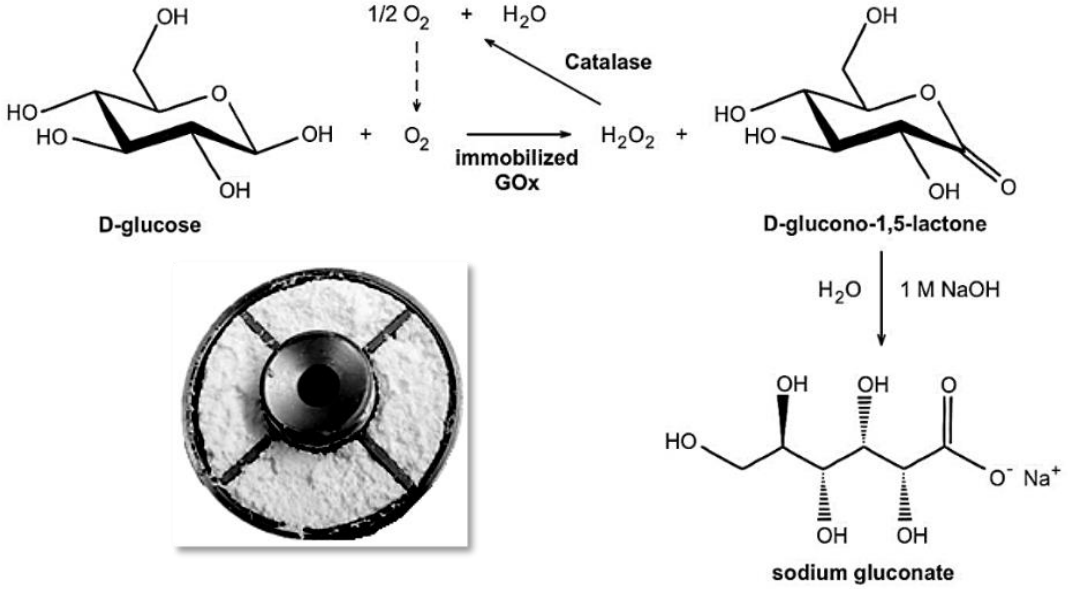

Scheme 1. Oxidation of D-glucose to D-glucono-1,5-lactone by covalently immobilized glucose oxidase (GOx) on epoxy-functionalized carriers in the presence of molecular oxygen and catalase [41]. A packed bed reactor with immobilized glucose oxidase on carriers (left, down).

2. Process intensification applying fine bubble technology

An oxidative biotransformation process catalyzed by immobilized glucose oxidase requires molecular oxygen. This was demonstrated (Scheme 1) in the previous section. As explained by S. Illner, the increase in surface area to volume ratio enhances the contact between the gas and liquid phases for the reaction catalyzed by the glucose oxidase enzyme in free form, resulting in an increased space-time yield [60]. Another example of increasing oxygen mass transfer is the use of fine bubble technology, applying microbubbles and nanobubbles to increase the surface area per volume of gas available for mass transfer at the gas-liquid interphase, as shown in our previous studies [61-63].

2.1. Characteristics of fine bubbles

In accordance with ISO 20480, fine bubbles are subdivided into ultrafine bubbles (d_B < 1 µm) and microbubbles (1 µm ≤ d_B < 100 µm) [64] (Figure 4, top). A reduction in the radius of the bubble results in an increase in internal pressure [37,62,65] (Figure 4, down), which becomes greater than the surrounding pressure as surface tension (σ) becomes dominant (Young-Laplace Equation, Equation 1).

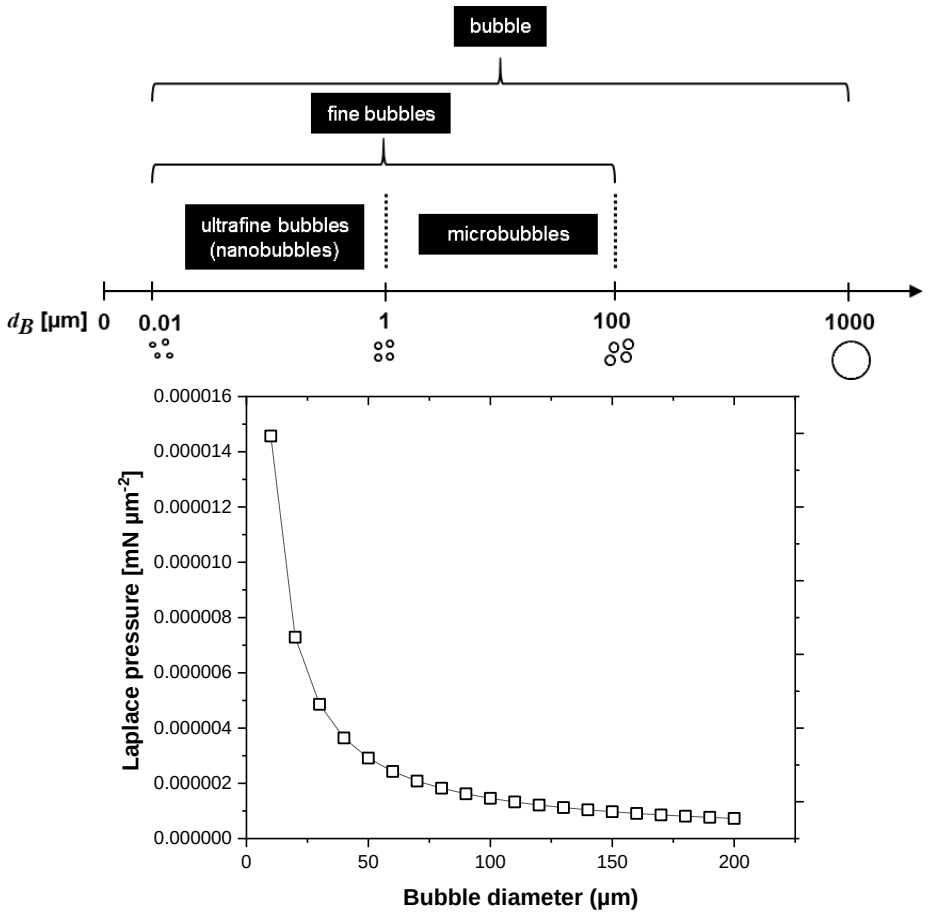

Figure 4. Redrawn from the scale diagram showing bubble diameters (top) [64]. Laplace pressure as a function of bubble diameter (down): The plot was generated using the data published for a water-air system at 20°C by N.R. Pallas [66].

$$\Delta P = \frac{4 \cdot \sigma}{d_B} \quad (1)$$

where ΔP in mN µm^{-2} is the Laplace pressure, σ in mN µm^{-1} denotes the surface tension and d_B in µm is the bubble diameter.

The elevation in the internal pressure of the bubble has the consequence of intensifying the partial pressure of the gas components within the bubble and, consequently, the saturation concentration. According to Henry's law (Equation 2), the concentration gradient at the interphase rises as the bubble diameter decreases, resulting in locally enhanced saturation concentrations [38,65], which contributes to high gas dissolution (Equation 3) [67].

$$H = \frac{p_i}{c_L^*} \quad (2)$$

where H in atm m^3 kmol^{-1} is the Henry's constant and p_i in atm denotes the partial pressure of the component i in the bubble, c_L^* in kmol m^{-3} is the saturation concentration of the gas molecule i in the liquid phase.

$$N_d = k_L \cdot A \cdot (p_i - p_i^*) / H \quad (3)$$

where N_d in mol s^{-1} is the dissolution rate, k_L in m s^{-1} is the liquid phase mass transfer coefficient, A in m^2 is the bubble surface area, p^* in atm is the partial pressure of the gas component i in equilibrium with the dissolved gas molecule in the liquid phase.

Fine bubbles have a large volume-specific surface area as well as a large interfacial area. As the diameter of the bubbles decreases, the effect of buoyancy becomes less dominant and the rate, at which the bubbles rise (Equation 4), decreases [65], thus increasing the residence time of the bubbles and the mass transfer into the reaction medium.

$$\vartheta_B = \frac{\rho \cdot g \cdot d_B^2}{18 \cdot \mu} \quad (4)$$

where ϑ_B in m s^{-1} is the bubble rising velocity, ρ in kg m^3 is the liquid density, g in m s^{-2} is the gravitational acceleration, d_B in m is the bubble diameter, μ in kg m^{-1} s^{-1} is the liquid dynamic viscosity.

2.2. Generation of fine bubbles

In the previous studies, the oxygen mass transfer was significantly improved with the use of fine bubbles (d_B < 100 µm) when compared to macrobubbles (100 µm ≤ d_B). Two distinct approaches (static and dynamic aeration) for the generation of fine bubbles have been reported [62,63,68].

2.2.1. Static aeration

Generation of fine bubbles via the static aeration approach is made achievable by utilizing the advantage of low power consumption. The fundamental principle underlying the static aeration approach is the use of spargers (Shirasu Porous Glass (SPG) membrane spargers and sintered frit porous metal spargers), whose material surface is composed of microscopic pores (Figure 5). The presence of these micropores facilitates the transfer of gas molecules into the liquid medium, thereby generating fine bubbles.

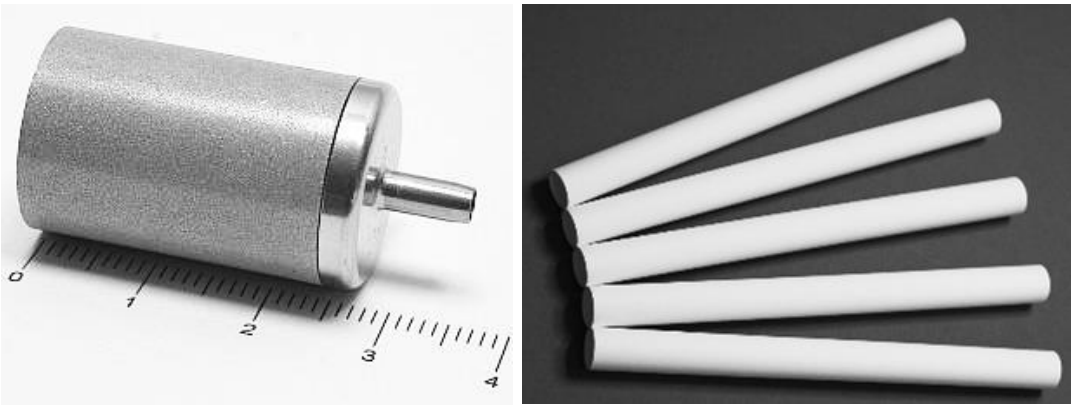

Figure 5. Porous spargers. Sintered frit sparger (left): pore size: 2 µm, stainless steel, TECHLAB GmbH, Braunschweig, Germany [69]. SPG membrane sparger (right): pore size: 0.1 - 50 µm, $Al_2O_3.SiO_2$ glass, SPG Technology Co. Ltd, Higashikaminaka Sadowaracho, Japan [69].

2.2.2. Dynamic aeration - pressurised dissolution method

An alternative method for the generation of fine bubbles is facilitated through the utilization of the pressurised dissolution method, which employs high-density bubble flows, necessitating the introduction of an additional liquid flow [71]. The liquid and gaseous phases are mixed and pressurized in the venture tube releaser to increase the concentration of dissolved gas. The liquid is pumped and transferred from the liquid inlet through to the venture tube releaser. The gas is sucked through the venture tube releaser, where the pressure is reduced and becomes less than atmospheric pressure. The liquid within the venture tube releaser is subjected to a process whereby the liquid becomes over-saturated with gas due to a pressure drop [71,72] (Figure 6). It is necessary to create a cavitation at the decompression nozzle to generate fine bubbles. The liquid volumetric flux at the nozzle throat affects the number density of cavitation fine bubbles, which are generated continuously [73]. The liquid, which contains fine bubbles, is pumped to the reactor, where a biotransformation reaction occurs.

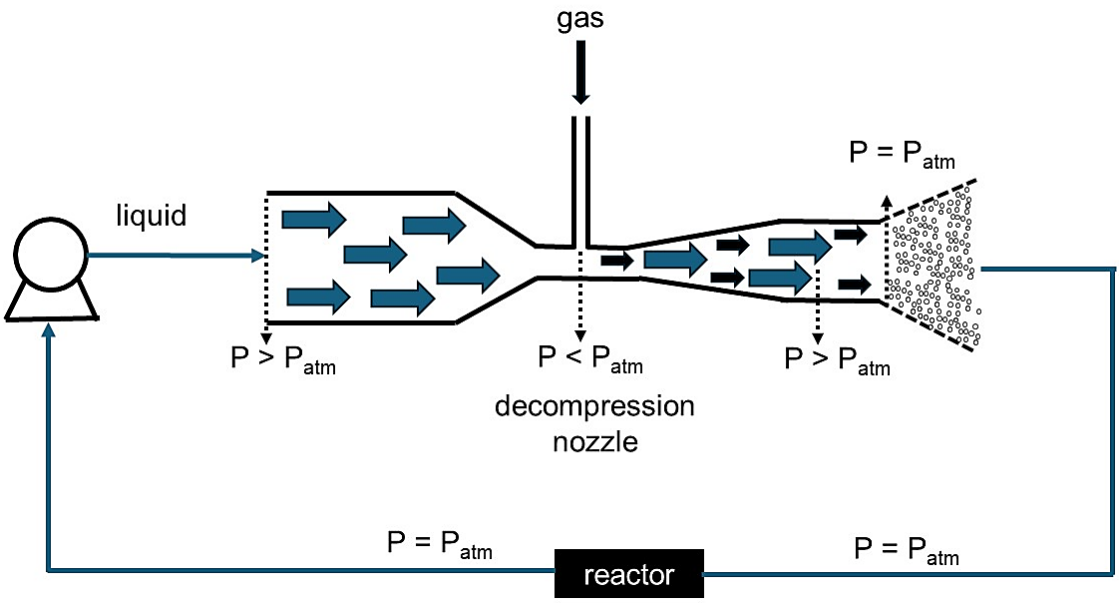

Figure 6. Generation of fine bubbles with a pressurized dissolution method. The figure was redrawn using the information provided in the referenced literature [71, 72].

Conclusion

To improve the performance of immobilized glucose oxidase in oxidative biotransformation reactors, it is necessary to increase the interfacial area using fine bubbles, thus enabling a high mass transfer rate of oxygen molecules through a given liquid medium at the same volume-specific aeration rate. This has been demonstrated in previous studies [62,63,68]. The novel aspect of this work is the implementation of fine bubble technology in a modified SpinChem® vessel V2 with a rotating packed bed basket S2, which is discussed in detail in section 2.4.

2.3. Utilization of molecular oxygen transferred from fine bubbles by oxidases

The underlying principle of oxygen transfer through a bulk medium via the two-film model is integrated with the oxygen demand of the enzyme glucose oxidase. The two-film theory assumes a one-dimensional mass transfer (Figure 7) of gas molecules in bubbles by diffusion at the boundary layer into the liquid medium under consideration of Fick's law.

$$\dot{N}_{O_2} = -D \cdot \frac{dc_{O_2}}{dy} \qquad (5)$$

where $\dot{N}_{O_2}$ in mol m^{-2} s^{-1} is the molar flow density, D in m^2 s^{-1} is the diffusion coefficient, and c in mol m^{-3} is the concentration of oxygen.

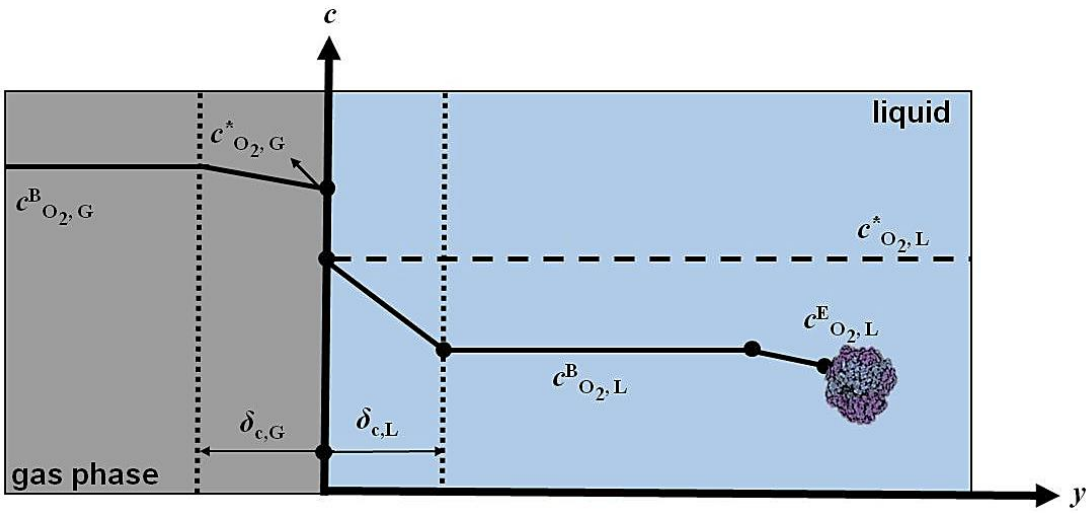

Figure 7. Two-film theory: Mass transfer of oxygen in the bulk gas phase through the bulk liquid medium [74]. The two-film theory is represented schematically, with the consumption of oxygen by the enzyme located in the bulk medium.

Well-mixed conditions are assumed in both bulk phases, where $c^{B}_{O_2,G}$ and $c^{B}_{O_2,L}$ are the concentrations of oxygen in the bulk gas and liquid phases, respectively. At the fluidic interface, the saturation concentration difference is observed and described by Henry's Law (Equation 2 in section 2.1), where $c^{*}_{O_2,G}$ and $c^{*}_{O_2,L}$ are described as the saturation concentration of oxygen in the gas phase and liquid phase. The oxygen molecules in the gas phase are transported and diffused at the boundary layer, where mass transfer occurs at the interface. The molar flow density $\dot{N}_{O_2}$ depends on the concentration difference at each interface, where $c^{B}_{O_2,G} - c^{*}_{O_2,G}$ and $c^{*}_{O_2,L} - c^{B}_{O_2,L}$ are the concentration differences at the gas phase and liquid phase interface, respectively.

$$\dot{N}_{O_2} = \beta_{G,O_2} \cdot (c^{B}_{O_2,G} - c^{*}_{O_2,G}) \quad (6)$$

$$\dot{N}_{O_2} = \beta_{L,O_2} \cdot (c^{*}_{O_2,L} - c^{B}_{O_2,L}) \quad (7)$$

The mass transfer coefficients β_{G,O_2} and β_{L,O_2} in m s^{-1} depend on the concentration boundary layer thickness in the gas $\delta_{c,G}$ in m and liquid phase $\delta_{c,L}$ in m, assuming that there is no back mixing into the bubbles and that the internal resistance of the bubbles is insignificant [75].

$$\beta_{O_2} = \frac{D}{\delta_c} \quad (8)$$

The oxygen mass transfer coefficient β_{G,O_2} for the gas phase is higher than the oxygen mass transfer coefficient for the liquid phase β_{L,O_2}, resulting in a lower boundary layer thickness in the gas phase ($\delta_{c,G} < \delta_{c,L}$) [71].

The dissolved oxygen and glucose in the bulk liquid medium are further consumed by the immobilized enzyme glucose oxidase [76]. The mass balance for the accumulated substrate layer within the carriers is defined by Equation 9.

$$\frac{dm_{\text{substrate}}}{dt} = \dot{V} \cdot c_{\text{sp}} - (\beta_{\text{substrate}} \cdot A_{\text{c}} \cdot r) \quad (9)$$

where $m_{\text{substrate}}$ in mg is the accumulated substrate on the layer of the carriers at time t, $\dot{V}$ in mL min^{-1} is the volume flow rate through the carriers, c_{sp} in mg mL^{-1} is the mass concentration of the substrate at the accumulation layer of the carriers, $\beta_{\text{substrate}}$ in m is the constant of the substrate on the layer, r in mg mL^{-1} min^{-1} is the reaction rate on the layer of carriers, A_{c} in m^2 is the surface area of the carriers.

The oxygen consumption rate OCR in mM min^{-1} is modeled as the design equation [77] of the batch operation by multiplying the reaction rate v_{R} in µmol min^{-1} mg$_{\text{GOx}}^{-1}$ with the enzyme concentration c_{enzyme} in mg$_{\text{GOx}}$ mL^{-1}. The oxygen concentration measured by the immersed sensor indicates the concentration of oxygen molecules $c_{\text{O}_2,\text{L}}^{\text{B}}$ present in the bulk liquid phase at time t, which is the total sum (Equation 10) of the oxygen transfer rate (OTR), oxygen consumption rate (OCR), and oxygen production rate (OPR).

$$\frac{dc_{\text{O}_2}}{dt} = OTR - OCR + OPR \quad (10)$$

$$OCR = \frac{dc_{\text{O}_2}}{dt} = v_{\text{R}} \cdot c_{\text{enzyme}} \quad (11)$$

$$v_{\text{R}} = \frac{v_{\max} \cdot c_{\text{glucose}} \cdot c_{\text{O}_2}}{K_{\text{m,glucose}} \cdot c_{\text{O}_2} + K_{\text{m,O}_2} \cdot c_{\text{glucose}} + c_{\text{glucose}} \cdot c_{\text{O}_2}} \quad (12)$$

where $v_{\max}$ in µmol min^{-1} mg$_{\text{GOx}}^{-1}$ is the maximum glucose oxidase mass-specific reaction rate, c_{glucose} in mM and c_{O_2} in mM are the glucose and oxygen concentrations and K_{m} in mM is the Michaelis-Menten constant.

The OPR is the reaction rate of hydrogen peroxide decomposition catalyzed by catalase in Scheme 1, producing ½ mole of oxygen as a by-product, which is reused in the reaction system by the enzyme glucose oxidase. The OCR is related to the reaction rate equation (12) and is directly proportional to the dissolved substrate concentrations. The mass balance of gaseous species, where the OTR in mmol min^{-1} L^{-1} is given by the time-dependent change in oxygen concentration in the circumstance of oxygen consumption being equal to zero, is demonstrated in Equation 13.

$$OTR = \frac{dc}{dt} = \frac{dn_{\text{G}}}{dt} \cdot \frac{1}{V_{\text{L}}} \quad (13)$$

where n_{G} in mmol is the moles of gas transferred from the bubbles into the liquid, V_{L} is the liquid volume in L, and c is the concentration of oxygen in mmol L^{-1}.

The value of the locally defined OTR is dependent upon the concentration gradient at the bubble interface $c^* - c(t)$, where c^* in mmol L^{-1} is the saturation concentration of dissolved molecular oxygen, and $c(t)$ in mmol L^{-1} is the dissolved oxygen concentration in the bulk medium at time t according to Equation 14. The liquid-side volumetric mass transfer coefficient $k_{\text{L}}a$ in h^{-1} is defined as the multiplication of the mass transfer

coefficient k_L and the specific interfacial area a in m^{-1}. In Equation 13, the OTR is replaced with Equation 14, in which the differential is solved to yield the parameter $k_L a$ in Equation 15 [41].

$$OTR = k_L a \cdot (c^* - c(t)) \quad (14)$$

The mass transfer performance is characterized by the liquid-side volumetric mass transfer coefficient $k_L a$ applying the dynamic method [78,79].

$$k_L a = ln\left(\frac{c^* - c_n}{c^* - c_0}\right) / (t_n - t_0) \quad (15)$$

where $t_n - t_0$ in h is the time interval.

2.4. The focus of the thesis: Application of immobilized oxidases in a modified SpinChem® vessel with a rotating packed bed basket

The focus of this work is the application of fine bubble aeration within the immobilized glucose oxidase in a rotating packed bed reactor as an efficient innovative reactor design for process intensification. The principal objective of this thesis is to develop solutions to the issue of mass transfer limitations:

1. Low solubility (0.254 mM at 1 atm and 25°C in water [21]) of oxygen in the reaction medium as a second substrate: The reaction is continuously supplied with oxygen to overcome this limiting factor, which results in a notable increase in gas consumption. The application of fine bubble aeration enables the surface area per unit volume of added oxygen in compressed air to be increased, thus facilitating a higher overall mass transfer rate of oxygen to the specified reaction volume.

2. Diffusion limitation in the rotating packed bed reactor: The solution to withstand the harsh process conditions is the immobilization of the biocatalysts [5] on a solid support, where a heterogeneous immobilized system is created. By immobilizing the enzyme on a solid support, the enzyme conformation is stabilized, making it more stable and resistant to changes under process conditions [80]. A higher level of stability and enzyme recycling is required to reduce the cost fraction of the biocatalyst, particularly for low-cost products [81]. Immobilizing enzymes on carriers provides a high biocatalyst concentration in the reactor, resulting in higher productivity for glucose oxidase [82]. Thus, the immobilization technique is an approach for implementing biocatalysis in practical applications, such as in flow biocatalysis [81]. To estimate the optimum operating time and reaction conditions, enzyme stability and kinetic studies under the targeted reaction conditions are required, which is the subject of this study.

The following investigations are the subject of this research to overcome mass transfer limitations and to enhance the performance of immobilized glucose oxidase in a rotating rotating packed bed reactor integrated with the fine bubble technology:

1. Design of system allowing improvement of reaction efficiency
2. Design of liquid model system and characterization of immobilized oxidases
3. Characterization of the rotating bed reactor focusing on hydrodynamics and mass transfer performance with inline oxygen measurements
4. Investigation of the stability of the immobilized oxidases with diffusion limitations
5. Characterization of system productivity based on reaction kinetics and kinetic modeling of the reaction rate equation
6. Demonstration of the applicability of fine bubble aeration by investigating the technological and economic performance of the innovative reactor concept

3. Materials and methods

3.1. Biocatalysts

Glucose oxidase (Enzyme Commission Number: 1.1.3.4) GOx type VII (G2133, 248878 units/mg solid, purity factor: 0.816) lyophilized powder from *Aspergillus niger* and peroxidase (Enzyme Commission Number: 1.11.1.7) type I (P8125, ≥ 50 units/mg solid) lyophilized powder from horseradish were purchased from Sigma-Aldrich/Merck KGaA (Darmstadt, Germany). Catalase (Enzyme Commission Number: 1.11.1.6) (C0052, ~2000 units/mg protein) solid powder from bovine liver was purchased from TCI Deutschland GmbH (Eschborn, Germany).

3.2. Chemicals

The substrate D-(+)-glucose (p.a., anhydrous), sodium acetate (> 100.1%, p.a., anhydrous), acetic acid 100% (≥ 99.8%, p.a.), acetic acid (25%, pure), dipotassium hydrogen phosphate (K_2HPO_4, 99.5%, anhydrous), and potassium-dihydrogen phosphate (KH_2PO_4, 99.8%) were purchased from Carl Roth GmbH (Karlsruhe, Germany) for the preparation of substrate and buffer solutions. Sodium hydroxide (NaOH, 99.5%, pellets) for inline titration as well as pH adjustment of solutions, o-dianisidine peroxidase substrate for the enzymatic assay of glucose oxidase, and antifoam 204 (A6426) as a surfactant (mixture of organic non-silicone polypropylene polyether dispersions) were purchased from Sigma-Aldrich/Merck (Darmstadt, Germany). For the Bradford protein assay, Coomassie Protein Assay Reagent (Blue G-250) was purchased from Themo Fisher Scientific GmbH (Rockford IL, USA). Sepabeads® EC-HFA and ReliZyme™ HFA 403 M grade carriers were purchased from Resindion S.r.l (Rome, Italy). Oxirane acrylic (1014 F) carriers were purchased from Röhl GmbH (Waldbüttelbrunn, Germany).

3.3. Carrier screening

0.1 g carriers supplied in wet form (Oxirane acrylic beads (1014F), Sepabeads® EC-HFA, Sepabeads® EC-EP 503/S and Lifetech ECR 8285b) were washed with 10 mL deionized water. Carriers remaining on the filter (diameter of 125 mm, Fisherbrand QL115, Fisher Scientific Schwerte, Germany) were left for 2 h in a vacuum drier.

Each type of dried epoxy functionalized carriers (0.05 g of Sepabeads® EC-HFA as well as Sepabeads® EC-EP 503/S, 0.05 g of Oxirane acrylic 1014F and 0.02 g of Lifetech ECR 8285b) was incubated separately with 1.4 mL of glucose oxidase solution (85.0 ± 2.4 μg_{GOx} mL^{-1}) at 4 ± 1°C and 40 rpm with the tube revolver Thermoscientific (USA) and for five days to establish the equilibrium between the carriers and enzyme at the end of immobilization. The enzyme glucose oxidase solution was prepared in 50 mM potassium phosphate buffer [83] at pH 7.0.

3.4. Buffer selection

0.07 g of ReliZyme™ HFA 403 M grade carriers were incubated with 1.4 mL of glucose oxidase solution (100 μg_{GOx} mL^{-1}) at 20 rpm with the tube revolver Thermoscientific (USA) and 4 ± 1°C for 20 h. The enzyme glucose oxidase solution was prepared in 100 mM potassium phosphate buffer at pH 7.0 and 10 mM sodium acetate buffer at pH 5.3 to study the buffers.

The term "unit definition of activity" U mL^{-1} (µmol min^{-1} mL^{-1}) represents the rate of oxidation of 1.0 µmol of β-D-glucose to D-glucono-1,5-lactone and H_2O_2 per minute. The reaction solution, prepared with 0.19 mM o-dianisidine, 8.84 mM D-(+)-glucose, and 1.93 U POD in a non-UV spectrophotometer cuvette, was saturated with compressed air for 20 minutes to ensure oxygen saturation of the reaction solution for a high glucose oxidase activity. The enzyme peroxidase facilitates the oxidation of o-dianisidine in the presence of hydrogen peroxide, which is a by-product of the oxidation of glucose by the enzyme glucose oxidase in the supernatant. The photometric investigations were performed under controlled temperature conditions using the UV/VIS photometer Uvikon XL, manufactured by Goebel Instrumentelle Analytik GmbH (Au in der Hallertau, Germany).

3.5. Preparation of carriers for the rotating packed bed basket

The amount of ReliZyme™ HFA 403 M grade carriers (25 g) supplied in wet form was washed with 500 mL deionized water. The carriers on the filter (Munktell Ahlstrom Folded Grade 3 Filters, d = 270 mm, Ahlstrom, Finland) were subjected to an overnight storage period at 52°C. To set up a SpinChem® rotating packed bed basket S2 (diameter = 45 mm), 8.2 g of ReliZyme™ HFA 403 M grade dried carriers was incubated with 90 mL of glucose oxidase solution (98 µg mL^{-1} and 685 µg mL^{-1}, which correspond to 1.07 mg_{GOx} $g_{carrier}^{-1}$ and 7.52 mg_{GOx} $g_{carrier}^{-1}$, respectively). The glucose oxidase solution was prepared in 10 mM sodium acetate buffer at pH 5.3. The immobilization experiments were carried out for 22 h at 4 ± 1°C and 300 rpm with the shaker Edmund Bühler GmbH (Bodelshausen, Germany). The supernatant was removed with a syringe needle. To remove unbound glucose oxidase from the carriers, they were washed three times with 20 mL of 10 mM sodium acetate buffer at pH 5.3 until no change in activity values of the washing solution was detected. Once the model reaction was run in the modified SpinChem® vessel V2 with a rotating packed bed basket S2 under fine bubble aeration, the rotating packed bed basket was washed three times with 100 mL of 10 mM sodium acetate buffer at pH 5.3, with the objective of eliminating any residual components. Following this process, the rotating packed bed basket was integrated into the experimental setup, where it was utilized to conduct a repetitive batch.

3.6. Reactor set-up

The generation of fine bubbles was achieved through the utilization of an AMB3 fine bubble generator and a sintered frit porous sparger. Consequently, two different reactor configurations were established in this study.

3.6.1. Reactor set-up 1: Generation of fine bubbles with an AMB3 nanobubble generator

Fine bubbles are generated by the pressurized dissolution method, as previously discussed in section 2.2.2, utilizing the AMB3 fine bubble generator in Figure 8 (HACK UFB Co., Ltd., Yamanashi, Japan). The ambient air is sucked (2), and the reaction medium is pumped from the liquid inlet (4) through to the mixing vessel (1). In the mixing vessel, the liquid is subjected to over-saturation, resulting in the generation of ultrafine bubbles, which are then pumped to the reactor from the liquid discharge point (5).

Figure 8. AMB3 fine bubble generator: 1 - mixing vessel: air with water, 2 - air suction, 3 - air control valve, 4 – liquid inlet, 5 – liquid discharge with fine bubbles [84].

The reactor setup (Figure 9) consists of a SpinChem® rotating packed bed basket S2 and a SpinChem® vessel V2 purchased from SpinChem AB (Sweden). To prevent carrier leaching, a stainless steel (SS316L, EN2348) filter (pore size 104 µm) was placed in the SpinChem® rotating bed basket S2 (Figure 2). The rotating packed bed basket was placed 19 mm from the bottom of the vessel. The shaft of the rotating packed bed basket was connected to the digital overhead stirring motor IKA RW 20 Digital from IKA-Werke GmbH & Co. KG (Staufen, Germany). The thermostat Thermohaake B5 Thermoscientific (USA) was connected to the SpinChem® vessel to maintain a constant temperature of 35°C during the reaction.

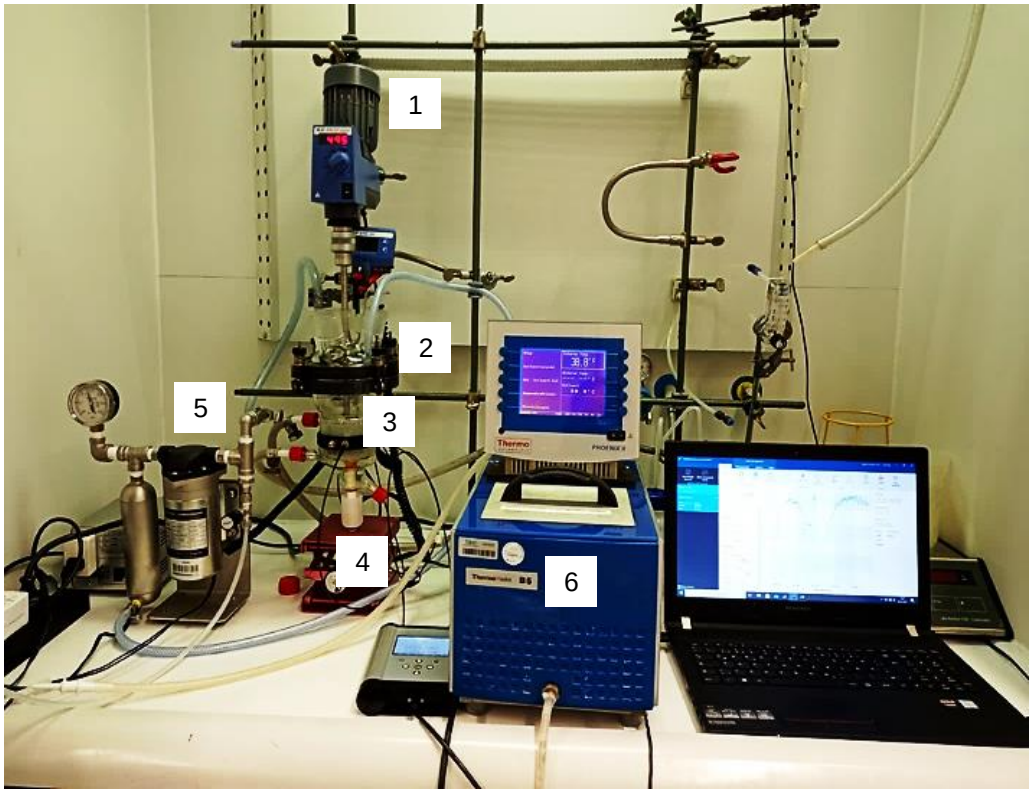

Figure 9. Experimental set-up 1. 1. Motor, 2. SpinChem® vessel V2 with a rotating packed bed S2 basket, 3. SP-PSt3-NAU-D10-YOP oxygen sensor spot, 4. Fiber optic oxygen meter Fibox 4, 5. AMB3 fine bubble generator, 6. Thermostat.

3.6.2. Reactor set-up 2: Generation of fine bubbles with 2 µm sintered frit sparger

The reactor setup consists of (Figure 10 and Figure 11) of a SpinChem® rotating packed bed basket S2 and a SpinChem® vessel V2 purchased from SpinChem AB (Sweden). To prevent carrier leaching, a stainless steel (SS316L, EN2348) filter (pore size 104 µm) was placed in the SpinChem® rotating bed basket S2 (Figure 2), which was filled with 8.2 g dried ReliZyme™ HFA 403 M grade carriers with immobilized glucose oxidase (Scheme 1). The shaft of the rotating packed bed basket was connected to the digital overhead stirring motor IKA RW 20 Digital from IKA-Werke GmbH & Co. KG (Staufen, Germany). The thermostat Thermohaake B5 Thermoscientific (USA) was connected to the SpinChem® vessel to maintain a constant temperature of 35°C during the course of the reaction.

The compressed air flow rate, which was regulated with a gas mass flow meter from Bronkhorst Deutschland Nord GmbH (Kamen, Germany), was supplied to the reaction medium using a sintered frit sparger from TECHLAB GmbH (Braunschweig, Germany) with a pore size of 2 µm (length 25.4 mm, diameter 12.7 mm) and an open tube sparger (opening diameter of 2 mm). At the bottom of the reactor, both spargers were placed vertically. The distance between the top of the sintered frit sparger and the bottom of the vessel was 26 mm. The rotating packed bed basket was positioned 41 mm from

the bottom of the vessel, with a distance of 15 mm between the top of the sintered frit sparger and the lower end of the rotating packed bed basket.

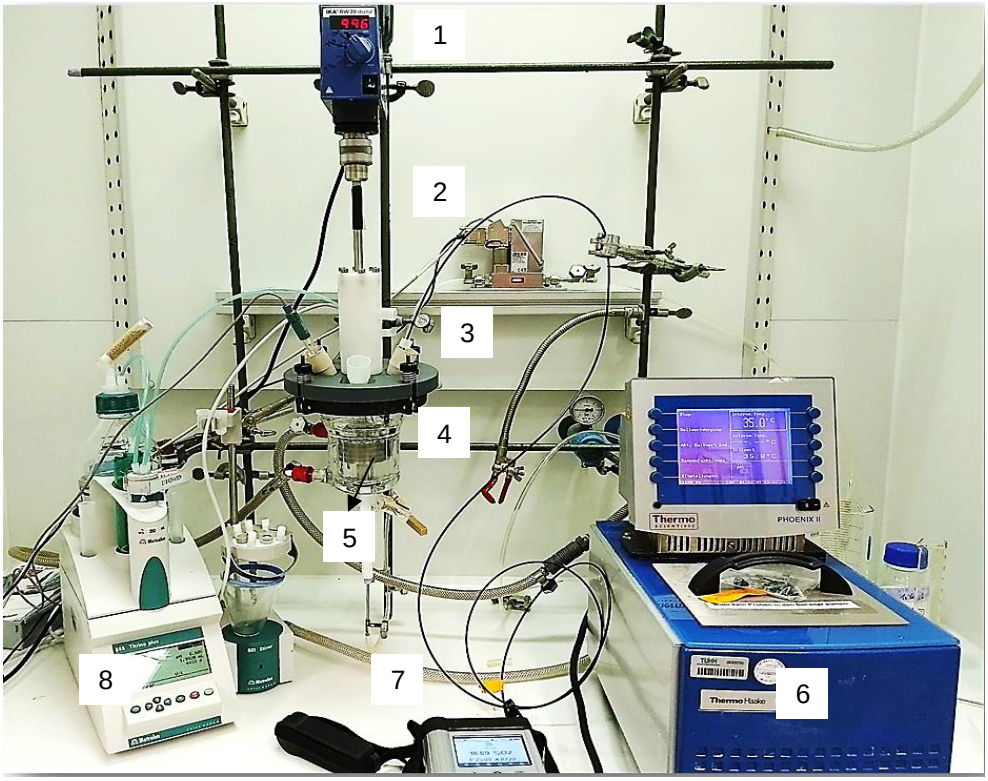

Figure 10. Experimental set-up 2. 1. Motor, 2. Bronkhorst gas flow meter, 3. SP-PSt3-NAU-D5-YOP oxygen sensor spot, 4. SpinChem® vessel V2 with a rotating packed bed reactor S2, 5. Sintered frit sparger with a pore size of 2 µm, 6. Thermostat, 7. Fiber optic oxygen meter Fibox 4, 8. Automated titrator Titrinoplus 848 Metrohm.

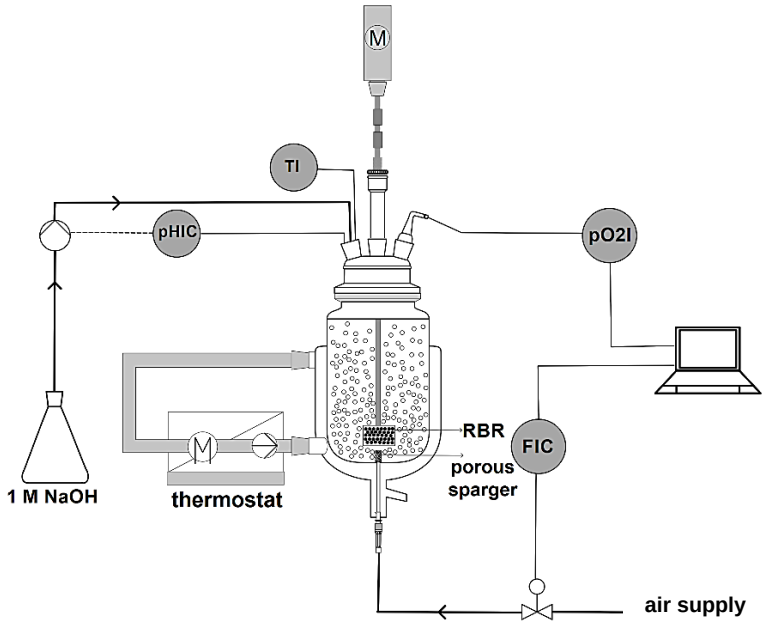

Figure 11. The Piping and Instrumentation Diagram (PID) of the experimental set-up (down, HiTech Zang RI-CAD software version 2.2).

3.7. Analytics

3.7.1. HPLC analysis

An offline HPLC analysis was established according to the literature [30] to detect the substrate D-glucose and gluconic acid (Figure 12).

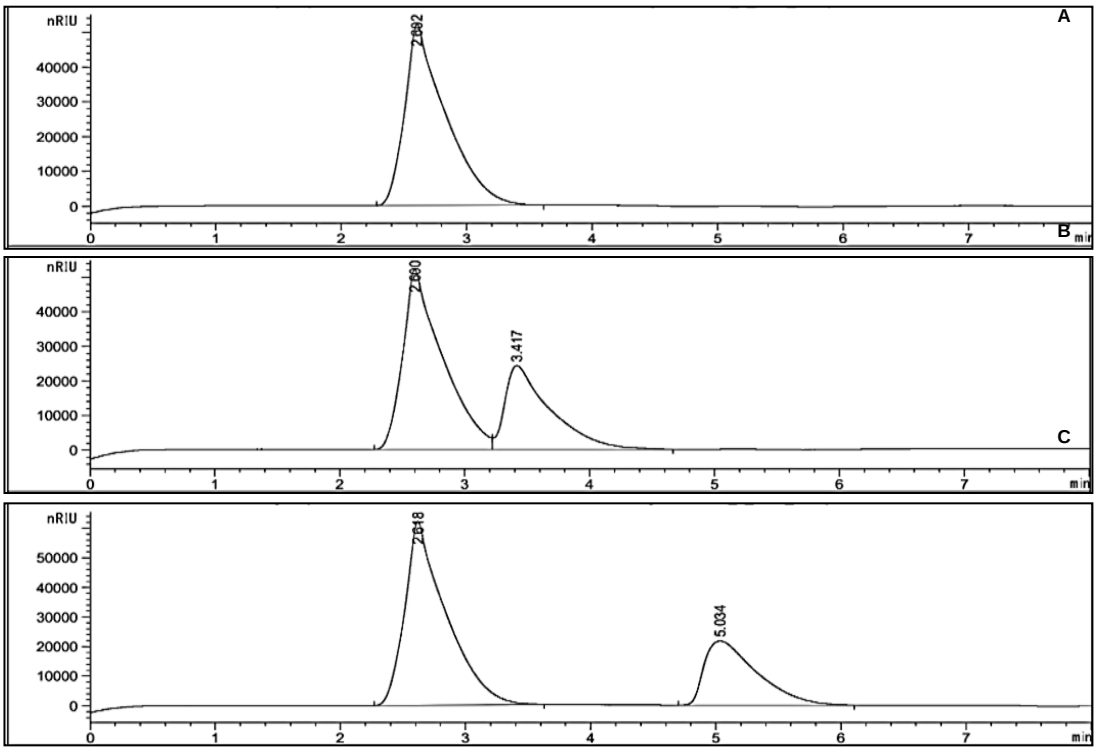

Figure 12. HPLC chromatograms. A) Blank: 50 mM potassium phosphate buffer with 20.8 mM NaOH (2.6 min), B) 20 mM D-glucose (3.4 min) in 50 mM potassium phosphate buffer with 20.8 mM NaOH, C) Gluconic acid (5.0 min) in 50 mM potassium phosphate buffer with 20.8 mM NaOH. HPLC column: Luna 5 µm NH_2 100 Å LC column 250 x 3.0 mm from Phenomenex Ltd, (Aschaffenburg, Germany), mobile phase flow rate: 0.5 mL min^{-1} of 20 mM of H_3PO_4 in deionized water, injection volume 10 µL, 30°C.

The analytes were identified using a refractive index detector and quantified with the peak areas of the calibration samples using the software OpenLab CDS ChemStation Edition (Figure 13).

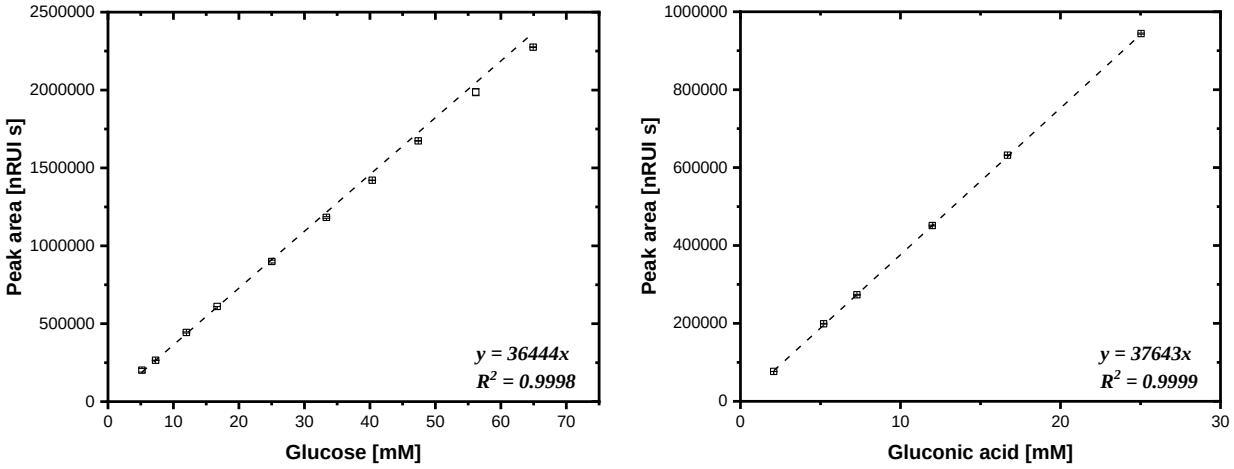

Figure 13. Calibration curves of D-glucose and gluconic acid. HPLC column: Luna 5 µm NH_2 100 Å LC column 250 x 3.0 mm from Phenomenex Ltd, (Aschaffenburg, Germany), mobile phase flow rate: 0.5 mL min^{-1} of 20 mM of H_3PO_4 in deionized water, injection volume 10 µL. Samples were prepared in 50 mM potassium phosphate buffer at pH 7 together with 20.8 mM NaOH, 30°C.

When the HPLC vials containing the samples taken from a reaction system were reinjected, an increase in the peak area of the product gluconic acid and a decrease in the peak area of glucose were observed (Figure 14).

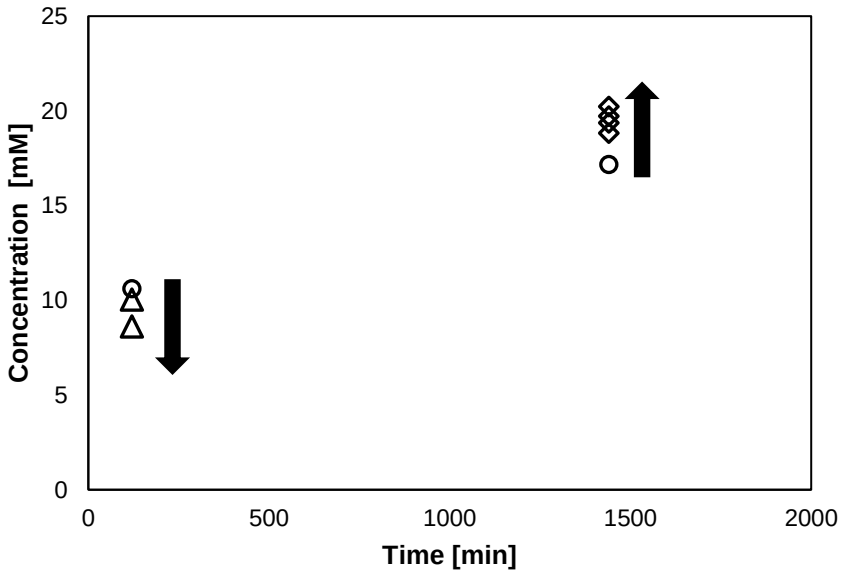

Figure 14. Re-analysis of the HPLC vials to control the change in peak area (20.8 mM NaOH was used to quench the reaction), circles: initial data point for glucose and gluconic acid, triangles for glucose after 1h and 4h, diamonds for gluconic acid of the same HPLC vial. Luna 5 µm NH_2 100 Å LC column 250 x 3.0 mm from Phenomenex Ltd, (Aschaffenburg, Germany), mobile phase: 0.5 mL min^{-1} of 20 mM of H_3PO_4 in deionized water, injection volume 10 µL. Samples were prepared in 50 mM potassium phosphate buffer at pH 7 together with 20.8 mM NaOH, 30°C.

In accordance with the literature [30], the sodium hydroxide concentration was increased to 480 mM in the HPLC vials to quench the reaction. However, the ability to separate the peaks was limited for a glucose concentration of 93 mM, as illustrated in Figure 15. Therefore, the inline automated titration analysis was established as described in section 3.7.1.

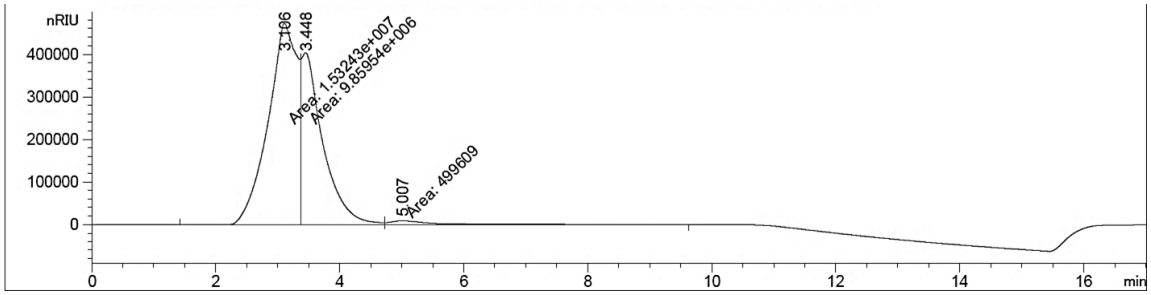

Figure 15. HPLC chromatogram of a reaction sample at 1 h. 93 mM D-glucose (3.4 min) and 7 mM gluconic acid (5.0 min) in 50 mM potassium phosphate buffer with 480 mM NaOH (3.1 min). HPLC column: Luna 5 µm NH_2 100 Å LC column 250 x 3.0 mm from Phenomenex Ltd, (Aschaffenburg, Germany), mobile phase: 0.5 mL min^{-1} of 20 mM of H_3PO_4 in deionized water, injection volume 10 µL. Samples were prepared in 50 mM potassium phosphate buffer at pH 7 together with 20.8 mM NaOH, 30°C.

3.7.2. Development of an automated inline analysis

Before starting the experiments, the automated titrator from Titrinoplus 848 Metrohm (Switzerland) was calibrated each time with the calibration solutions at pH 4.00 ± 0.02 as well as pH 7.00 ± 0.02 from Carl Roth GmbH + Co. KG (Karlsruhe, Germany). To avoid overtitration during the titration, the pumping rate of 1 M NaOH was adjusted for each substrate concentration, ranging from 8.8 - 1000 mM. For macrobubble aeration, the reaction rate was much slower than during fine bubble aeration. Thus the pumping rate of NaOH was kept at a lower level compared to the reactions performed for fine bubble aeration.

Table 1. Adjustment of titration parameters: Reagent 1 M NaOH, 35°C, pH sensor, time interval 120 s. The lag phase was explained in sections 3.7.1.2 and 4.8.

	Fine bubble aeration (2 µm sintered frit)		**Macrobubble aeration (Open tube: 2 mm orifice diameter)**	
D-glucose [mM]	**Before lag phase**	**After lag phase**	**Before lag phase**	**After lag phase**
	1 M NaOH pumping rate [mL min^{-1}]			
8.8	0.05-0.1	0.2-0.3	-	-
25	0.05-0.1	0.2-0.3	0.03	30
50	0-05-0.1	0.2-0.3	-	-
100	0.1	0.2-0.3	-	-
300	0.1	0.45- 0.5	0.03	30
600	0.1	0.55-0.6	0.03	30
1000	0.1	0.55-0.6	-	-

3.7.2.1. Validation of the inline titration method

The chemical transformation is not limited, and the acid dissociation constant of gluconic acid pK_a of 3.5 was calculated with Equation 16 at 35°C using the value of pK_a 3.6 of gluconic acid at 25°C published by the European Chemical Agency [85].

$$ln\,K = \frac{\Delta G}{R \cdot T} \qquad (16)$$

where K is the equilibrium constant, R in J K^{-1} mol^{-1} is the molar gas constant, ΔG in J mol^{-1} is the Gibbs free energy.

The acid dissociation constant of gluconic acid pK_a of 3.5 is lower than the value of pH 5.3 of the reaction causing deprotonation of the carboxylic acid group of gluconic acid. The quantitative product determination for the biotransformation of D-glucono-1,5-lactone to gluconic acid was validated on a mole basis, as one mole of NaOH consumed corresponds to one mole of gluconic acid produced. The ratio of the total mole of product n_{product} at the end of the reaction to the initial mole of D-glucose $n_{\text{glucose},0}$ given to the system, shown in Equation 17, corresponds to the reaction yield.

$$Yield\,[\%] = \frac{n_{\text{product}}}{n_{\text{glucose},0}} \cdot 100 \qquad (17)$$

A representative calculation is described for a glucose concentration of 300 mM, corresponding to 60.000 µmole of glucose to be oxidized by the enzyme glucose oxidase in 200 mL of reaction medium. Continuous titration of the product D-glucono-1,5-lactone shifted the reaction to the product side, allowing a yield of 96.2 ± 2.5%. Based on this finding, as presented in section 4.9, if all the glucose molecules in the reaction medium are oxidized, 60.000 µmole of gluconic acid would be produced, corresponding to the need for 60 moles of 1 M NaOH, resulting in a total volume of 60 mL of 1 M NaOH pumped into the system as shown in Figure 16. The titration method was well established for inline analysis and ensured a fixed pH value of pH 5.5 ± 0.2, which is required for maximum activity of glucose oxidase.

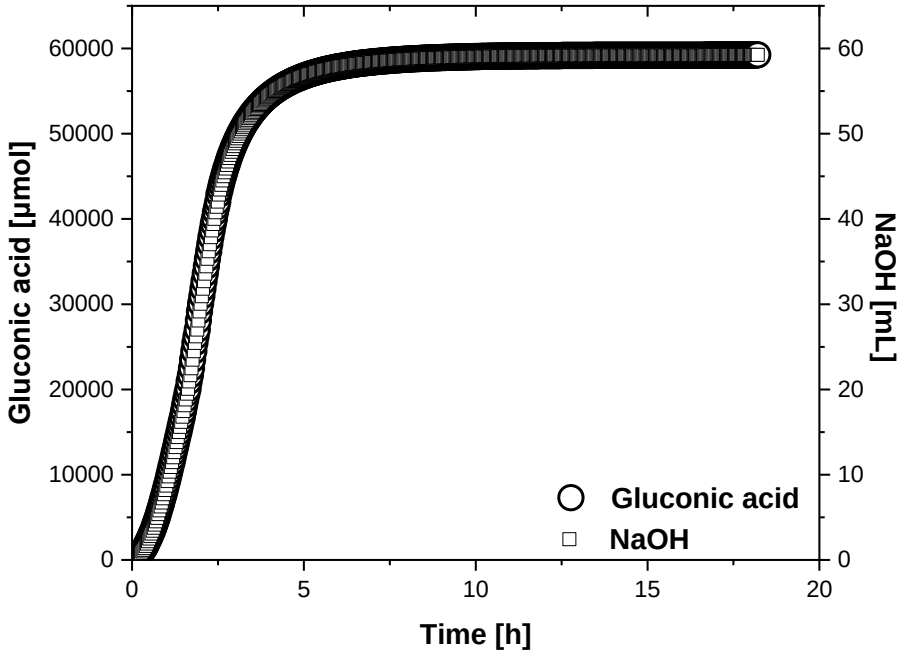

Figure 16. Inline determination of gluconic acid during the course of the reaction. 1000 rpm, 35 ± 1°C, 8.2 g carriers, initial volume 200 mL, 1 vvm, pH 5.5 ± 0.2. 300 mM glucose solution was prepared in 10 mM sodium acetate buffer at pH 5.3. Calculated activity of catalase (free) / calculated activity of glucose oxidase (immobilized):1.70. The experiment was performed in duplicate. Error bars show the standard deviation obtained from duplicate measurements.

3.7.2.2. Determination of the glucose oxidase-specific activity of immobilized and free oxidases in a rotating packed bed reactor

The amount of product was quantified using inline titration analysis. The slope of the progress curve between 10-25% of yield (10% yield is the start of the linear region after the lag phase) yielded the amount of product produced in micromoles per minute (U). The slope was quantified using linear data fitting in the Origin2023a software. The amount of product determined is correlated to the amount of substrate consumed in a 1:1 stoichiometric ratio without side product production as described in section 3.2.2. The glucose oxidase-specific activity in U mg^{-1} is defined as the amount of substrate consumed in micromoles per minute per mg of enzyme.

3.8. Investigation of mass transfer in a gas-liquid multiphase flow

The mass transfer performance for the rotating packed bed reactor used as an impeller was measured with 8.2 g of dry ReliZyme™ HFA 403 M grade carriers without immobilized enzymes in 200 mL of the liquid model solution (10 mM sodium acetate buffer at pH 5.3 at 35°C) using compressed air and nitrogen as the stripping gas. The concentration of oxygen was monitored inline with an immersed oxygen sensor spot SP-PSt3-NAU-D5-YOP connected to the Fiber Optic Oxygen Meter Fibox 4 from PreSens Precision Sensing GmbH (Regensburg, Germany). The position of the sensor

spot was fixed for all experiments at 2 mm near the rotating packed bed basket and 4 mm above the bottom of the rotating packed bed basket.

The oxygen was provided through the utilization of compressed air, which was regulated by the Bronkhorst gas flow meter and connected to a 2 µm sintered frit in the SpinChem® vessel V2. The accuracy of the air flow rate given by the Bronkhorst gas flow meter was investigated through a series of experiments. In each experiment, a measuring cylinder was filled to capacity with deionized water, and a thin tube was placed under the measuring cylinder. As the air flow rate was initiated, the gas was introduced into the measuring cylinder, resulting in the water being removed from the measuring cylinder. The measurement time was set at one minute, after which the remaining water volume in the cylinder was quantified. The difference between the initial water volume and the remaining water volume represents the volume of air (ml) placed with water, indicating the air flow rate (mL) per minute (Figure 17).

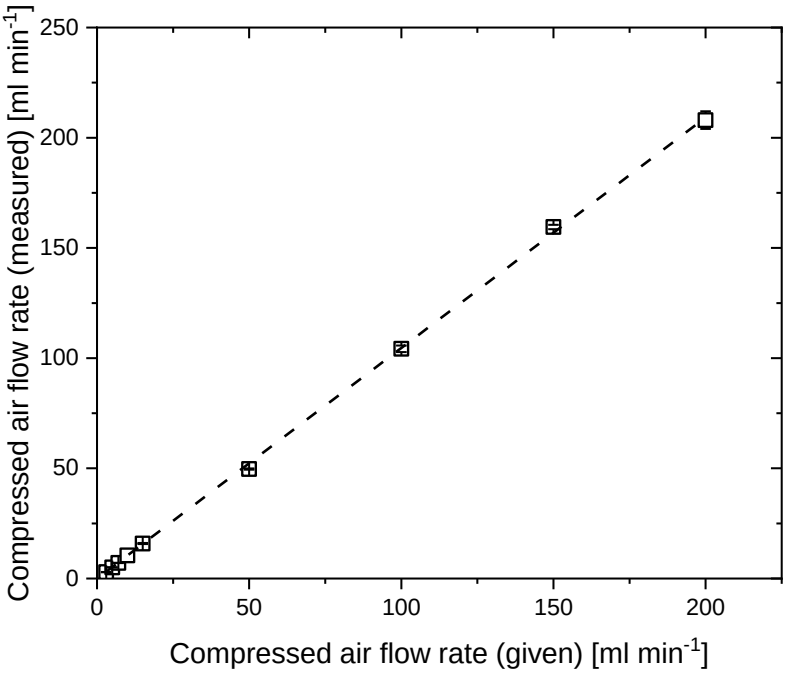

Figure 17. Calibration test of the Bronkhorst gas flow meter at 23 ± 1°C, deionized water.

4. Results and discussion

In the following section, the applicability of the fine bubble technology in the modified SpinChem® vessel with a rotating packed bed basket is demonstrated by:

- Investigation of the mass transfer and biocatalytic performance for a SpinChem® vessel with a rotating packed bed basket (SpinChem® rotating packed bed reactor)
- Investigation of process parameters for efficient use of the SpinChem® rotating packed bed reactor under fine bubble aeration
- Approaches to overcome mass transfer limitations: internal diffusion limitations and mass transfer in the gas-liquid multiphase system
- Stability and reuse of immobilized glucose oxidase in the rotating packed bed reactor
- Kinetic studies and reaction rate modeling
- Comparison of simulated and experimental reaction rates
- Lab-scale techno-economic performance of the immobilized glucose oxidase

At the end of this chapter, the reader will find the answers to the following questions: How can the use of fine bubble technology in the innovative SpinChem® rotating packed bed reactor concept be applied:

- in a cost-efficient manner compared to the conventional aeration method?
- while contributing to more environmentally friendly biotransformations?

4.1. Establishment of an enzyme-carrier system

The choice of immobilization strategy is critical for the reaction system (Scheme 1), utilizing two enzymes: either both enzymes are used in immobilized form, or the cost-driving enzyme is immobilized, and the other enzyme is used in its free form. The enzyme glucose oxidase is the cost driver in immobilization when its price (624 Euro per gram solid for 250,000 Units per gram solid [86]) is compared with the price of the carriers (780 Euro per kg ReliZyme™ HFA 403 M grade carrier [87]) and the second enzyme catalase (91 Euro per gram solid for 2200 Units per mg solid [88]). Therefore, carrier screening tests were carried out with the enzyme glucose oxidase to achieve a reasonable catalyst loading on the carriers in the rotating packed bed reactor.

The qualitative analysis of the purity of the enzyme glucose oxidase (GOx) was conducted via SDS-PAGE analysis. The stock glucose oxidase solution was diluted in series, injected into the gel and gel-electrophoresis was started.

Table 2. A serial dilution of the stock glucose oxidase (0.816 mg mL^{-1}) for the SDS-PAGE analysis.

Glucose oxidase solution in the gel bands [mg mL^{-1}]								
1	**2**	**3**	**4**	**5**	**6**	**7**	**8**	**9**
0.816	0.272	0.091	0.071	0.052	0.043	0.034	0.017	0.008

Three bands appeared in Figure 18 for each glucose concentration. Glucose oxidase is a dimer protein (80 kDa) with a molecular weight of 160 kDa according to Sigma Aldrich/Merck (Darmstadt, Germany) [86] and an impurity factor of 0.816 [89]. The bands in Figure 18 between 75 and 100 kDa are the glucose oxidase dimers. The bands close to 150 kDa are glucose oxidase protein (160 kDa).

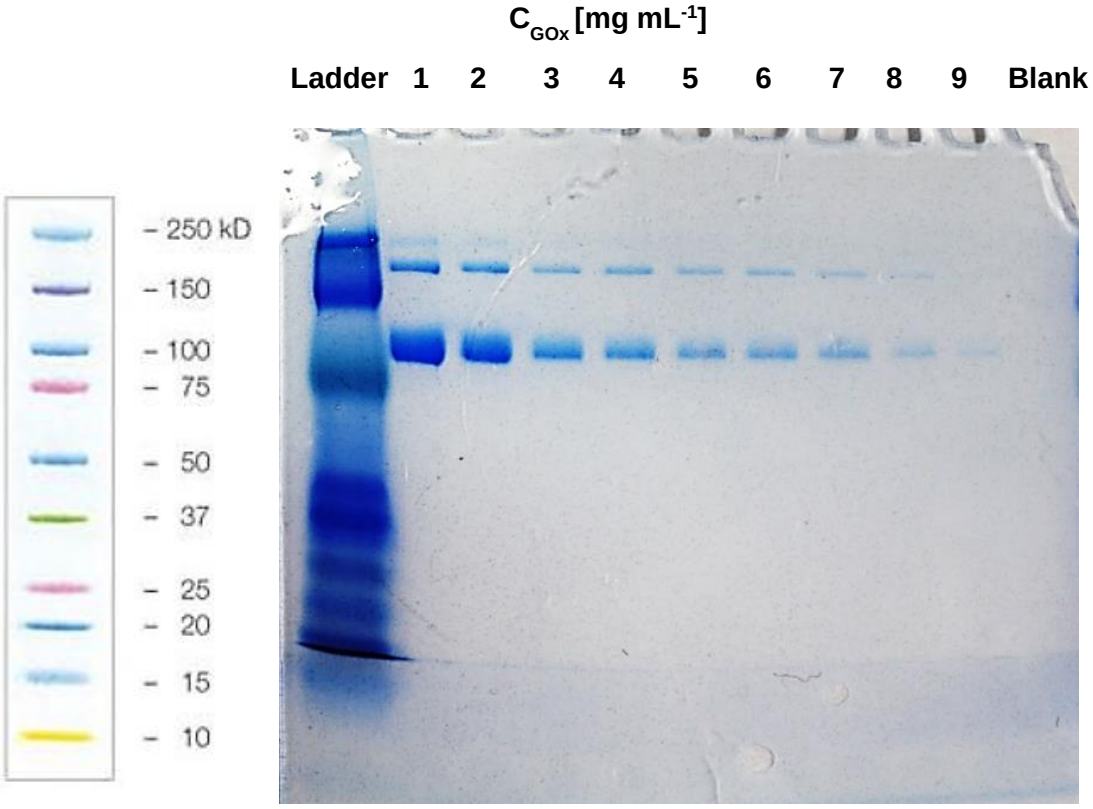

Figure 18. SDS-Page analysis of the enzyme glucose oxidase performed by the technician Maren Breuer.

The immobilization yield was quantified with the Bradford protein assay by determining the absorbance ratio (590 nm / 450 nm) detected at 35°C, according to T. Zor [90]. Glucose oxidase at various concentrations was used for the preparation of the calibration curve of the Bradford assay (Figure 19). Equation 18 defines the mass-specific yield depending on the protein loss in the supernatant, which is the ratio of the amount of enzyme immobilized on carriers to the amount of enzyme in the initial solution [91].

$$Immobilization\ yield = (1 - \frac{c_s \cdot V_s}{c_0 \cdot V_0}) \cdot 100 \qquad (18)$$

where c_0 in µg mL^{-1} and c_s in µg mL^{-1} denote the initial enzyme concentration and the enzyme concentration in the supernatant at the end of immobilization, V_0 in mL and V_s in mL describe the volume of the initial enzyme solution and the volume of the supernatant at the end of the immobilization process.

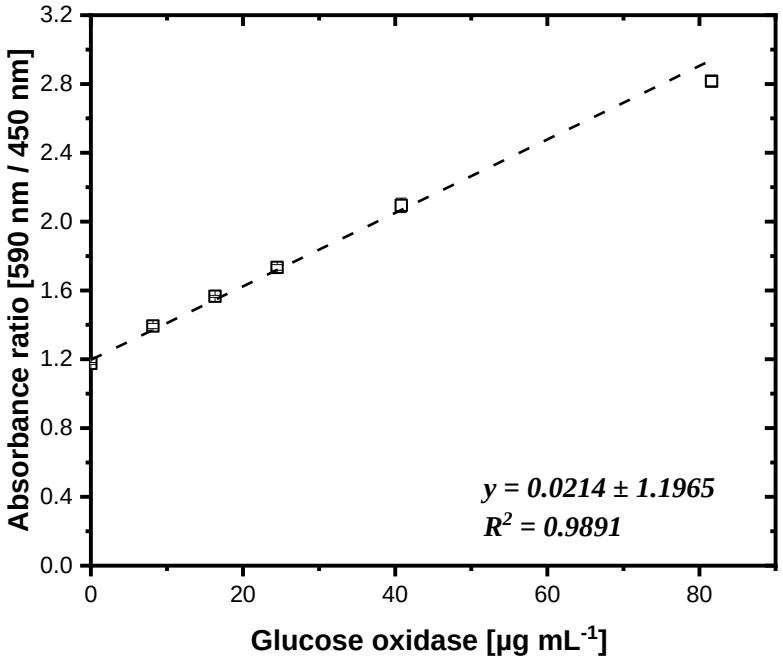

Figure 19. Bradford assay calibration curve. Enzyme solutions were prepared in 1.4 mL of 50 mM potassium phosphate buffer at pH 7.0. Experiments were performed in duplicate at 37 ± 1°C.

The enzyme loadings on different epoxy-functionalized carriers were compared in terms of immobilization yield. The screening tests (Table 3) were first performed with 50 mM potassium phosphate buffer at pH 7 as described in the literature [83]. The carriers applied show differences in particle size, pore diameter, and oxirane active group content. Therefore, a concrete comparison between the carriers could not be described, even though the carriers have epoxy functional groups, and the same immobilization procedure was applied. However, the aim of this investigation is not only to find a cost-optimized carrier, but also to find a carrier type that is commercially available on the market, since the use of a rotating packed bed reactor requires a relatively higher amount of carriers.

Table 3. Particle screening and buffer selection for glucose oxidase immobilization. Measurement conditions: 4 ± 1 °C, 40 rpm, 10 mM sodium acetate buffer pH = 5.3, volume of immobilization: 1.4 mL, initial glucose oxidase concentration 85 µg mL^{-1}, carriers were incubated for 5 days, experiments were performed in duplicate.

Carrier screening				
Carrier type	**Functional group**	**Oxirane content**	**Buffer**	**Immobilization yield [%]**
Sepabeads® EC-EP 503/S[a]	Epoxy [53]	NA	50 mM of potassium phosphate buffer at pH 7.0	8.5 ± 1.7
Lifetech ECR 8285[b]	Epoxy [92]	NA		13.6 ± 0.8
Oxirane acrylic beads (1014F)[c]	Epoxy [93]	minimum 0.4%		38.5 ± 4.7
Sepabeads® EC-HFA[a]	Amino-epoxy [53]	minimum 30 µmol per g wet		68.3 ± 4.3

a. 0.05 g carriers, b. 0.02 g carriers. Sepabeads® EC S grade carriers have a smaller particle size (100 - 300 µm) and pore diameter (10 - 20 nm) [53].
b. Lifetech ECR 8285 (methacrylate type resin) have a particle size of 250 - 1000 µm (pore diameter: 40 to 60 nm [92]).
c. Oxirane acrylic beads (1014F, copolymer of methacrylamide) carriers have a particle size of 205 µm [93].

The carriers Lifetech ECR 8285 and Oxirane acrylic beads (1014F) resulted in a lower immobilization yield than the Sepabeads® EC carriers. An immobilization yield (68.3 ± 4.3%) was achieved with Sepabeads® EC-HFA resin and Resindion S.r.l. reported that their product Sepabeads® EC provides irreversible (covalent) immobilization [53]. Further investigations were described in section 4.2 to increase the amount of immobilized glucose oxidase per gram of carriers to improve the catalyst concentration in a given volume of the rotating packed bed reactor.

4.2. Characterization of enzyme-carrier system

4.2.1. Effect of buffer concentration, pH and immobilization volume

The carrier giving a high immobilization yield was studied in different buffers [83] with the ReliZyme™ HFA 403 M grade carrier instead of Sepabeads® EC carriers due to the discontinuity in the Sepabeads® production line. Resindion S.r.l. is offering the ReliZyme™ HFA 403 M grade carrier as an improved carrier type of the Sepabeads® EC HFA resin, according to their own description, with a larger carrier size, which is the advantage to avoid possible diffusion limitations in the rotating packed bed reactor. Sepabeads® EC S grade carriers have a smaller particle size (100-300 µm), and pore diameter (10-20 nm) compared to ReliZyme™ HFA 403 M grade carriers (particle size: 200-500 µm, pore diameter: 40-60 nm; [83]). ReliZyme™ HFA M grade carriers are used in many biocatalytic immobilizations [58,59,94].

The activity yield of immobilization was determined using Equation 19 [91], which is the ratio of the remaining activity in U after 22 h to the initial activity in the supernatant in U by the initial rate measurements in the presence of peroxidase at 520 nm according to the glucose oxidase (GOx)/peroxidase (POD) photometric assay [24,95] from Sigma-Aldrich / Merck (Darmstadt, Germany) at pH 5.3 and 35°C. The activity on the carriers in U $mg_{carrier}^{-1}$ (Equation 20) is the ratio of the calculated activity on the carriers after immobilization with enzymes per milligram of carriers.

$$Activity\ yield = \left(\frac{v_0 \cdot V_0 - v_s \cdot V_s}{v_0 \cdot V_0}\right) \cdot 100 \qquad (19)$$

$$Activity\ on\ carriers = \frac{v_0 \cdot V_0 - v_s \cdot V_s}{m_{carrier}} \qquad (20)$$

G. Ozyilmaz [83] reported that the concentration of the buffer has no effect on the activity of immobilized glucose oxidase, whereas it has a considerable effect on the activity of the free form of the enzyme, where the similar activity of glucose oxidase for its free and immobilized forms was obtained in the literature with 100 mM potassium

phosphate buffer [83]. The experiments with the free form of glucose oxidase were carried out in further investigations of this study. Therefore, the buffer concentration was increased to 100 mM, and the activity yield of ReliZymeTM HFA 403 M grade carrier was measured as 51.9 ± 0.6% at this buffer concentration, as shown in Table 4.

Table 4. Effect of pH and immobilization volume on the activity yield.

Buffer type	Activity yield [%]	Immobilization volume [mL]
100 mM of potassium phosphate buffer at pH 7.0	51.9 ± 0.6	1.4[a]
10 mM of sodium acetate buffer at pH 5.3	> 99	1.4[a]
10 mM of sodium acetate buffer at pH 5.3	> 98	90[b]

[a]0.07 g carriers, initial glucose oxidase concentration 100 µg mL^{-1}, 20 rpm, 4 ± 1°C, 10 mM sodium acetate buffer pH = 5.3, volume of immobilization: 1.4 mL, 20 h, experiments were performed in duplicate.

[b]8.2 g carriers, initial glucose oxidase concentration 97.9 µg mL^{-1}, 300 rpm, 4 ± 1°C, 10 mM sodium acetate buffer pH = 5.3, volume of immobilization: 90 mL, 22 h, experiments were performed in triplicate.

An activity yield of 51.9 ± 0.6% was achieved with 100 mM of potassium phosphate buffer at pH 7.0 and further investigation was required to improve the activity yield. The ReliZyme^{TM} HFA 403 M grade carrier interacts with the amino group of the enzyme and irreversible covalent bonding occurs between the oxyrane (epoxy) group of the carrier and the amino group of the enzyme as shown in Figure 3 without the need for a prior activation step with a functional agent such as glutaraldehyde [53]. During this interaction, the pH of the immobilization solution is a key factor as it affects the charge of the proteins in solution. As reported by B. Saha [96], at pH above the isoelectric point of the protein, where the net charge of a protein is zero, the protein is deprotonated and becomes negatively charged. The isoelectric point of glucose oxidase is reported as 4.2 and the highest activity yield was obtained at pH 5.5 for the immobilized glucose oxidase, which was adjusted with sodium acetate buffer [83]. The enzyme glucose oxidase is deprotonated at pH 5.3, which could increase the interaction between the carriers and the protein, resulting in immobilization of all defined amounts of enzyme on the carriers, depending on the available carrier surface area. Over 98% of the activity yield was achieved with 10 mM sodium acetate buffer at pH 5.3, indicating that almost all the enzymes incubated with ReliZyme^{TM} HFA 403 M grade supports were immobilized.

For the investigations with fine bubbles, the salt concentration of the buffer influences the electrostatic interaction, resulting in the formation of less stable bubbles [97]. The bubble exit diameter from the porous sparger is indirectly proportional to the electrolyte concentration [98]. To minimize the bubble exit diameter from the porous sparger, the concentration of the sodium acetate buffer was adjusted to 10 mM according to the previous study [68]. Furthermore, to operate the biocatalytic reactions at the highest glucose oxidase activity, both in free and immobilized form, a reaction at 35°C with 10 mM sodium acetate buffer was sufficient to maintain the optimal pH of 5.5 [63,83].

4.2.2. Enzyme loading capacity on carriers

ReliZyme™ HFA 403 carriers were incubated with five different concentrated glucose oxidase solutions (Table 5) to determine the highest achievable enzyme loading on the carriers and to utilize the available carrier surface area for glucose oxidase immobilization.

Table 5. Enzyme loadings corresponding to the measured initial activity.

Immobilization solution				
1	**2**	**3**	**4**	**5**
Enzyme loadings [mg_{GOx} $g_{carrier}^{-1}$]				
1.67	3.35	6.71	12.7	25.5
Initial activity [U $mg_{carrier}^{-1}$]				
0.08 ± 0.01	0.15 ± 0.02	0.34 ± 0.05	0.40 ± 0.02	1.11 ± 0.16

As summarised in Table 5, the measured initial activity prior to immobilization increased with increasing enzyme concentration. The initial glucose oxidase-specific activity for the enzyme glucose oxidase was measured by the method of initial rate as shown on the x-axis of Figure 20. The y-axis (left) of Figure 20 represents the activity measured after the end of immobilization. The y-axis (right) represents the activity yield, which was calculated for each enzyme concentration using Equation 20.

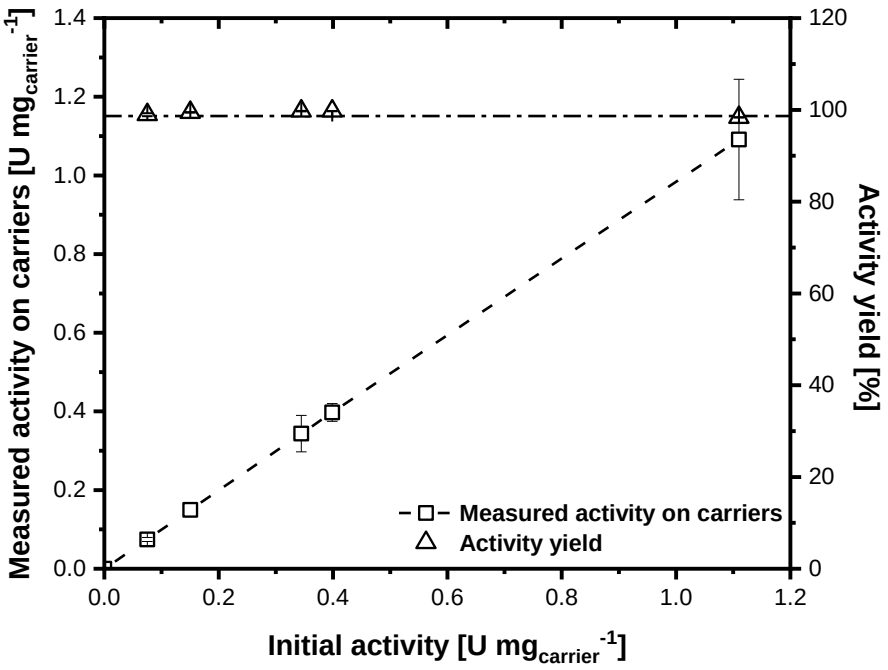

Figure 20. Investigation of the maximum achievable activity yield. Measured activity on ReliZyme™ HFA 403 M grade carriers (square) and the activity yield for each data point (triangle). 0.07 g carriers, 20 rpm, 4 ± 1°C, 10 mM sodium acetate buffer pH 5.3, volume of immobilization: 1.4 mL. Carriers were incubated for 20 h.

At data points in Figure 20, where the activity yield is greater than 98%, the saturation capacity of the carriers was not reached even at an enzyme loading of

25.5 $mg_{GOx}\ g_{carrier}^{-1}$. This finding agrees with L. Hilterhaus [94] that the saturation point for Sepabeads® EC carriers is above 100 $mg_{enzyme}\ g_{carrier}^{-1}$ (i.e., Cal B and endoglucanase, Table 6). Table 6 gives an overview of the glucose oxidase immobilization with three different enzyme loadings on carriers. The enzyme loadings 1.07 $mg_{GOx}\ g_{carrier}^{-1}$ and 7.52 $mg_{GOx}\ g_{carrier}^{-1}$ were used to determine the influence of enzyme concentration on the glucose oxidase-specific activity measured with a rotating packed bed reactor and 25 $mg_{GOx}\ g_{carrier}^{-1}$ was used for the literature comparison with L. Hilterhaus [94].

Table 6. Overview of glucose oxidase (GOx) immobilization on the carriers ReliZyme™ with two different enzyme loadings and literature comparison.

Carrier type	GOx in the supernatant [$\mu g_{GOx}\ mL^{-1}$]	Validation batch			Activity yield [%]	Initial activity [$U\ mg_{carrier}^{-1}$]	Applied enzyme loading on carriers [$mg_{GOx}\ g_{carrier}^{-1}$]
			Prior to immobilization [$U\ mL^{-1}$]	After immobilization [$U\ mL^{-1}$]			
ReliZyme™ HFA 403/GOx	98[a]	1	3.0 ± 0.1	0.04 ± 0.01	> 98	0.04 ± 0	1.07
		2	3.5 ± 0.1	0.02 ± 0	> 99		
		3	3.7 ± 0.1	0.01 ± 0			
	685[a]	1	33.7 ± 0.9	0.03 ± 0.01	> 99	0.34 ± 0.03	7.52
		2	29.9 ± 1.2	0.06 ± 0.01			
		3	28.7 ± 4	0.06 ± 0.01			
	1272[b]	1	62.2 ± 4.9	1.08 ± 0.76	> 98	1.11 ± 0.16	25.5
		2	48.8 ± 0.9	0.83 ± 0.01			
Sepabeads EC/CALB [94]	-	-			100	-	20
	69000				85		139
Sepabeads EC/endo-glucanase [94]	2400				94		20

[a]8.2 g carriers, 300 rpm, 4 ± 1°C, 10 mM sodium acetate buffer pH = 5.3, volume of immobilization: 90 mL, 22 h, experiments were performed in triplicate. 0.28 ± 0.06 mg mL^{-1} antifoam 204 was used for the enzyme loading of 7.52 $mg_{GOx}\ g_{carrier}^{-1}$.

[b]0.07 g carriers, 20 rpm, 4 ± 1°C, 10 mM sodium acetate buffer pH = 5.3, volume of immobilization: 1.4 mL, 20 h, experiments were performed in duplicate.

With the initial rate measurements (Table 6) prior to the biocatalytic oxidation in a rotating packed bed reactor, over 98% of the immobilization activity yield was measured for all enzyme loadings, as the residual activity in the supernatant after 22 h was less than 0.07 U mL^{-1} and the activity of glucose oxidase in the washing solutions for each applied enzyme loading on carriers (1.07 $mg_{GOx}\ g_{carrier}^{-1}$ and 7.52 $mg_{GOx}\ g_{carrier}^{-1}$) was determined as 0.018 ± 0.003 U mL^{-1} and 0.04 ± 0.02 U mL^{-1}, respectively). There was no significant enzyme leaching after each washing process. No washing procedure was performed for 25 $mg_{GOx}\ g_{carrier}^{-1}$ enzyme loading. Triplicates

were used for all assays and sample measurements. Due to the high enzyme concentration required, the experiment to determine the enzyme loading of 25.5 mg_{GOx} $g_{carrier}^{-1}$ was carried out in duplicate. According to the findings of L. Hilterhaus [94], where 85% of the bound enzyme was reported at the enzyme loading of 139 mg_{enzyme} $g_{carrier}^{-1}$, an increased glucose oxidase loading on carriers could be applied on ReliZyme™ HFA 403 carriers, however, during the biocatalytic oxidation in a SpinChem® vessel with a rotating packed bed basket, no enzyme loading higher than 7.52 mg_{GOx} $g_{carrier}^{-1}$ was used to investigate the effect of the enzyme concentration on the reaction rate. A detailed explanation is given in section 4.4.3.

4.3. Generation of fine bubbles in a modified SpinChem® vessel

The mass transfer performance of sintered frit spargers (porosities of 0.5 µm, 5 µm and 10 µm) as well as Shirasu Porous Glass (SPG) membrane sparger were compared by B. Thomas [68] with the bubbles generated by the AMB3 fine bubble generator in a stirred tank reactor in the same designed liquid medium as used in this study (10 mM sodium acetate buffer at pH 5.3). It could be shown that the measured volumetric mass transfer coefficient $k_L a$ of nanobubbles generated with an AMB3 fine bubble generator is similar to the parameter $k_L a$ obtained with 0.5 µm and 2 µm sintered frit metal porous sparger and 1 µm membrane sparger under identical measurement conditions [68].

To generate fine bubbles in the SpinChem® vessel V2 with the rotating packed bed basket S2, an AMB3 fine bubble generator was integrated into the setup of a SpinChem® vessel V2 with the rotating packed bed basket S2, as illustrated in the reactor set-up 1. Generating a high number of fine bubbles resulted in a milky appearance when compared with macrobubble aeration by an open tube sparger with a 2 mm orifice diameter (Figure 21).

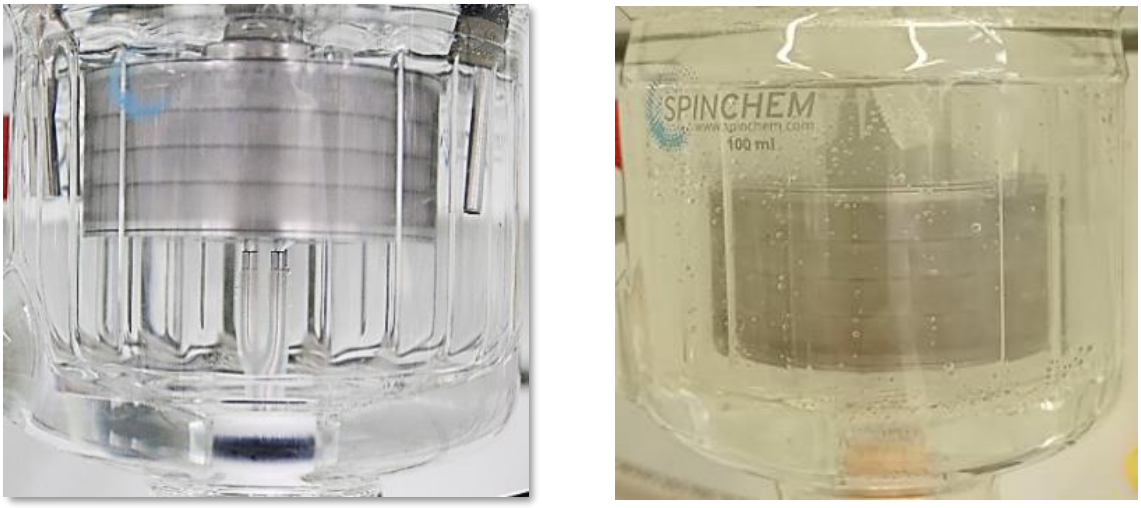

Figure 21. The SpinChem® vessel V2 equipped with two different aerators. Aeration by the open tube sparger (orifice diameter: 2 mm) with macrobubbles (left), milky with fine bubbles generated (right) by the AMB3 fine bubble generator.

The time-resolved oxygen concentration profile (Figure 22) was measured with an AMB3 fine bubble generator, whose operational principle is described in section 2.2. The time-resolved oxygen concentration profile reveals an increase in oxygen saturation concentration (in air) from 21% measured with an open tube (orifice diameter: 2 mm) to 30% measured with an AMB3 fine bubble generator, however further investigation is required to confirm the results.

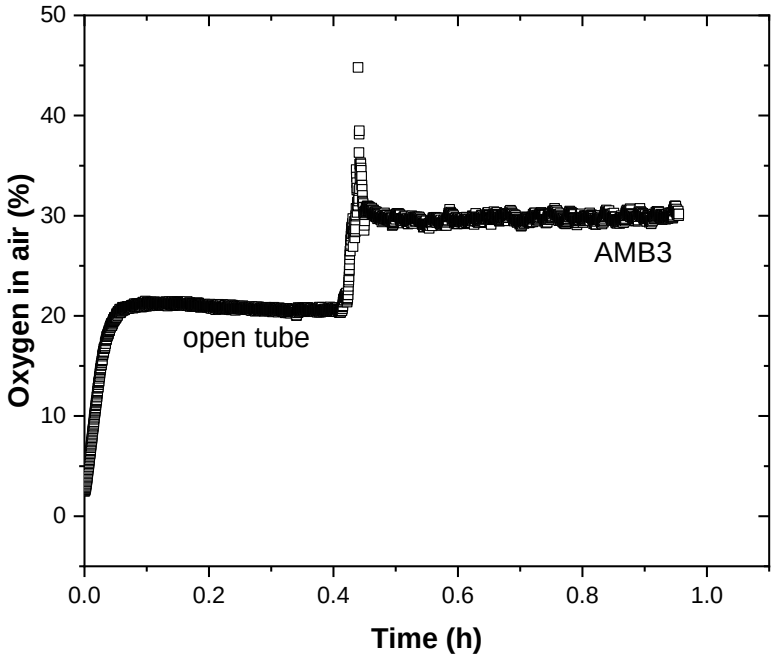

Figure 22. Dynamic measurement of the time-resolved concentration profile. An open tube (orifice diameter: 2 mm) and AMB3 fine bubble generator were implemented in the SpinChem® vessel V2 with the empty rotating bed basket S2. 500 rpm, 35 ± 3°C, 400 mL, deionized water. The internal pressure in the mixing chamber is 0.2-0.4 mPa.

4.3.1. Mass transfer performance

An alternative fine bubble generation was enabled with the 2 µm sintered frit porous sparger, which has a non-complex design and is easy to implement compared to the AMB3 nanobubble generator system. In addition, sintered frit spargers are currently available on the market with different pore sizes. The microbubbles that are of interest in this study are generated by the integration of a 2 µm sintered frit porous sparger into the modified SpinChem® vessel V2 with a rotating packed bed basket S2 (Figure 23). The SpinChem® vessel V2 is baffled to improve the mixing of the reaction medium.

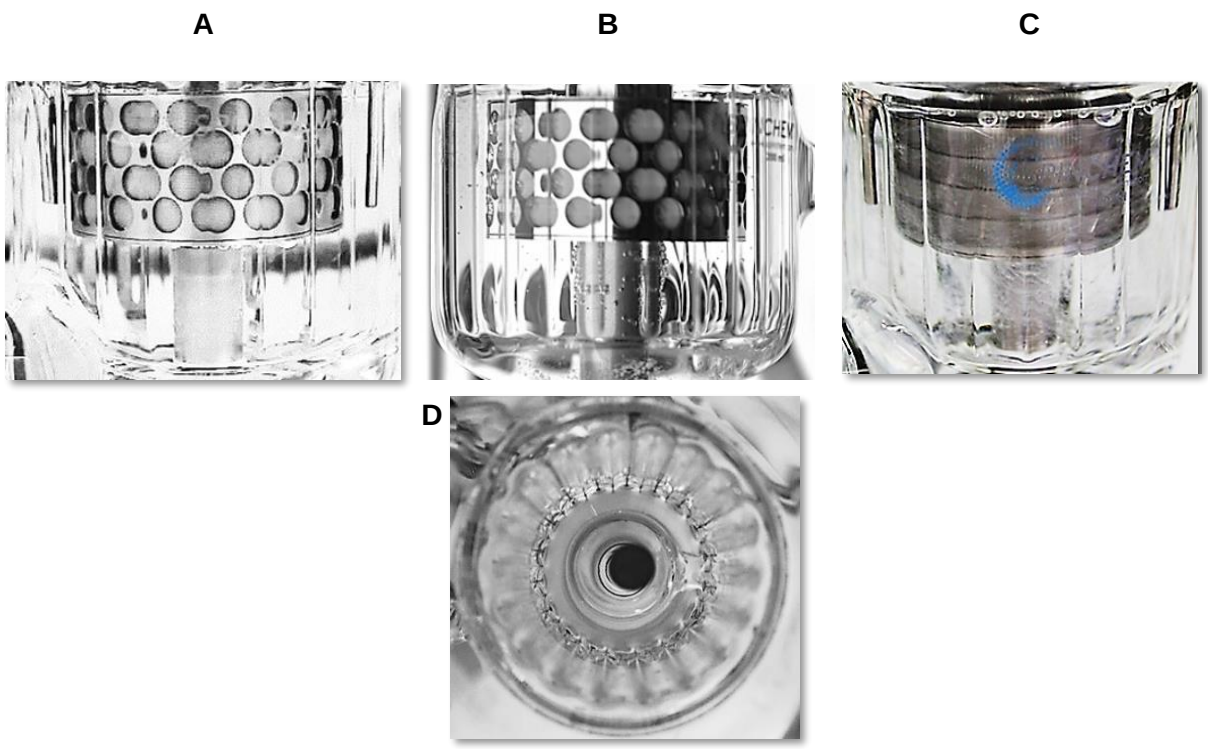

Figure 23. Sintered frit porous spargers in the SpinChem® vessel V2. A) 2 µm sintered frit implemented into the SpinChem® vessel V2 without air flow and rotation. B) Start of air flow without rotation of the rotating packed bed reactor (10 µm sintered frit, source: Lotta Kursula). C) The microbubbles are dispersed in the liquid with air flow and rotation of the rotating packed bed reactor (2 µm sintered frit, right). D) The inner structure of the baffled vessel.

The mass transfer performance was characterized by the volumetric mass transfer coefficient $k_L a$ (Equation 15) for an open tube (macrobubbles) and the 2 µm sintered frit applying the dynamic measurement method [78,79] with compressed air and nitrogen as stripping gas. During the dynamic measurement of the time-resolved oxygen concentration profile, nitrogen was used to degas the oxygen from the reaction medium, where a decrease in the percentage of oxygen was observed. Subsequently, the nitrogen gas was turned off and oxygen was supplied as compressed air by a 2 µm sintered frit sparger. An increase in the dynamic measurement of the time-resolved oxygen concentration profile was monitored. This step was performed five times as shown in Figure 24. To evaluate the liquid-side volumetric mass transfer coefficient ($k_L a$), a data range of 20% to 80% of the O_2 saturation profile was selected.

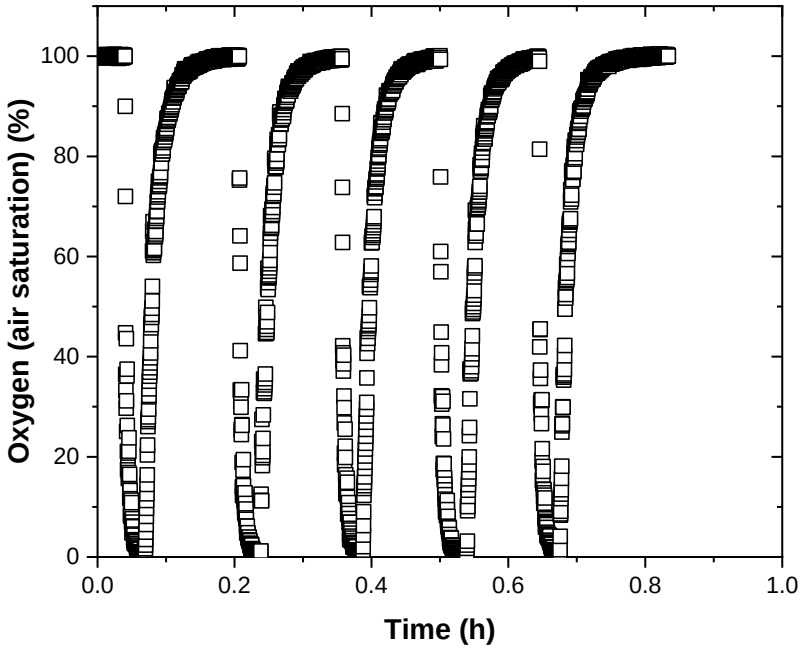

Figure 24. Dynamic measurement of the time-resolved concentration profile: 2 µm sintered frit sparger. 8.2 g carriers without biocatalyst, 1000 rpm, 35 ± 1°C, 200 mL, 1 vvm, 10 mM sodium acetate buffer at pH 5.3.

Many studies typically report process parameters as a function of stirring rate [99-101] for mechanically agitated reactors. For efficient mixing in the turbulent flow regime, it is necessary to define the Reynolds number Equation 21 [102,103]. To calculate the impeller Reynolds number, the density (994 kg m^{-3}) and dynamic viscosity (0.720 mPa s) of water are used due to the negligible difference in density and dynamic viscosity for 10 mM sodium acetate buffer.

$$Re_{\text{impeller}} = \rho \cdot N \cdot D^2 \cdot \mu^{-1} \qquad (21)$$

where ρ in kg m^{-3} is the density of the liquid, N in s^{-1} is the rotational rate, D in m is the diameter of the rotating packed bed basket, and μ in Pa s is the dynamic viscosity.

The impeller Reynolds number was chosen for the SpinChem® rotating bed basket S221 (diameter 45.5 mm) used as an impeller for mixing in the single-phase liquid reaction medium in the investigations by H. K. Larsson [104]. Further investigation is necessary to characterize the Reynolds number of the rotating bed basket for biphasic flow [105], since the formulation of the Reynolds number depends on physical parameters [104], including the design of the rotating bed basket and the viscosity as well as density of the continuous phase. Turbulent flow is typically used for efficient mass transfer performance and to minimize inhomogeneities. To ensure efficient mixing in the SpinChem® vessel using the rotating bed basket as the impeller, the impeller Reynolds number for a rotating packed bed reactor with macrobubble aeration (open tube with a 2 mm orifice diameter) under two stirring rates (500 rpm, Re_{impeller} = 2.3x10^5 and 1000 rpm, Re_{impeller} = 4.7x10^5) was calculated using Equation 21, which ensures a fully turbulent regime according to H. K. Larsson [104].

The mass transfer performance was first measured under macrobubble aeration at two stirring rates 500 rpm and 1000 rpm. As described by D. Wenzel [106] for liquid-liquid extraction in a rotating bed reactor, the concentration boundary layer becomes thinner with increasing stirring rate. Other studies carried out with rotating bed reactors in various configurations have reported an increasing trend in the volumetric mass transfer coefficient with increasing stirring rate [107,108]. Applying the same principle to the gas-liquid system, the higher the stirring rate, the higher the rate of mass transfer of the gas molecules into the bulk medium should be. The measurements with macrobubble aeration confirm this principle as shown in Figure 25.

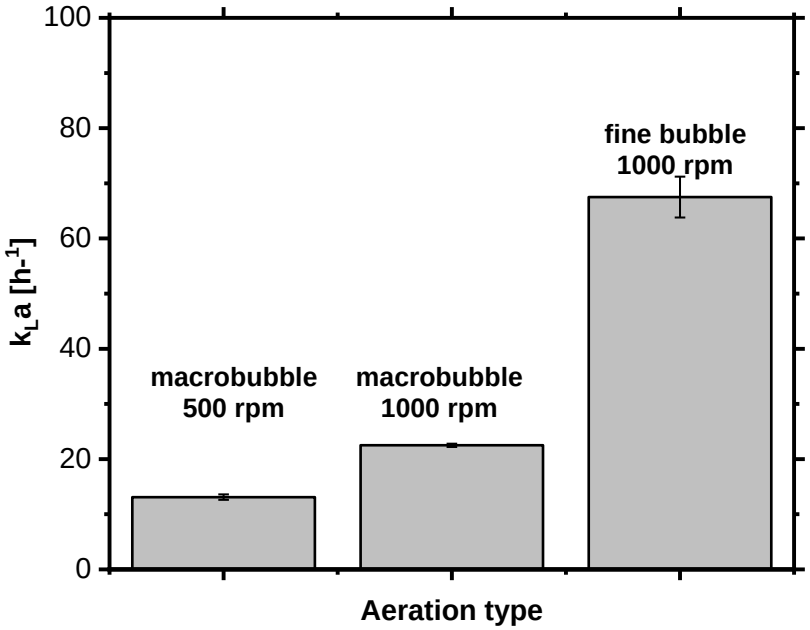

Figure 25. Influence of stirring rate and aerator type on the mass transfer performance. An open tube (orifice diameter: 2 mm) and a 2 µm sintered frit have been integrated under the rotating packed bed basket S2, where macro and fine bubbles are generated. 35 ± 1°C, 1000 rpm, 8.2 g carriers without biocatalyst, 200 mL, 1 vvm, 10 mM sodium acetate buffer at pH 5.3, error bars show the standard deviation obtained from five measurements.

The volumetric mass transfer coefficient k_La under macrobubble aeration was doubled, as shown in Figure 25, by increasing the stirring rate from 500 rpm (13.1 ± 0.5 h^{-1}) to 1000 rpm (22.5 ± 0.3 h^{-1}). The volumetric mass transfer coefficient k_La = 67.3 ± 3.7 h^{-1} obtained with the 2 µm sintered frit was tripled compared to macrobubble aeration k_La = 22.5 ± 0.3 h^{-1} under identical measurement conditions at 1000 rpm and 1 vvm. This improvement is due to the increased interfacial area available for efficient mass transfer of molecular oxygen through the reaction medium at the identical volume-specific aeration rate, which has been demonstrated in previous studies [61-63].

The effect of the position of the sintered frit sparger 2 µm in the SpinChem® vessel V2 on the volumetric mass transfer coefficient k_La was investigated. In position 1, the sintered frit sparger 2 µm was placed under the rotating packed bed reactor. In position 2, the position of the 2 µm sintered frit sparger was raised and placed inside the rotating bed packed reactor (Figure 26).

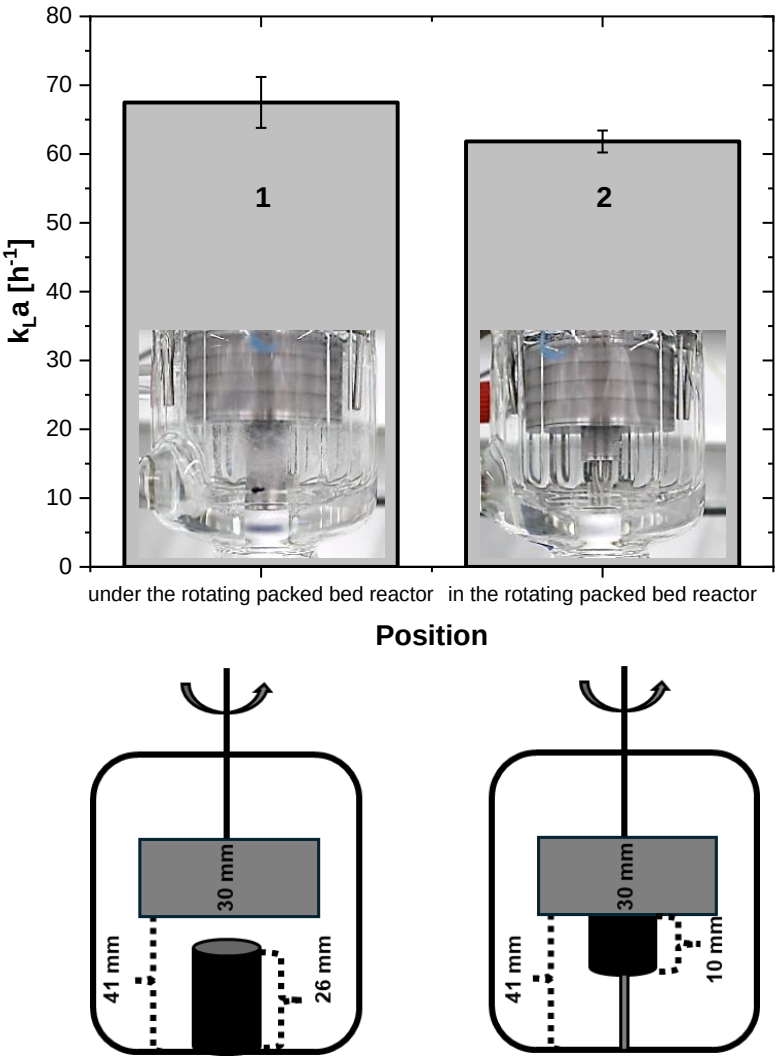

Figure 26. Influence of the position of the aerator on the mass transfer performance: 2 µm sintered frit in the SpinChem® vessel V2. 8.2 g carriers without biocatalyst, 1000 rpm, 35 ± 1°C, 200 mL, 1 vvm, 10 mM sodium acetate buffer at pH 5.3, error bars show the standard deviation obtained from five measurements.

The mass transfer performance for the rotating packed bed reactor was measured for each condition, where the parameter k_La was determined to be 67.5 ± 3.7 h^{-1} for the position 1 and 61.8 ± 1.6 h^{-1} for the position 2. To ascertain the effect of the position of the 2 µm sintered frit sparger, a larger distance between the rotating packed bed basket and the 2 µm sintered frit would be required, which is not technically possible for this SpinChem® vessel V2. Consequently, the subsequent experiments were performed utilizing the 2 µm sintered frit in position 1.

Investigation of the influence of the aeration rate on the mass transfer performance for both types of aeration is critical in this study to establish similar reaction rates for biocatalytic oxidation as described in section 4.5. To determine the similar mass volumetric transfer coefficient k_La achieved for both types of aeration, the effect of the aeration rate in the range of 0.125 - 1 vvm on the parameter k_La values for fine bubble aeration were determined and compared with the macrobubble aeration in the following section.

4.3.2. Aeration rate: Comparison of macrobubble and fine bubble aeration

According to A. T. Pedersen [30], the stirring rate of 1000 rpm, which created the turbulent conditions with efficient mixing as shown at the beginning of the section 4.3, was chosen to investigate the effect of volume specific-aeration rate (Equation 22) for both macrobubble and fine bubble aeration.

$$vvm = \frac{\dot{v}_{\mathrm{air}}}{V_{\mathrm{L}}} \qquad (22)$$

where vvm is the volume-specific aeration rate as the ratio of the air flow rate $\dot{v}_{\mathrm{air}}$ in mL min^{-1} to the volume of the liquid volume V_{L} in mL.

To determine the liquid-side volumetric mass transfer coefficient $k_{\mathrm{L}}a$ for each measurement condition, the dynamic measurement of the time-resolved concentration curve was plotted in Figure 27A. The $k_{\mathrm{L}}a$ values were determined using the data from the dynamic measurement of the time-resolved concentration curve and calculated with Equation 15 as shown in Figure 27B.

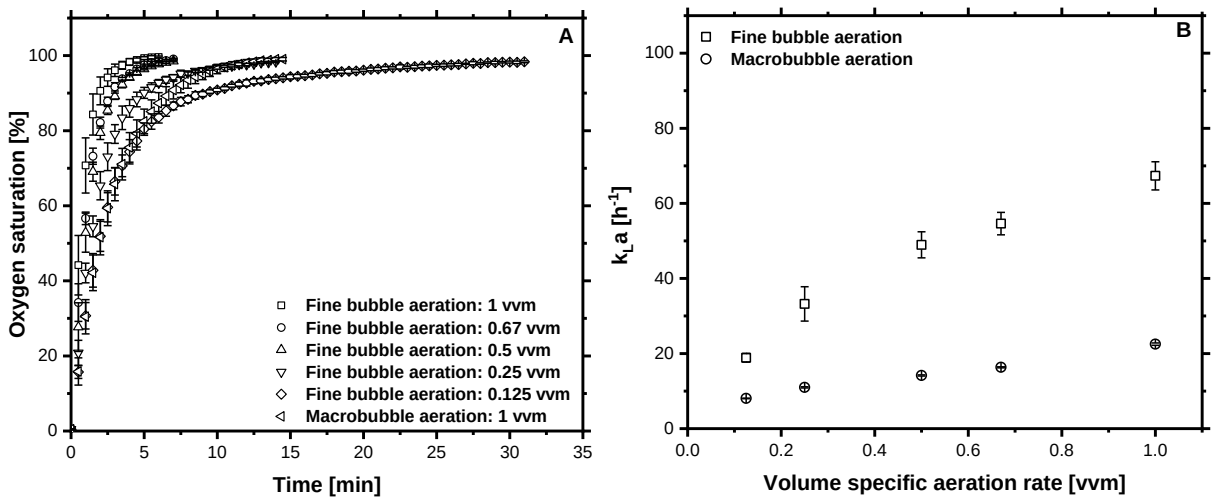

Figure 27. Comparison of mass transfer performances: Fine bubble aeration with 2 µm sintered frit and macrobubble aeration with open tube (orifice diameter: 2 mm). A) The dynamic measurement of the time-resolved concentration curve. B) Comparison of the volumetric mass transfer coefficients $k_{\mathrm{L}}a$ for macrobubble and fine bubble aeration. 8.2 g carriers without biocatalyst, 1000 rpm, 200 mL, 1 vvm, 35 ± 1°C, 10 mM sodium acetate buffer at pH 5.3, error bars show the standard deviation obtained from five measurements.

The $k_{\mathrm{L}}a$ was dependent on the aeration rate and increased with increasing the volume-specific aeration rate, as observed in other studies. [24, 63,109-111]. The dynamic measurement of the time-resolved concentration curve shows the same saturation point for all measurements.

Conclusion

- the higher the stirring rate, the higher the mass transfer rate
- the smaller the bubbles, the higher the mass transfer rate and the enhanced local oxygen concentration, however, no oversaturation was achieved with fine bubbles generated with the 2 µm sintered frit sparger
- the higher the aeration rates, the higher the mass transfer rate for each aerator
- the comparable volumetric mass transfer coefficient was observed for macrobubble aeration $k_L a$ = 22.5 ± 0.3 h^{-1} at 1 vvm and fine bubble aeration $k_L a$ = 18.9 ± 1.2 h^{-1} at 0.125 vvm.

4.4. Biocatalyst performance in a rotating packed bed reactor

The performance of immobilized glucose oxidase was measured by evaluating the productivity for glucose oxidase and the product concentration as the performance metrics [112]. These parameters depend on the operational process parameters, the selectivity [113] as well as the activity of the enzyme glucose oxidase, and whether it is applied in free or immobilized form [114]. The solubility of the substrate is a crucial factor in the increase of glucose oxidase-specific activity, as a greater amount of substrate allows the enzyme glucose oxidase to become more saturated with it [115]. The performance of oxidases is in principle proportional to:

- the available oxygen concentration in the reaction medium
- in-depth understanding of optimal operating conditions
- immobilized enzyme stability

In the previous section, the improvement in local oxygen concentration was described by mass transfer measurements using fine bubble aeration without the utilization of glucose oxidase. The following section focuses on the:

- mass transfer limitation observed under macrobubble aeration for different substrate (glucose) concentrations
- effect of fine bubble aeration on the enhanced performance of immobilized glucose oxidase
- investigation of process parameters (enzyme loading and substrate concentration) for efficient use of a rotating packed bed reactor
- improvement in gas utilization through fine bubble aeration
- biocatalyst stability in a rotating packed bed basket
- approaches to overcome internal diffusion limitations with kinetic parameter estimation
- reaction rate modeling with comparison to experimental results

4.4.1. Investigation of mass transfer limitation

To investigate the mass transfer limitation on the performance of immobilized glucose oxidase, it is necessary to saturate the enzyme with its substrate. For this purpose, the

substrate concentration is maintained at a level exceeding its characteristic constant [114], namely the affinity constant as the Michaelis-Menten constant K_m, which represents the substrate concentration at which half of the maximum reaction is achieved [116].

The model reaction shown in section 1.3 (Scheme 1) uses two substrates (glucose and oxygen), whose concentrations in the bulk medium affect the glucose oxidase-specific activity. The first substrate, glucose, has a solubility of 57.3 g glucose per 100 g water at 1 atm and 35°C (corresponding to 3.2 M at 1 atm and 35°C and 2.8 M at 1 atm and 25°C as calculated from Figure 28). However, the solubility of oxygen is reported to be 0.254 mM at 1 atm and 25°C in water [21], which is considerably lower than the solubility of glucose. Thus, the insufficient oxygen solubility limits the performance of glucose oxidase.

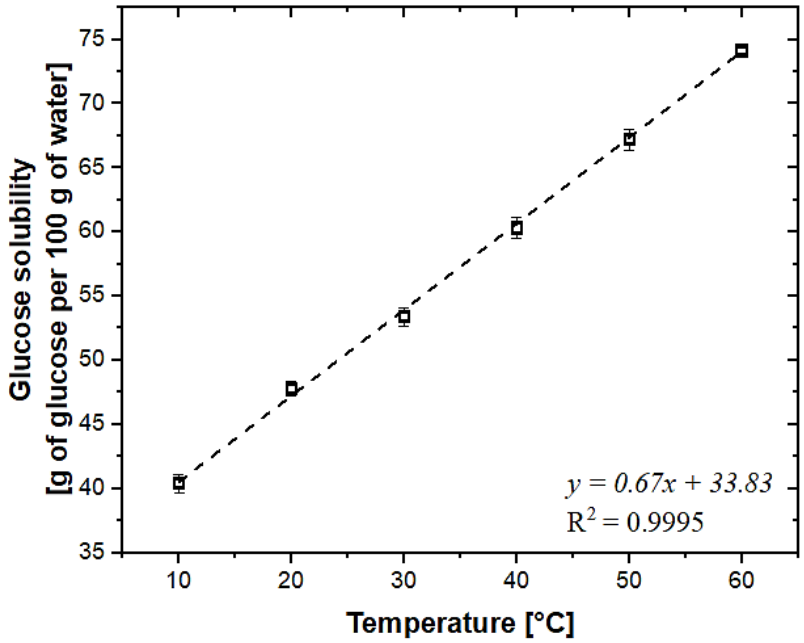

Figure 28. Solubility of glucose in water as a function of temperature at 1 atm. The graph was plotted using the solubility data from the literature [117].

The rate of mass transfer of molecular oxygen through the reaction medium is thus a crucial parameter, since the glucose oxidase-specific activity depends on the availability of dissolved oxygen in the reaction medium as shown in the reaction rate equation (Equation 12). The amount of oxygen available in the reaction medium is based on the oxygen mass transfer rate, which is characterized by the volumetric mass transfer coefficient $k_L a$. Higher volume-specific aeration rates resulted in a reduced saturation time for oxygen and an increased volumetric mass transfer coefficient $k_L a$ values as previously demonstrated in Figure 27.

The volume-specific aeration rate was chosen to be 1 vvm according to T. Pedersen [30] and the experiment was performed under macrobubble aeration, where the reaction rate was measured as 24.2 ± 0.6 µmol min^{-1}. Subsequently, the enzyme loading and substrate concentration were increased by a factor of 12 and 7,

respectively, to avoid the limitations of insufficient substrate or enzyme concentration (Table 7).

Table 7. Overview of the effect of the aeration rate, enzyme loading and substrate concentration on the reaction rate under macrobubble aeration. 8.2 g carriers, 35 ± 1°C, 1000 rpm, initial volume 200 mL, 1 vvm, pH 5.5 ± 0.2. Glucose solutions were prepared in 10 mM sodium acetate buffer at pH 5.3.

Aeration rate [vvm]	Enzyme loading [$mg_{GOx}\ g_{carrier}^{-1}$]	Glucose [mM]	Reaction rate (measured) [µmol min^{-1}]
Macrobubble aeration with open tube (orifice diameter: 2 mm)			
1	1.07	25	24.2 ± 0.6[a] R^2 = 0.9962
	7.52	300[c]	33.8 ± 5.4[b] R^2 = 0.9999
	7.52	600	28.5 ± 2.4[b] R^2 = 0.9999

a. Calculated activity of catalase (free) / calculated activity of glucose oxidase (immobilized):1.38. The experiment was performed in duplicate. Error bars show the standard deviation obtained from duplicate measurements.
b. Calculated activity of catalase (free) / calculated activity of glucose oxidase (immobilized):1.70. The experiment was performed in duplicate. Error bars show the standard deviation obtained from duplicate measurements. 0.28 ± 0.06 mg mL^{-1} antifoam 204 was used for the enzyme loading of 7.52 $mg_{GOx}\ g_{carrier}^{-1}$.
c. The data points for 300 mM are evaluated including the data point from the supervised B.Sc. thesis [118].

A 1.2-fold of increase in the reaction rate (24.2 ± 0.6 µmol min^{-1} to 33.8 ± 5.4 µmol min^{-1}) was observed. At the identical aeration rate and enzyme loading, when the substrate concentration was doubled from 300 mM to 600 mM, similar reaction rates were measured, within the range of variation. Table 7 shows that no significant enhancement in the reaction rate values under macrobubble aeration was obtained when substrate concentration, aeration rate, and enzyme concentrations were increased in subsequent experiments. To explain this observation of no enhancement in the reaction rate, the oxygen saturation of the molecular oxygen during the course of the reaction was measured inline under macrobubble aeration at the substrate concentration of 25 mM and compared with the oxygen saturation profile during the course of the reaction at the substrate concentration of 300 mM (Figure 29).

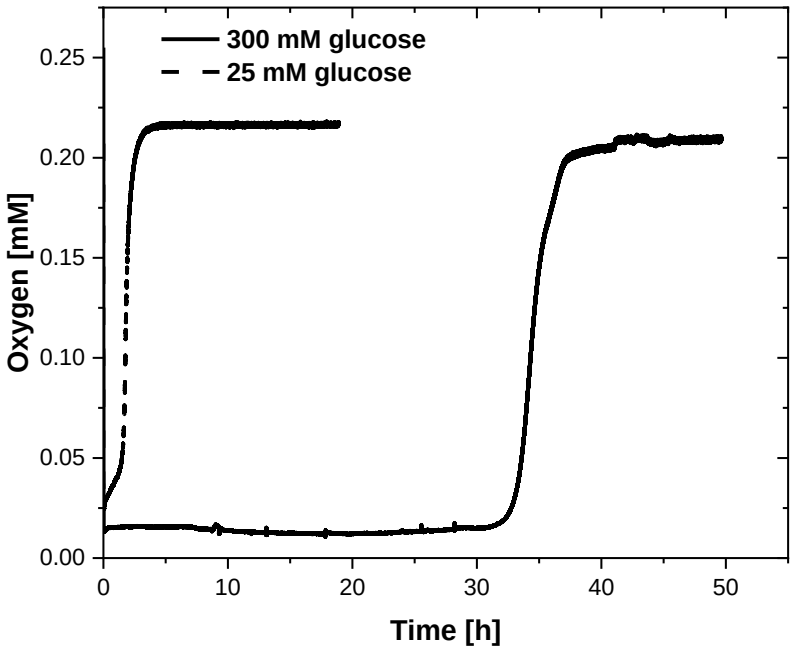

Figure 29. Effect of dissolved substrate (glucose) on the measured oxygen concentration in the bulk liquid medium. Macrobubble aeration (open tube: orifice diameter: 2 mm - dash line: 25 mM glucose, line: 300 mM glucose). The measurement conditions are detailed in Table 7.

In Figure 29, the oxygen concentration per time dropped at the beginning of the reaction for both substrate glucose concentrations (25 mM and 300 mM), when the reaction was started. For the glucose concentration of 25 mM, the oxygen concentration reached its lowest value of 0.025 mM at 0.055 h, instantly started to increase again during the reaction, and nearly reached the saturation point before the end of the reaction. This measurement implies that the oxygen transfer rate was higher than the reaction rate under the given experimental conditions and no strong mass transfer limitation was observed during the reaction. A logarithmic increase in the yield curve was observed instead of a linear increase (Figure 30, square), which is another indication that the reaction rate is not limited by oxygen mass transfer. When the substrate glucose concentration was increased to 300 mM, the oxygen level decreased at the beginning of the reaction, however, it did not reach the saturation point during the course of the reaction.

The reaction at 300 mM glucose concentration was strongly limited by oxygen mass transfer, since the concentration of oxygen stays at 0.016 mM for 31 h during the reaction (Figure 29, line) and was far below its saturation concentration under continuous oxygen supply. It started to increase again at the 31st h and reached the saturation level at the end of the reaction. At the 31st h, the yield value was measured as 96.6% and the final yield value was measured as 97.2%, confirming that the reaction (Figure 30, circle) was almost complete.

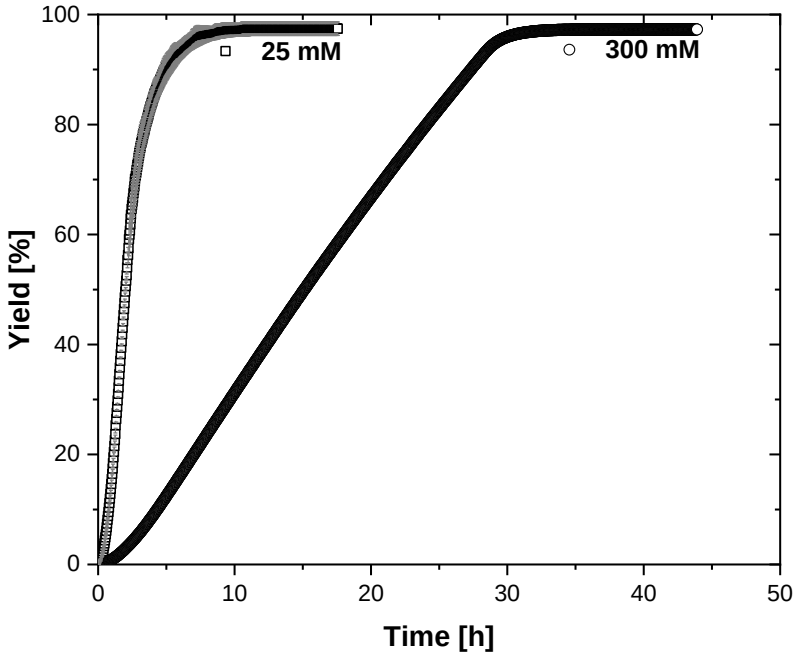

Figure 30. Oxidation of substrate glucose under macrobubble aeration (open tube with an orifice diameter of 2 mm). 8.2 g carriers, 1000 rpm, 35 ± 1°C, initial volume 200 mL, pH 5.5 ± 0.2, 1 vvm. Glucose solutions were prepared in 10 mM sodium acetate buffer at pH 5.3. Squares: 25 mM glucose, enzyme loading on carriers: 1.07 mg_{Gox} $g_{carrier}^{-1}$, catalase (free) / calculated activity of glucose oxidase (immobilized):1.38, and circles: 300 mM glucose, enzyme loading on carriers: 7.52 mg_{Gox} $g_{carrier}^{-1}$, antifoam 204: 0.28 ± 0.06 mg mL^{-1}, catalase (free) / calculated activity of glucose oxidase (immobilized):1.70. The data at 300 mM were included from the supervised B.Sc. thesis [118].

The reaction rate for the substrate glucose concentration of 300 mM was linearly dependent on only one reactant concentration, the available oxygen concentration in the reaction medium, resulting in a linear increase in the progress curve rather than a logarithmic increase (Figure 30, square). The reason for observing a lag phase at the beginning of progress curves (up to 1 h) is explained in section 4.8.

To understand the relationship between the substrate concentration and the oxygen consumption rate, the fundamental knowledge of oxygen transfer through the bulk medium via the two-film model is considered with the oxygen demand of the enzyme glucose oxidase as described in section 2.3 (Figure 7). As the reaction rate, i.e. the oxygen consumption rate, increases at high glucose concentrations, less oxygen is available in the bulk medium per time due to the higher oxygen consumption rate of the enzyme glucose oxidase, which was observed in Figure 29. Using the same principle, but with the opposite effect, increasing the oxygen mass transfer rate at the identical substrate concentration will bring the measured oxygen concentration closer to the saturation point, thus contributing to overcoming the mass transfer limitation.

4.4.2. Overcoming the mass transfer limitation by fine bubble aeration

The advantage of fine bubble aeration is that it increases the surface-to-volume ratio at the same volume-specific aeration rate, providing a higher overall mass transfer rate of oxygen molecules in the same given liquid volume compared to macrobubble aeration. The volumetric mass transfer rate was tripled by fine bubble aeration $k_L a$ = 67.3 ± 3.7 h^{-1} when compared to macrobubble aeration $k_L a$ = 22.5 ± 0.3 h^{-1} at the equal volume-specific aeration rate (as described in Figure 27). Using this advantage, the measured oxygen concentration and the yield progression curve at the substrate glucose concentration of 300 mM under fine bubble and macrobubble aeration are compared in Figure 31 and Figure 32.

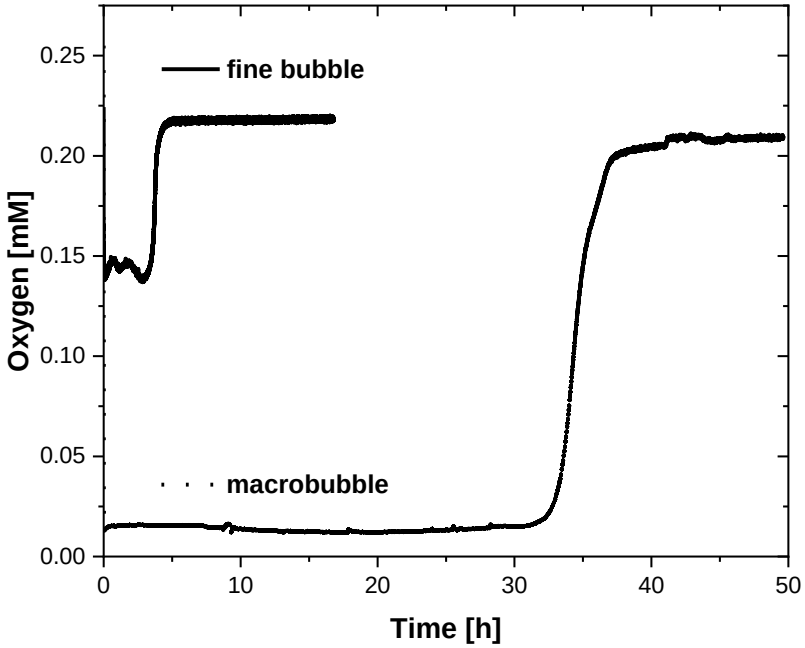

Figure 31. Effect of aeration method on the measured oxygen concentrations in the bulk liquid medium: Macrobubble aeration with open tube: orifice diameter: 2 mm, fine bubble aeration with 2 µm sintered frit. 8.2 g carriers, 1000 rpm, 35 ± 1°C, initial volume 200 mL, 1 vvm, pH 5.5 ± 0.2. Glucose solution (300 Mm) was prepared in 10 mM sodium acetate buffer at pH 5.3. enzyme loading on carriers: 7.52 mg_{GOx} $g_{carrier}^{-1}$, catalase (free) / calculated activity of glucose oxidase (immobilized):1.70, antifoam 204: 0.28 ± 0.06 mg mL^{-1}.

In Figure 31, a higher concentration of oxygen was measured at all times for fine bubble aeration compared to macrobubble aeration at the substrate concentration of 300 mM. As described in the previous section, the reaction at 300 mM substrate glucose concentration under macrobubble aeration was strongly inhibited by oxygen mass transfer. With fine bubble aeration, it was still limited by oxygen mass transfer as the measured oxygen concentration was not reaching to the saturation point during the course of the reaction Figure 31 and a linear increase in the yield progression curve was observed (Figure 32, circle).

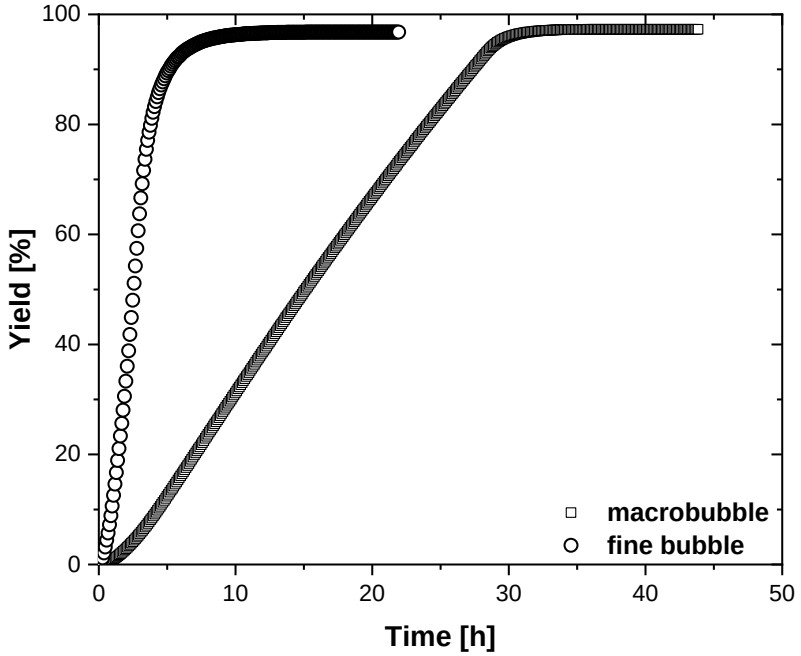

Figure 32. Effect of aeration method on the oxidation of the substrate glucose. Macrobubble aeration with open tube: orifice diameter: 2 mm, fine bubble aeration with 2 µm sintered frit. 8.2 g carriers, enzyme loading on carriers: 7.52 $mg_{GOx}\ g_{carrier}^{-1}$, catalase (free) / calculated activity of glucose oxidase (immobilized): 1.70, 35 ± 1°C, 1000 rpm, initial volume 200 mL, 1 vvm, pH 5.5 ± 0.2. Glucose solution (300 mM) in 10 mM sodium acetate buffer at pH 5.3. Antifoam 204: 0.28 ± 0.06 mg mL^{-1}. The yield data were taken from the supervised B.Sc. thesis [118].

The focus of this section was to prove that fine bubble aeration contributes to overcoming the mass transfer limitation of oxygen during the reaction. The reaction rate was significantly enhanced under fine bubble aeration (237 ± 50 µmol min^{-1}), when compared to macrobubble aeration (33.8 ± 5.4 µmol min^{-1}, Figure 32, square). The effect of process parameters (enzyme loading on carriers, substrate concentration, aeration rate, stirring rate, biocatalyst activity, and stability) on the reaction rate was investigated and discussed in detail in the following sections for the understanding of the process of biocatalytic oxidation in the rotating packed bed reactor using immobilized glucose oxidase.

4.4.3. Characterization of process parameters under fine bubble aeration

4.4.3.1. Enzyme loading on carriers

The enzyme glucose oxidase is the cost driver in this two-enzyme (glucose oxidase and catalase) reaction. In this study, two different enzyme loadings (1.07 $mg_{GOx}\ g_{carrier}^{-1}$ and 7.52 $mg_{GOx}\ g_{carrier}^{-1}$) at a substrate glucose concentration of 25 mM were investigated under identical reaction conditions with fine bubble aeration (Table 8).

Table 8. Effect of enzyme loading on the reaction rate. 8.2 g carriers, 1000 rpm, 35 ± 1°C, initial volume 200 mL, 1 vvm, pH 5.5 ± 0.2. Glucose solution 25 mM in 10 mM sodium acetate buffer at pH 5.3.

Stirring rate [rpm]	Aeration rate [vvm]	Enzyme loading [mg_{GOx} $g_{carrier}^{-1}$]	Glucose [mM]	Reaction rate (measured) [µmol min^{-1}]
Fine bubble aeration with 2 µm sintered frit				
1000	1	1.07[a]	25	38.9 ± 9.1 R^2 = 0.9997
		7.52[b]		43.7 ± 7.8 R^2 = 0.9999

a. Enzyme loading on carriers: 1.07 mg_{GOx} $g_{carrier}^{-1}$, catalase (free) / calculated activity of glucose oxidase (immobilized):1.38. The standard deviation value was obtained from triplicate measurements.

b. Enzyme loading on carriers: 7.52 mg_{GOx} $g_{carrier}^{-1}$, catalase (free) / calculated activity of glucose oxidase (immobilized):1.70, antifoam 204: 0.28 ± 0.06 mg mL^{-1}. The standard deviation value was obtained from duplicate measurements.

At 25 mM glucose concentration, the reaction rate was increased 1.12-fold even though the enzyme loading was increased 7-fold. The difference in reaction rate was not significant when compared to the increase in enzyme loading, as the reaction rate was shown to be substrate-dependent and a substrate concentration ($c_m > K_m$) is required to see a significant change in reaction rate. To determine the substrate glucose concentration required for sufficient enzyme-substrate saturation, the kinetic studies were performed and described in section 4.8.2. On the other hand, the result of the previous section indicates that 300 mM substrate concentration is sufficient to investigate the performance of immobilized glucose oxidase in a rotating packed bed reactor. For this reason, the effect of the aeration rate and stirring rate on the reaction rate was investigated at two substrate concentrations (25 mM and 300 mM) and shown in the following section.

4.4.3.2. Aeration rate, stirring rate and substrate concentration

As shown in the reaction rate equation (Equation 12), the mass transfer rate of molecular oxygen through the reaction medium is a critical parameter because the glucose oxidase-specific activity depends on the availability of dissolved oxygen in the reaction medium. By increasing the volume-specific aeration rate, a higher local oxygen concentration with a higher volumetric mass transfer rate was reached (Figure 27B).

To investigate the effect of aeration rate on the glucose oxidase-specific activity, three different volume-specific aeration rates were studied at 0.125 vvm ($k_L a$ = 18.9 ± 1.2 h^{-1}, Figure 27B), 0.75 vvm ($k_L a$ = 57.7 ± 6.8 h^{-1} calculated from Figure 27B), and 1 vvm ($k_L a$ = 67.3 ± 3.7 h^{-1} Figure 27B). The parameter $k_L a$ values were determined in 200 mL

of 10 mM sodium acetate buffer at pH 5.3 using 8.2 g carriers without glucose oxidase at 35 ± 1°C and 1000 rpm. The resulting reaction rates are listed in Table 9.

Table 9. Effect of aeration rate and substrate concentration on the reaction rate. 1000 rpm, 35 ± 1°C, 8.2 g carriers, initial volume 200 mL, 1 vvm, pH 5.5 ± 0.2. Glucose solutions were prepared in 10 mM sodium acetate buffer at pH 5.3.

Stirring rate [rpm]	Aeration rate [vvm]	Enzyme loading [$mg_{GOx}\ g_{carrier}^{-1}$]	Glucose [mM]	Reaction rate (measured) [$\mu mol\ min^{-1}$]
Fine bubble aeration with 2 µm sintered frit				
1000	0.125	1.07[a]	25	23.5 ± 4.4 R^2 = 0.9994
	1	1.07[a]		38.9 ± 9.1 R^2 = 0.9997
	1	7.52[b]		43.7 ± 7.8 R^2 = 0.9999
1000	0.75	7.52[b]	300	164 ± 1 R^2 = 0.9987
	1			237 ± 50 R^2 = 0.9987

a. Enzyme loading on carriers: 1.07 $mg_{GOx}\ g_{carrier}^{-1}$, catalase (free) / calculated activity of glucose oxidase (immobilized):1.38. The experiment was performed in duplicate. The standard deviation value was obtained from duplicate measurements.

b. Enzyme loading on carriers: 7.52 $mg_{GOx}\ g_{carrier}^{-1}$, catalase (free) / calculated activity of glucose oxidase (immobilized):1.70, antifoam 204: 0.28 ± 0.06 mg mL^{-1}. The experiment was performed in duplicate. The standard deviation value was obtained from duplicate measurements, additionally including the data from the supervised B.Sc. thesis [118] for 300 mM substrate concentration.

At the substrate glucose concentration of 25 mM the effect of volume-specific aeration rates of 0.125 vvm and 1 vvm were compared. A 1.66-fold improvement in the reaction rate can be achieved with a 3-fold increase in the volumetric mass transfer coefficient $k_L a$ under conditions of an 8-fold increase in the volume-specific aeration rates. Since eight times more gas must be supplied to the system to increase the reaction rate by only 1.66 times, the enhancement is not significant. This result leads to the analysis of the oxygen consumption during the reaction (shown in Figure 33) at 1 vvm.

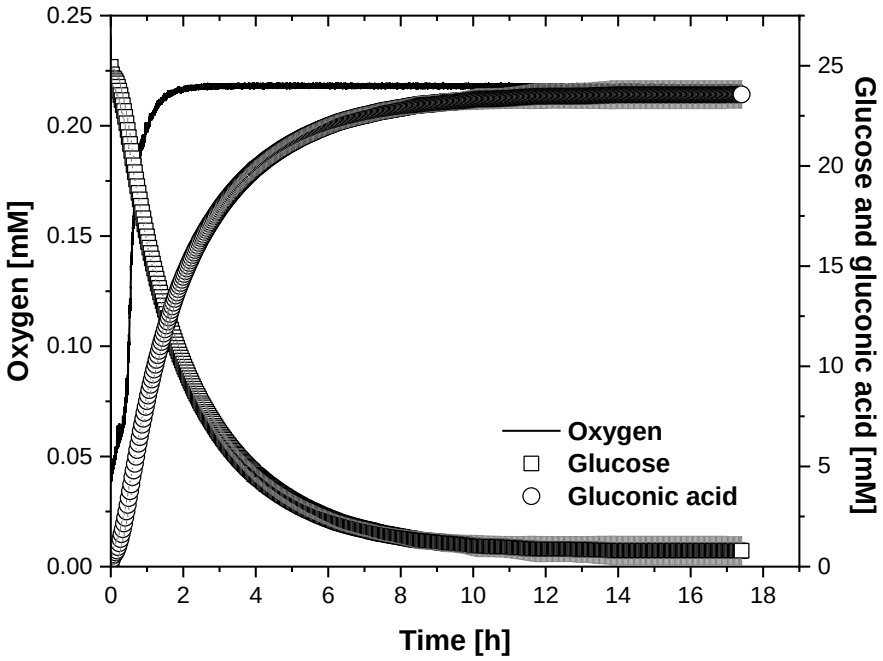

Figure 33. Biocatalytic oxidation of glucose under fine bubble aeration: 2 µm sintered frit. 8.2 g carriers, 1000 rpm, 35 ± 1°C, catalase (free) / calculated activity of glucose oxidase (immobilized):1.38, enzyme loading on carriers: 1.07 mg_{GOx} $g_{carrier}^{-1}$, 25 mM glucose solution in 10 mM sodium acetate buffer at a pH of 5.5 ± 0.2, initial volume 200 mL, 1 vvm, experimental results.

In Figure 33, the oxygen concentration decreased per time at the beginning of the reaction due to the oxygen consumption by the enzyme glucose oxidase. However, the oxygen concentration rapidly increased again and reached almost the saturation point under continuous oxygen supply during the reaction, which means that the oxygen transfer rate is above the reaction rate under the given experimental conditions at 1 vvm and 25 mM substrate concentration.

The following approach investigated the effect of aeration at higher substrate concentrations. At 300 mM substrate glucose concentration, the volume-specific aeration rate of 0.75 vvm, $k_L a$ = 57.7 ± 6.8 h^{-1} calculated from Figure 27B, and 1 vvm, $k_L a$ = 67.3 ± 3.7 h^{-1}, measured in Figure 27B, was investigated. When the volume-specific aeration rate was increased 1.3-fold (from 0.75 vvm to 1 vvm), the parameter $k_L a$ increased by 1.2 fold, and the reaction rate was enhanced by 1.4 fold (Table 9). A further increase in the reaction rate could be observed when the system is aerated with more than 1 vvm. During the preliminary tests, a higher aeration rate was investigated, and leakage was observed in 0.5 µm sintered frit sparger at 14.1 vvm. All experiments were repeated with a new 2 µm sintered frit sparger at relatively lower aeration rates based on the literature [30].

The potential of the rotating bed basket as an impeller for providing a sufficient energy input to facilitate biotransformation reactions was evaluated by conducting experiments with solubilized glucose oxidase and catalase without the use of carriers in the rotating bed basket. The oxidation reaction was completed in one hour with a full conversion

under fine bubble aeration (Figure 34), thereby demonstrating that the rotating bed basket provides sufficient mixing performance as an impeller.

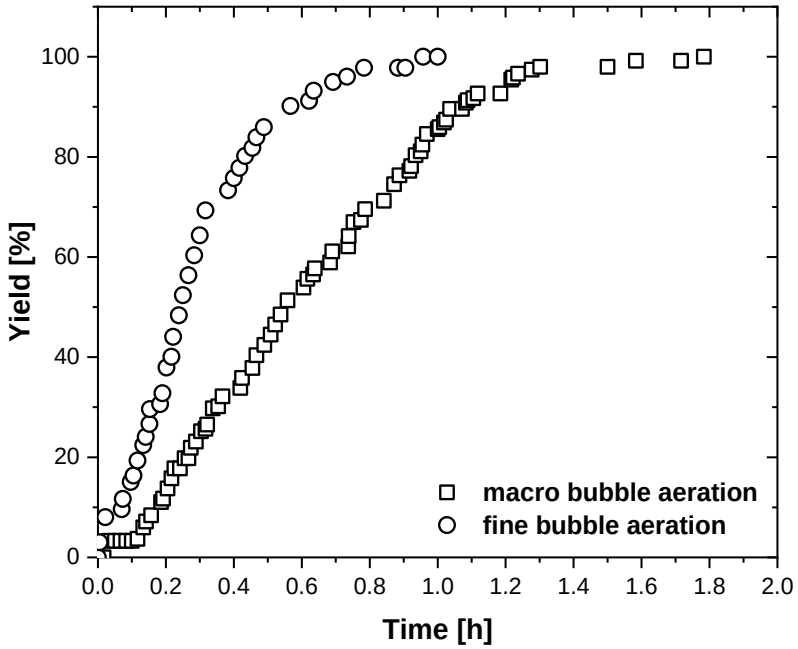

Figure 34. Application of free glucose oxidase and catalase in the SpinChem® vessel V2 with a rotating bed basket S2 without carriers. 500 rpm, 37 ± 1°C, initial volume 256 mL, 14.1 vvm, 78.1 mM glucose solution in 50 mM potassium phosphate buffer at pH 7, calculated activity of catalase / calculated activity of glucose oxidase: 0.52. Enzymes are used in their free form in the SpinChem® vessel V2 with a rotating bed basket S2 integrated with a 0.5 µm sintered frit sparger and perforated tube (2 mm). The experiment under macrobubble aeration was measured with manual titration and the yield values of both experiments were correlated to full conversion.

The effect of the stirring rate was investigated at 500 rpm and 1000 rpm on the reaction rate under fine bubble aeration with immobilized glucose oxidase in the rotating packed bed reactor, ensuring that both stirring rates provide turbulent flow conditions as determined in section 4.3. Subsequently, the substrate glucose concentration was investigated, and the findings are summarised in Table 10.

Table 10. Influence of the stirring on the reaction rate. 1000 rpm, 35 ± 1°C, 1 vvm, initial volume 200 mL, pH 5.5 ± 0.2. Glucose solutions were prepared in 10 mM sodium acetate buffer at pH 5.3.

Stirring rate [rpm]	Volume-specific aeration rate [vvm]	Enzyme loading [mg_{GOx} $g_{carrier}^{-1}$]	Glucose [mM]	Reaction rate (measured) [µmol min^{-1}]
Fine bubble aeration with 2 µm sintered frit				
500	0.67	1.07[a]	8.8	10.5 ± 0.6 R^2 = 0.9925
500	0.67	1.07[a]	25	24.4 ± 0.5 R^2 = 0.9924
1000	1	7.52[b]	8.8	19.4 ± 5.1 (calculated)[c]
1000	1	7.52[b]	25	43.7 ± 7.8 R^2 = 0.9999
1000	1	7.52[b]	300	237 ± 50 R^2 = 0.9987
1000	1	7.52[b]	600	368 ± 14 R^2 = 0.9739

a. Enzyme loading on carriers: 1.07 mg_{GOx} $g_{carrier}^{-1}$, catalase (free) / calculated activity of glucose oxidase (immobilized), pH = 6. The experiment was performed once for each single batch. The standard deviation was obtained from repetitive batches (batch 1 and batch 2) by data fitting using the Origin 2023b software.

b. Enzyme loading on carriers: 7.52 mg_{GOx} $g_{carrier}^{-1}$, catalase (free) / calculated activity of glucose oxidase (immobilized):1.70, antifoam 204: 0.28 ± 0.06 mg mL^{-1}, pH = 5.5. The standard deviation was calculated from duplicate experiments by data fitting using the Origin 2019b and 2023b software.

c. The reaction rate was calculated using the Michaelis-Menten function in Equation 12, which is derived from the kinetic measurements in section 4.8.2 at the same aeration rate 1 vvm, stirring rate 1000 rpm and enzyme loading 7.52 mg_{GOx} $g_{carrier}^{-1}$.

A comparison of the results obtained at 8.8 mM substrate glucose concentration at 500 rpm and 1000 rpm revealed that an increase in the stirring rate resulted in a doubling of the reaction rate (10.5 ± 0.6 µmol min^{-1} to 19.4 ± 5.1 µmol min^{-1}, Table 10). This is due to overcoming external diffusion limitations by reducing the gas-liquid boundary layer for mass transfer and increasing the convective flow in the reaction vessel. At the same stirring rate of 500 rpm, the reaction rate under fine bubble aeration was measured for two different substrate concentrations (8.8 mM and 25 mM) as 10.5 ± 0.6 µmol min^{-1} and 24.4 ± 0.5 µmol min^{-1}, respectively). The result supports the theory of the dominance of the substrate concentration over the reaction rate, since a 2.3-fold increase was observed when the substrate concentration was increased by a factor of 2.8.

During the kinetic studies presented in Section 4.8, the dependence of the reaction rate on the substrate concentration at 1000 rpm was investigated. It was observed that the reaction exhibited a Michaelis-Menten behaviour, with the highest reaction rate measured at 600 mM substrate glucose concentration. The detailed discussion for the

kinetic parameters is given in section 4.8.2 with the investigation of internal diffusion limitation. The performance of the immobilized glucose oxidase in a rotating packed bed reactor under macrobubble and fine bubble aeration was compared at 600 mM glucose concentration in the following section.

4.4.3.3. Reaction rate comparison: Macrobubble and fine bubble aeration

The rotating packed bed reactor was operated at its highest efficiency at 600 mM, as no further increase in the reaction rate was observed at 1000 mM (section 4.8.2, Figure 43). Therefore, the performance of the 2 µm sintered frit was compared to the open tube sparger (orifice diameter: 2 mm) at a substrate concentration of 600 mM (Figure 35). For 600 mM substrate concentration, three times the catalase (free) activity (90200 U) was used in the duplicate experiment, and a ratio of the calculated catalase (free) activity to the calculated glucose oxidase (immobilized) activity was calculated as 4.79. The final yield value obtained at 600 mM glucose substrate concentration with the higher catalase concentration is the same as the result obtained with the ratio of the calculated catalase (free) activity to the calculated glucose oxidase (immobilized) activity of 1.70. The catalase activity in its free form over 32000 U did not influence the reaction rate.

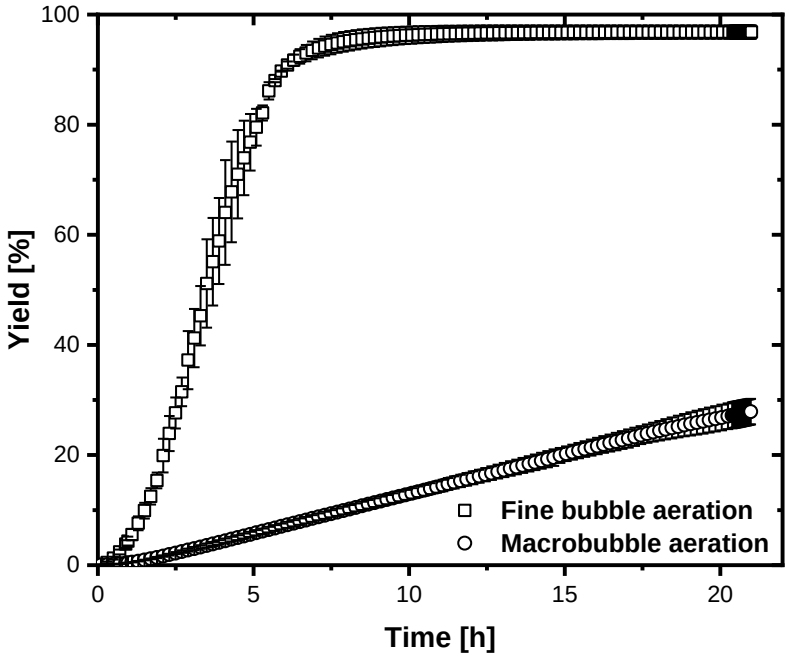

Figure 35. The effect of the aerator type on the reaction rate. Macrobubble aeration with open tube - orifice diameter: 2 mm; fine bubble aeration with 2 µm sintered frit. 8.2 g carriers, 35 ± 1°C, 1000 rpm, 7.52 mg_{GOx} $g_{carrier}^{-1}$, 600 mM glucose in 10 mM sodium acetate buffer pH 5.5 ± 0.2, initial volume before titration 200 mL, 1 vvm, 0.28 ± 0.06 mg mL^{-1} antifoam 204.

The higher liquid-side volumetric mass transfer coefficient ($k_L a$ = 67.3 ± 3.7 h^{-1}) with the 2 µm sintered frit was utilized to increase the reaction rate by 12.9 ± 1.6 times, and the reaction was completed in 8 h under fine bubble aeration (Table 11). The reason for observing a lag phase at the beginning of progress curves is explained in section 4.8.

Table 11. Summary of the reaction rates for fine bubble and macrobubble aeration[a].

Aeration rate [vvm]	Enzyme amount on carriers [$mg_{GOx}\ g_{carrier}^{-1}$]	Glucose [mM]	Reaction rate measured [µmol min^{-1}]	GOx-specific activity measured [U mg_{GOx}^{-1}]
Macrobubble aeration with open tube (orifice diameter: 2 mm)				
1	7.52	600	28.5 ± 2.4 R^2 = 0.9999 k_La = 22.5 ± 0.3 h^{-1}	0.46 ± 0.04
Fine bubble aeration with 2 µm sintered frit				
1	7.52	600	368 ± 14 R^2 = 0.9739 k_La = 67.3 ± 3.7 h^{-1}	5.82 ± 0.23

[a]8.2 g carriers, 35 ± 1°C, catalase (free) / calculated activity of glucose oxidase (immobilized): 1.70, antifoam 204: 0.28 ± 0.06 mg mL^{-1}, 1000 rpm, 10 mM sodium acetate buffer at pH 5.5 ± 0.2, initial volume before titration 200 mL. Data fitting was applied by the Origin 2019b software for linear regression. The standard deviation was obtained from duplicate measurements.

4.5. Gas utilization

In the previous section, the benefit of fine bubbles in biocatalytic oxidation reactions was shown as an increase in reaction rate and a reduction in process time. In the previous study [63], the gas consumption for the same model reaction catalyzed by the free form of glucose oxidase has been shown to be increased by a factor of 25 under microbubble aeration in a stirred tank reactor by performing the reaction at the equal liquid-side volumetric mass transfer coefficient k_La at 160 h^{-1}.

An identical mass transfer rate of molecular oxygen enables the same local oxygen concentration to be provided to the reaction medium, resulting in a comparable reaction rate with fine bubble and macrobubble aeration. In this study, the reaction was run at the comparable mass transfer rate of molecular oxygen (macrobubble aeration k_La = 22.5 ± 0.3 h^{-1} at 1 vvm and fine bubble aeration k_La = 18.9 ± 1.2 h^{-1} at 0.125 vvm) as described in the end of section 4.3. Using this outcome, the comparable GOx-specific reaction rates for macrobubble aeration (2.81 ± 0.07 U mg_{GOx}^{-1}, open tube with a 2 mm orifice diameter, 1 vvm, k_La = 22.5 ± 0.3 h^{-1}) and fine bubble aeration (2.74 ± 0.5 U mg_{GOx}^{-1}, 2µm sintered frit, 0.125 vvm, k_La = 18.9 ± 1.2 h^{-1}) at similar mass transfer rates were achieved, where the gas consumption was reduced 8 times at the substrate concentration of 25 mM. The experiments were performed in duplicate. Further investigations are necessary in order to gain a more comprehensive understanding of the matter.

4.6. Stability of the immobilized biocatalyst in a rotating packed bed reactor

The SpinChem® vessels with rotating packed bed reactors are designed as an alternative reactor concept to conventional fixed bed reactors, allowing convective flows in the reaction medium through the fixed bed, where the immobilized catalysts are packed. At this point, the stability of the immobilized biocatalyst within the substrate scope is the key consideration for the operational parameters to determine the half-life of enzymes [119]. Investigation of biocatalyst stability and an understanding of the factors that reduce the half-life of enzymes are essential to enable biocatalyst reuse in the rotating packed bed reactor. The main reason for the deactivation of the glucose oxidase used in this study is the accumulation of hydrogen peroxide [120] within the carriers, where the oxidative biotransformation reaction takes place.

In this section, the results of the effect of substrate concentration on the activity as well as the stability of immobilized glucose are presented and the optimum substrate concentration for the operation of a rotating packed bed reactor was determined.

4.6.1. Influence of the substrate concentration

With a higher concentration of substrate, a higher amount of hydrogen peroxide is produced as a by-product within the carriers. To prevent the deactivation effect of hydrogen peroxide, the second enzyme catalase is used as shown in previous studies [30,121,122].

In this study, the first choice is to immobilize the biocatalyst glucose oxidase and use catalase in its free form, whose cost is considerably lower than that of glucose oxidase as mentioned in section 4.1. The effect of substrate glucose concentration on the stability of immobilized glucose oxidase in a rotating packed bed reactor was investigated at three different glucose concentrations, in conditions above (300 mM > $K_{\mathrm{m,glucose}}$) and below (8.8 mM < $K_{\mathrm{m,glucose}}$ and 25 mM < $K_{\mathrm{m,glucose}}$) the Michaelis-Menten constant (section 4.8.2) of immobilized glucose oxidase for its substrate glucose. The glucose oxidase mass-specific activities obtained for the repetitive batches are listed in Table 12.

Table 12. Overview of immobilized glucose oxidase (GOx) stability in rotating packed bed reactor under fine bubble aeration with 2 µm sintered frit. 8.2 g carriers, 35 ± 1°C, 1000 rpm, initial volume 200 mL, 1 vvm, pH 5.5 ± 0.2. Glucose solutions were prepared in 10 mM sodium acetate buffer at pH 5.3.

Repetitive batches	**1**	**2**	**3**	**4**
Substrate glucose: 8.8 [mM][a]				
Time [h]	0.5	17.4	-	
Glucose oxidase-specific activity [U mg_{GOx}^{-1}]	1.30±0.04	1.21±0.08		
Yield [%]	94.6	98.7		
Substrate glucose: 25 [mM][a]				
Time [h]	0.8	23	-	
Glucose oxidase-specific activity [U mg_{GOx}^{-1}]	4.05±0.04	3.68±0.02		
Yield [%]	94.7	98.9		
Substrate glucose: 300 [mM][b]				
Time [h]	1.19±0.66	24.27±3.27	49.33±7.87	71.1
Glucose oxidase-specific activity [U mg_{GOx}^{-1}]	4.25±1.15	2.28±0.27	0.62±0.88	0

a. Enzyme loading on carriers: 1.07 mg_{GOx} $g_{carrier}^{-1}$, catalase (free) / calculated activity of glucose oxidase (immobilized):1.38 The experiment was performed once for each single batch. The standard deviation was obtained from data fitting using the Origin 2023b software.

b. Enzyme loading on carriers: 7.52 mg_{GOx} $g_{carrier}^{-1}$, catalase (free) / calculated activity of glucose oxidase (immobilized):1.70, antifoam 204: 0.28 ± 0.06 mg mL^{-1}. The experiment was performed in duplicate. Data fitting was applied by the Origin 2023b software for linear regression. The standard deviation was obtained from duplicate measurements. (Supervised B.Sc. thesis [118]).

The repetitive batches were performed for each substrate concentration. The time required for the substrate concentrations of 8.8 mM and 25 mM was measured to be 17 h and 23 h, respectively, to lose 5% and 9% of its glucose oxidase-specific activity indicating that the immobilized glucose oxidase is stable enough to maintain its activity for the subsequent batch under the given experimental conditions (Figure 36). The comparable final yield results of each batch at each substrate glucose concentration were achieved (repetitive batches for 8.8 mM glucose concentration - batch 1: 94.6% and batch 2: 98.7%; repetitive batches for 25 mM glucose concentration - batch 1: 94.7% and batch 2: 98.9%). The statistical analysis of the final yield values is described in section 4.9.

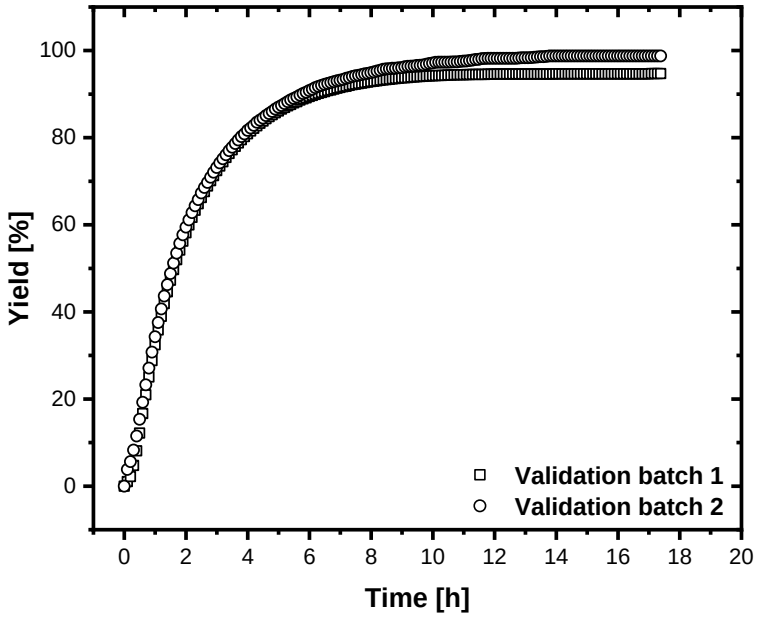

Figure 36. Validation of repetitive batches under fine bubble aeration: 2 µm sintered frit. 35 ± 1°C, 1000 rpm, 8.2 g carriers, initial volume 200 mL, 1 vvm, pH 5.5 ± 0.2. 25 mM glucose solution was prepared in 10 mM sodium acetate buffer at pH 5.3, enzyme loading on carriers: 1.07 mg_{GOx} $g_{carrier}^{-1}$, catalase (free) / calculated activity of glucose oxidase (immobilized):1.38.

A representative yield progress curve for the substrate concentration of 25 mM was shown in Figure 36, where the glucose oxidase mass-specific reaction rates for the validation batch 1 (4.05 U mg_{GOx}^{-1}) and batch 2 (3.68 U mg_{GOx}^{-1}) were achieved. No carrier leaching from the rotating packed bed reactor as well as enzyme leaching from the carriers into the reaction medium could be quantified by glucose oxidase activity measurements, allowing the validation of the repetitive batches with the reuse of biocatalysts. 98.5% of the carriers were found to be in the range of 200 - 500 µm (Figure 37).

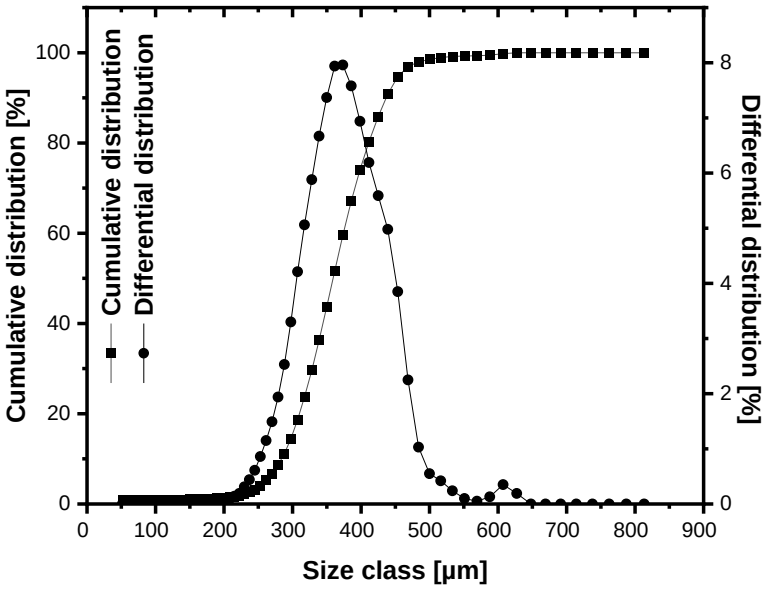

Figure 37. Particle size distribution of ReliZyme™ HFA 403 M grade carriers. The software (version 6.0.3.1008, 0249) of the Camsizer XT particle size analyser from Retsch GmbH (Haan, Germany).

To validate the repetitive batches under fine bubble aeration, subsequent batches were conducted at a higher substrate glucose concentration (300 mM). A strong deactivation was observed at the substrate concentration of 300 mM > $K_{m,glucose}$ (Tables 12). The time required for the substrate concentration of 300 mM to lose 46% of its activity in the subsequent batch (repetitive batches: batch 1: 4.25 ± 1.15 U mg_{GOx}^{-1} and batch 2: 2.28 ± 0.27 U mg_{GOx}^{-1}) was determined as 24 h, although the ratio of the calculated catalase (free) activity to the calculated glucose oxidase activity as 1.70 was higher than the conditions for the substrate concentration of 8.8 mM and 25 mM (1.38). This outcome could raise the question of whether the provided catalase (free) amount is enough to decompose the hydrogen peroxide produced within the carriers.

In section 4.4.3.3, the ratio of the calculated catalase (free) activity to the calculated glucose oxidase (immobilized) activity on the glucose oxidase-specific activity at the substrate concentration of 600 mM was investigated. No difference in glucose oxidase-specific activity was observed for each batch when the ratio of calculated catalase (free) activity to calculated glucose oxidase (immobilized) activity of 1.70 and 4.79 was used separately. The finding of no difference in the glucose oxidase-specific activity with a higher ratio of catalase activity indicates that the catalase (free) can get through the pores and decompose hydrogen peroxide. To confirm this information, the mean pore diameter of ReliZyme™ HFA 403 M grade carriers (40-60 nm [53]) was compared with the Stokes radius of catalase. The molecular weights of *Aspergillus niger* glucose oxidase and bovine liver catalase are reported to be 160 kDa [86] and 250 kDa [88], respectively. The Stokes radius of each protein was calculated (glucose oxidase: 3.97 nm, catalase: 4.31 nm, R^2 = 0.9196) using the hyperbolic function (shown in Figure 38) fitted to the Stokes radius of proteins of different masses as reported by H. P. Erickson [123].

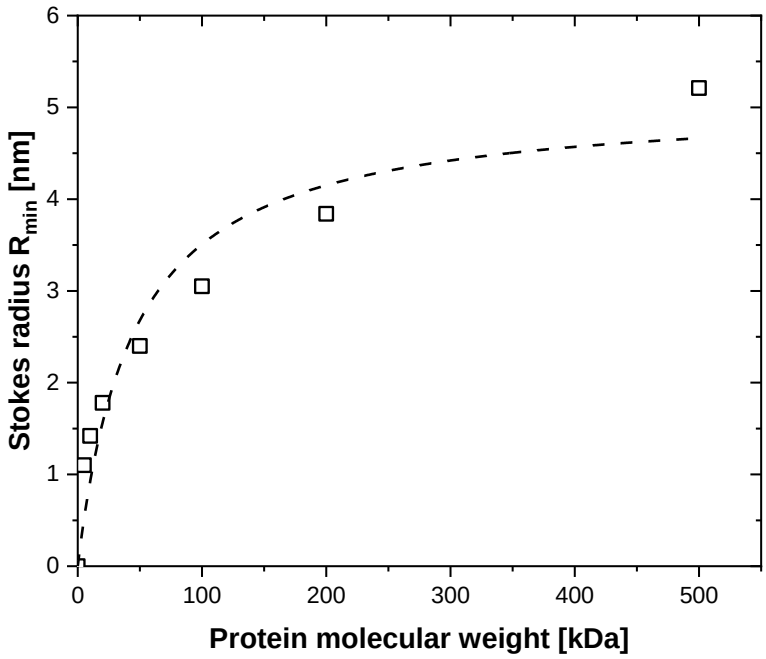

Figure 38. The fitted function of the Stokes radius of proteins with different masses. The graph was plotted from the data published by H. P. Erickson [123].

The mobility of the enzyme conformation is achieved by selecting carriers with a pore size larger than the size of the enzymes [124]. The pore size of ReliZyme™ HFA 403 M grade carriers is larger than the Stokes diameter of both enzymes, thus avoiding a reduction in immobilized glucose oxidase conformational mobility and allowing the free form of catalase to penetrate through the pores. However, when highly concentrated substrates are used, large amounts of inhibitor (hydrogen peroxide with a mean pore diameter: 0.25 nm and mean length: 0.28 nm [125]) are produced as a by-product.

The batch 2 of repetitive batches exhibited a loss of glucose oxidase-specific activity at the substrate concentration of 300 mM, which could indicate that the production rate of hydrogen peroxide is higher than the diffusion rate of catalase through the pores and the diffusion rate of hydrogen peroxide out of the pores. The hydrogen peroxide could precipitate within the carriers, where the reaction occurs, resulting in enzyme deactivation as well as a lag phase in the beginning of the reaction as always observed for each substrate concentration. Therefore, the stability of the enzyme in the second batch at a higher substrate concentration was decreased due to the severe internal diffusion limitation. The half-life of the immobilized glucose oxidase and the approach to overcome the internal diffusion limitation are described in the following sections.

4.6.2. Effect of substrate concentration on the biocatalyst half-life

To express the degree of activity loss mathematically, the measured glucose oxidase-specific activity was plotted (Figure 39) over time. An exponential decay function (Equation 23) was fitted to the measured data points shown using the Origin 2023b software. The data at 300 mM were taken from the supervised B.Sc. thesis [118]. The vertical error bars reflect the deviation in glucose oxidase-specific activity for the duplicate and the horizontal error bars reflect the time difference due to the measurement time and start of the experiments.

$$v_n = v_0 \cdot e^{-k_{deac} \cdot (t_n - t_0)} \qquad (23)$$

where v_n is the glucose oxidase-specific activity in U mg_{enzyme}^{-1} at time t_n in h, v_0 is the glucose oxidase-specific activity in U mg_{enzyme}^{-1} at time t_0 in h, k_{deac} is the deactivation constant in h^{-1}, $t_n - t_0$ is the time interval.

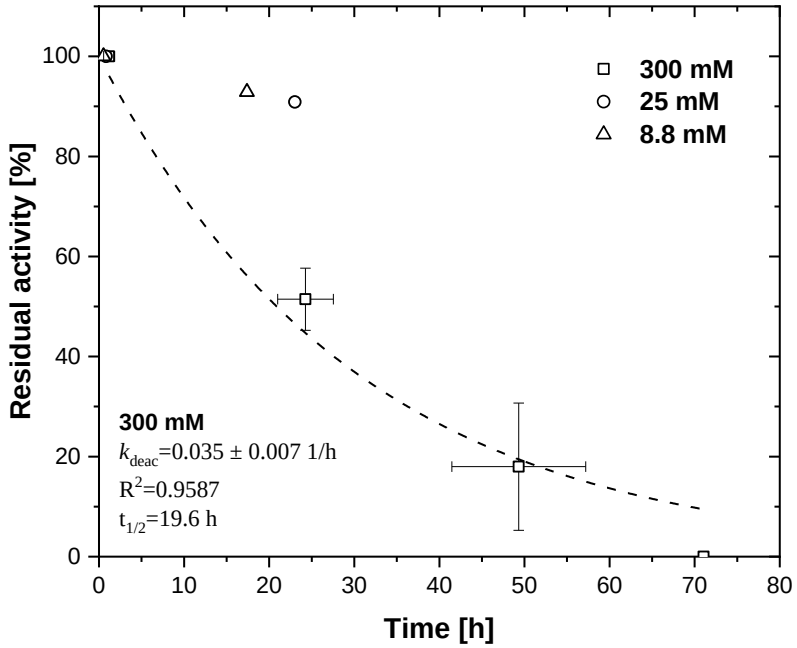

Figure 39. Stability of immobilized glucose oxidase under fine bubble aeration: 2 µm sintered frit sparger. 8.2 g carriers, 35 ± 1°C, 1000 rpm, initial volume 200 mL, pH 5.5 ± 0.2. Glucose solutions were prepared in 10 mM sodium acetate buffer at pH 5.3.

a. 300 mM - 1 vvm: enzyme loading on carriers: 7.52 mg_{GOx} $g_{carrier}^{-1}$, catalase (free) / calculated activity of glucose oxidase (immobilized):1.70, antifoam 204: 0.28 ± 0.06 mg mL^{-1}.
b. 25 mM - 1 vvm: enzyme loading on carriers: 1.07 mg_{GOx} $g_{carrier}^{-1}$, catalase (free) / calculated activity of glucose oxidase (immobilized):1.38.
c. 8.8 mM - 0.67 vvm: enzyme loading on carriers: 1.07 mg_{GOx} $g_{carrier}^{-1}$, catalase (free) / calculated activity of glucose oxidase (immobilized):1.38.

For a further concrete comparison, the half-life $t_{1/2}$ of immobilized glucose oxidase was calculated as 19.6 h for the substrate glucose concentration of 300 mM using the Equation 24, with the glucose oxidase-specific activity reduced by half ($v_n = \frac{1}{2} \cdot v_0$).

$$t_{1/2} = \frac{ln2}{k_{deac}} \qquad (24)$$

To compare the stability of the immobilized glucose oxidase at the substrate glucose concentration of 25 mM, where 9% loss of the activity was observed in 23 h, the time required to lose 9% of the glucose oxidase-specific activity of 300 mM substrate concentration was calculated as 2.7 h using Equation 24 with the deactivation constant k_{deac}. To achieve a high productivity for glucose oxidase in batch operation, a substrate concentration ($c_s > K_m$) is necessary to operate the rotating packed bed reactor efficiently. However, a severe internal diffusion limitation was observed at 300 mM substrate concentration.

4.7. Interim summary

In the first part of the thesis the following main results were achieved:

- A suitable enzyme-carrier system in the designed liquid medium (10 mM sodium acetate at pH 5.3) was established with an immobilization activity yield of over 98%.
- The established enzyme-carrier system was utilized in the SpinChem® rotating packed bed reactor and the oxidative biotransformation reaction was catalyzed by the immobilized glucose oxidase with a reaction yield of 96.2 ± 2.5%.
- The mass transfer performance for the SpinChem® vessel with rotating packed bed basket under fine bubble and macrobubble aeration was compared:
  - At the equal volume-specific aeration rate, the volumetric mass transfer coefficient for fine bubble aeration (67.3 h^{-1}) was three times that of macrobubble aeration (22.5 h^{-1}).
  - A comparable volumetric mass transfer coefficient for fine bubble aeration (0.125 vvm) was achieved at a reduced aeration rate compared to macrobubble aeration (1 vvm).
- The mass transfer limitations during the biocatalytic oxidation have been studied under two different conditions, when the enzyme glucose oxidase is unsaturated and when it is saturated with its substrate glucose:
  - When the enzyme glucose oxidase was not saturated at 25 mM glucose, no oxygen mass transfer limitation was observed.
  - When the enzyme glucose oxidase was oversaturated with substrate glucose (300 mM and 600 mM), severe mass transfer limitations were observed. The mass transfer limitation was overcome by fine bubble aeration using the advantage of a higher volumetric mass transfer coefficient at a substrate concentration ($c_s > K_m$).
- The stability of the immobilized biocatalyst in the rotating packed bed reactor was investigated:
  - When the enzyme glucose oxidase was not saturated with glucose at 25 mM, the stability of the immobilized glucose oxidase was longer than when the enzyme glucose oxidase is oversaturated with its substrate glucose (300 mM and 600 mM).

In the following section, the reason for the loss of enzyme stability in conjunction with the diffusion limitations and the approaches to overcome the internal diffusion limitation are reported.

4.8. Approaches to overcome internal diffusion limitation

In the previous section, severe internal diffusion limitation was observed at a substrate glucose concentration (300 mM) for the case where the immobilized enzyme glucose oxidase was used, and the second enzyme catalase was used in its free form (Figure 40). To overcome the diffusion limitation the co-immobilization approach [126] was applied to improve the reaction rate. In addition, the free form of both enzymes in the SpinChem® vessel, in which the rotating packed bed basket was filled with the carriers but without enzymes, was used as a reference point to determine the maximum achievable reaction rate, reflecting the case where there is no internal diffusion limitation.

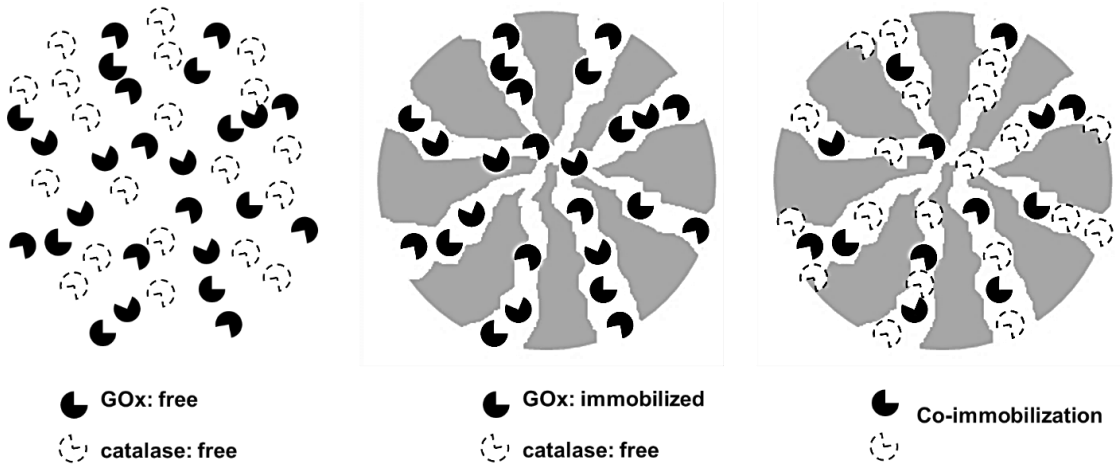

Figure 40. Application of biocatalysts in the SpinChem® vessel V2 with the rotating packed bed basket S2. A) Free form of glucose oxidase (solid) and catalase (dash), B) Immobilized glucose oxidase (GOx) within the carriers and free catalase in the bulk medium, C) Co-immobilization of glucose oxidase with catalase.

For the reaction to take place, two substrates (glucose and oxygen) are required to enter the pores of the carriers placed in the rotating bed basket. A lag phase (until reaching 10% yield) was observed for each substrate concentration (25 mM, 300 mM, and 600 mM, Figure 41).

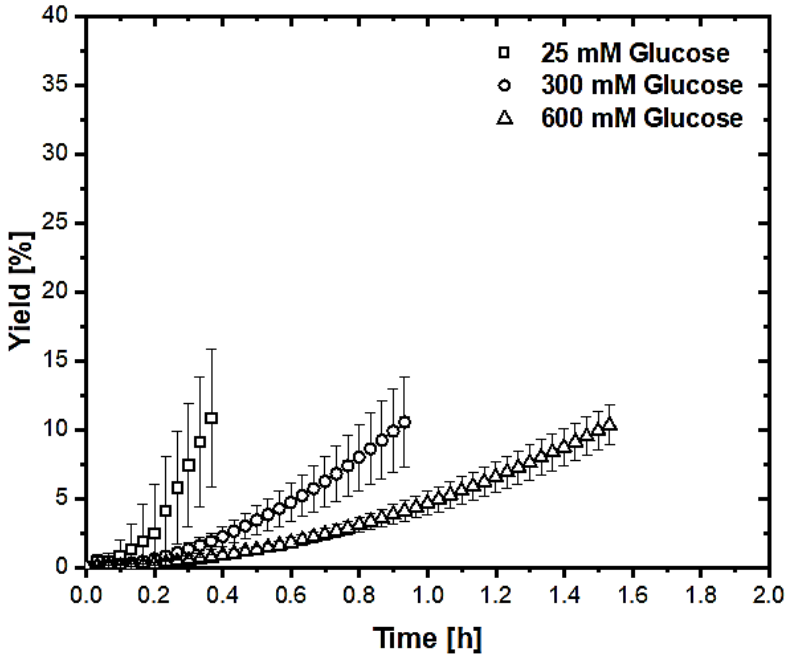

Figure 41. Lag phase observed for each substrate concentration under fine bubble aeration: 2 µm sintered frit. 8.2 g carriers, 1000 rpm, 35 ± 1°C, initial volume 200 mL, 1 vvm, pH 5.5 ± 0.2. Enzyme loading on carriers: 7.52 mg_{GOx} $g_{carrier}^{-1}$, catalase (free) / calculated activity of glucose oxidase (immobilized): 1.70, antifoam 204: 0.28 ± 0.06 mg mL^{-1}. Glucose solutions were prepared in 10 mM sodium acetate buffer at pH 5.3, For the duplicate experiment at 600 mM substrate glucose was performed with the ratio of catalase (free) to the calculated activity of glucose oxidase (immobilized) is 4.79. Error bars show the standard deviation obtained from duplicate measurements. The graph is generated by additionally integrating the results of the supervised B.Sc. thesis [118] and the project work [127].

At a low substrate glucose concentration of 25 mM, the duration of the lag phase was found to be relatively short, in contrast to the lag phase obtained with a 300 mM and 600 mM substrate concentration. A longer lag phase was observed at a higher substrate concentration and was attributed to diffusion limitations. To properly interpret the lag phase exhibited by each yield progress curve, it is essential to consider the underlying reaction kinetics (section 4.8.1), and it is reasonable to consider that the diffusion limitation could be associated with the second enzyme, catalase, which is utilized for the decomposition of hydrogen peroxide accumulated in the pores of carriers [128]. To improve the reaction rate and reduce the lag phase, the co-immobilization approach [126] was used and the results are presented in Figure 42 for comparison.

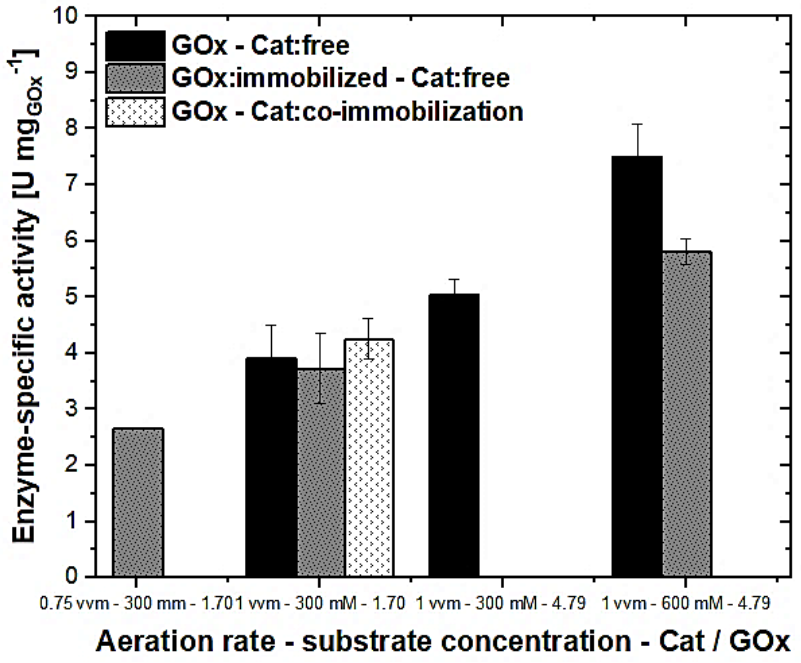

Figure 42. Application of immobilized glucose oxidase in the SpinChem® vessel V2 with the rotating packed bed basket S2 under fine bubble aeration with 2 µm sintered frit. 8.2 g carriers, 1000 rpm, initial volume 200 mL, 35 ± 1°C, 1 vvm, pH 5.5 ± 0.2. Glucose solutions in 10 mM sodium acetate buffer at pH 5.3, enzyme loading on carriers: 7.52 mg_{GOx} $g_{carrier}^{-1}$, antifoam 204: 0.28 ± 0.06 mg mL^{-1}, Cat/GOx: the ratio of calculated activity of catalase (Cat) / calculated activity of glucose oxidase (GOx). The experiments were performed in duplicate. Error bars show the standard deviation obtained from duplicate measurements. For 600 mM (GOx: immobilized, Cat: free): The error bar represents the deviation between the experiments for the ratio of calculated activity of catalase / calculated activity of glucose oxidase 1.70 and 4.79, where no significant difference was observed. The experiment at the volume-specific aeration rate of 0.75 vvm was performed once. Error bars show the standard deviation obtained from data fitting using the Origin 2023b software. The graph is generated by additionally integrating the results of the supervised B.Sc. thesis [118] and the supervised project work [127].

In Figure 42, the first result was measured with a lower (0.75 vvm) volume-specific aeration rate to illustrate the oxygen dependency of the biocatalytic reaction. A lower volume-specific aeration rate (0.75 vvm) results in a lower glucose oxidase-specific activity compared to the glucose oxidase-specific activity measured at 1 vvm. The effect of the aeration rate on mass transfer performance and reaction rate was discussed in sections 4.3.2 and 4.4.3.

According to M. Nouaimi-Bachmann [129], it is required to optimize the ratio of the amount of two enzymes for the co-immobilization approach, as competition between enzymes (glucose oxidase and catalase) for the binding site is potential. The results in Figure 42 demonstrate that there was no significant change in the glucose oxidase-specific activity for any of the three approaches at a ratio of calculated activity of catalase to the calculated activity of glucose oxidase: 1.70 at a substrate concentration of 300 mM, indicating that there could be no competition between the two enzymes.

The pore diameter of the carriers (40-60 nm) is larger than the size of both proteins (Stokes radius: glucose oxidase: 3.97 nm, catalase:4.31 nm), i.e., the pores are not closed by one of the proteins.

The size of the substrate glucose (0.84-0.86 nm [130] for ring molecule and 1.5 nm for open structure [131]) and the by-product hydrogen peroxide (0.25 nm [132]) are relatively smaller than the pore size of ReliZyme^{TM} HFA 403 M grade carriers (40-60 nm) as well as the Stokes radius of the enzymes glucose oxidase (3.97 nm) and catalase (4.31 nm) [123]. The substrate glucose can pass through the pores, reach the immobilized glucose oxidase and is oxidized to D-glucono-1,5-lactone, producing the by-product hydrogen peroxide. Ideally, the by-product hydrogen peroxide should interact with the co-immobilized catalase, as in the case of free catalase in the bulk reaction medium. Therefore, no improvement in the glucose oxidase-specific activity was observed with the co-immobilization approach (Figure 42).

The further approach was to increase the ratio of calculated activity of catalase to calculated activity of glucose oxidase by using both enzymes in their free form to enhance the reaction rate for the oxidative biotransformation. When the ratio of calculated activity of catalase to calculated activity of glucose oxidase was increased from 1.70 to 4.79, the glucose oxidase-specific activity was increased by 1.3-fold at the substrate concentration of 300 mM. Increasing the amount of catalase in its free form would increase the glucose oxidase mass-specific reaction rate by increasing the decomposition rate of hydrogen peroxide, thus decreasing its deactivation effect.

At a higher substrate concentration (600 mM), the use of the free form of both enzymes improved the glucose oxidase-specific activity by 29% (Figure 42) at the equal ratio of the calculated activity of catalase (free) to the calculated activity of glucose oxidase (immobilized), indicating that immobilization caused a reduction in the enzyme activity of glucose oxidase [133] at the higher substrate concentration, where a higher amount of by-product hydrogen peroxidase was produced within the carriers. Thus, the function of catalase was hindered due to its lower diffusion rate, when compared to the production rate of the by-product hydrogen peroxidase. Kinetic parameters of the immobilized and free forms of glucose oxidase were investigated to determine the relevant enhancement of the glucose oxidase-specific activity for each substrate concentration and to further explain the internal diffusion limitation.

4.8.1. Kinetic parameter determination for free and immobilized glucose oxidase

Carrying out biocatalytic oxidation in a porous structure of a carrier could reduce the measured reaction rate compared to the application of enzymes in their free form, floating in the medium buffer. This phenomenon can be attributed to the limited mobility of enzymes and solutes [134]. The potential decrease in the reaction rate is mathematically explained by the effectiveness factor η (Equation 25), which is the ratio of the maximum glucose oxidase-specific activity v_{max} in U mg^{-1} achieved for immobilized and free forms of biocatalysts [133].

$$\eta = \frac{v_{\text{max,immobilized glucose oxidase}}}{v_{\text{max,free glucose oxidases}}} \quad (25)$$

The maximum achievable reaction rates for immobilized and free form of biocatalysts were determined by measuring the glucose oxidase-specific activity in U mg^{-1} over a wide range of substrate concentrations (Figure 43). The kinetic investigations were carried out in the substrate concentration range of 25 mM - 1000 mM.

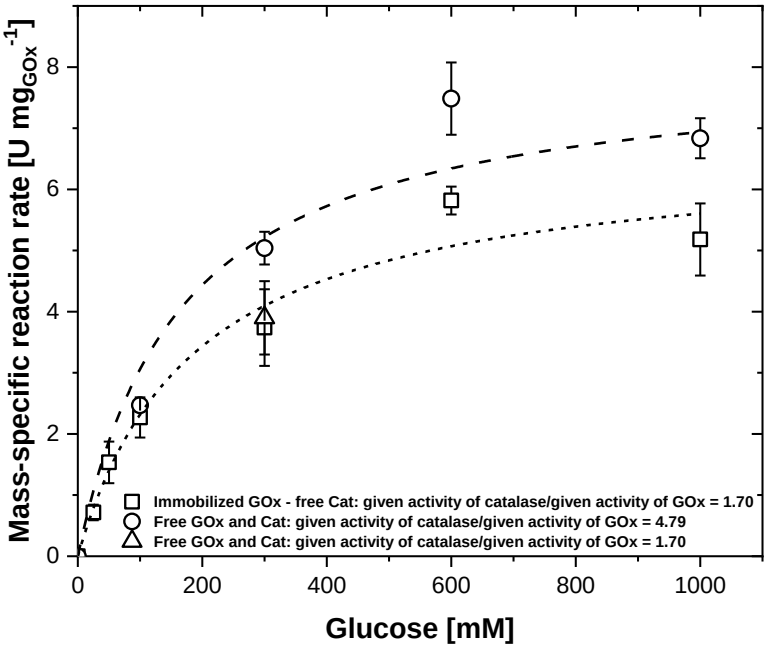

Figure 43. Kinetic parameter estimation for free and immobilized forms of enzymes in the SpinChem® vessel V2 with the rotating packed bed basket S2 under fine bubble aeration with 2 µm sintered frit: 8.2 g carriers, enzyme loading on carriers: 7.52 mg_{GOx} $g_{carrier}^{-1}$, 35 ± 1°C, 1000 rpm, 1 vvm, initial volume 200 mL, pH 5.5 ± 0.2, antifoam 204: 0.28 ± 0.06 mg mL^{-1}. Glucose solutions were prepared in 10 mM sodium acetate buffer at pH 5.3. Error bars show the standard deviation obtained from duplicate measurements. The experiment at 100 mM glucose concentration with free enzyme was performed once. Error bars show the standard deviation obtained from data fitting using the Origin 2023b software. The graph is generated by additionally integrating the results of the supervised B.Sc. thesis [118] and the project work [127].

In the context of kinetic investigations with both enzymes in their free form, an increase in catalase concentration resulted in an enhancement of the glucose oxidase-specific activity for the biocatalytic oxidation (the data point triangle and circle at the substrate concentration of 300 mM). When the ratio of the given activity of catalase to the given activity of Gox was tripled (from 1.70 to 4.79), the glucose oxidase-specific activity increased by a factor of 2.8. It was measured as 5.04 ± 0.27 U mg_{GOx}^{-1} at a ratio of 4.79 for the free form of the enzymes in comparison to the glucose oxidase-specific activity of 3.90 ± 0.6 U mg_{GOx}^{-1} at a ratio of 1.70 for the free form of the enzymes. Therefore, to ensure that the measured reaction rates are not limited by the decomposition of hydrogen peroxide by the catalase enzyme, the calculated catalase

activity was tripled to obtain the highest glucose oxidase-specific activity for the free form of both enzymes, which is the denominator of the effectiveness factor (Equation 25).

In both cases of enzyme application (free and immobilized forms), the reaction rate is found to be proportional to the substrate concentration. This is explained by the fact that an increase in substrate concentration results in a higher reaction rate (Equation 12). The glucose oxidase-specific activity (2.27 ± 0.33 U mg_{GOx}^{-1}) was measured with immobilized glucose oxidase and free catalase, whereas it was measured as 2.47 U mg_{GOx}^{-1} with the free form of both enzymes at the identical substrate concentration of 100 mM. The difference in both values is in the experimental range.

The rate of substrate consumption within the carriers (in the pores and/or on the surface) is comparable to the reaction rate in the bulk phase with free forms of biocatalysts for both biocatalyst applications at the substrate concentration of 100 mM, resulting in an immobilization with an effectiveness factor (Equation 25) of 0.92 ($c_s < K_m$). The enzyme activity is expected to be similar for both applications at a substrate concentration lower than 100 mM, as the enzyme glucose oxidase is not saturated with its substrate ($c_s < K_m$, see Table 13). The effect of diffusion limitation on the reaction rate is expected to be reduced and the system behaves as if free enzymes are used. Accordingly, kinetic investigations with free-form glucose oxidase were initiated at a substrate concentration of 100 mM, and the resulting kinetic parameters are presented in Table 13 for comparison.

Table 13. Comparison of kinetic parameters using the SpinChem® vessel V2 with the rotating packed bed basket S2 under fine bubble aeration: 2 µm sintered frit. 8.2 g carriers, 35 ± 1°C, 1000 rpm, 10 mM sodium acetate buffer at pH 5.5 ± 0.2, 7.52 mg_{GOx} $g_{carrier}^{-1}$, initial volume before titration 200 mL, antifoam 204: 0.28 ± 0.06 mg mL^{-1}. Data fitting was applied by the Origin 2023b software.

Parameter	Glucose oxidase free[b]	Glucose oxidase immobilized[c]
v_{max} [U mg^{-1}]	8.08 ± 0	6.65 ± 0.62
$K_{m,glucose}$ [mM]	164 ± 34	187 ± 54
R^2 [-]	0.956	0.964
K_{m,O_2} [mM][a]	0.010 ± 0.002	0.084 ± 0.019
Effectiveness factor η [-]	0.82	

[a] K_{m,O_2} for free glucose oxidase was determined under the experimental conditions: 250 mM glucose, 30°C, 100 mM phosphate buffer at pH 7, 1 mL. K_{m,O_2} for immobilized glucose oxidase was determined under the experimental conditions: 250 mM glucose, 30°C, 100 mM phosphate buffer at pH 7, 2 mL [135].
[b] calculated activity of catalase (free) / calculated activity of glucose oxidase: 4.79
[c] calculated activity of catalase (free) / calculated activity of glucose oxidase: 1.70

The measured Michaelis-Menten constant 187 ± 54 mM of immobilized glucose oxidase for its substrate glucose is higher than the free form of glucose oxidase

164 ± 34 mM. In the presence of mass transport limitation, a lower affinity to the substrate could be observed, resulting in a higher Michaelis-Menten constant [136], which was observed in this study for immobilized glucose oxidase. A substrate concentration exceeding 164 mM is necessary for the generation of a sufficient driving force within the carriers to overcome the diffusion limitation.

At 300 mM glucose the glucose oxidase-specific activity for the immobilized glucose oxidase and free catalase and for free form of both enzymes are comparable (3.74 ± 0.63 U mg_{GOx}^{-1} and 3.9 ± 0.6 U mg_{GOx}^{-1}, respectively) at the identical experimental conditions, where the ratio of calculated catalase activity to the calculated glucose oxidase activity was used as 1.70. However, when the ratio of calculated catalase activity to the calculated glucose oxidase activity was tripled for the free form of enzymes, 5.04 ± 0.27 U mg_{GOx}^{-1} glucose oxidase-specific activity was obtained. This indicates that a catalase activity above 90200 U is necessary to avoid the deactivation effect of hydrogen peroxide on the enzyme glucose oxidase.

At higher substrate concentrations (600 mM and 1000 mM), the effect of glucose oxidase immobilization on the glucose oxidase-specific activity can be clearly seen, as the difference of the glucose oxidase-specific activity for two systems (immobilized glucose oxidase-free catalase and free form of the enzymes) is increased. The application of the free form of the enzymes indicates no diffusion limitation. Therefore, the higher substrate concentration can accelerate the reaction rate more than under immobilization conditions (Figure 43).

The highest glucose oxidase-specific activity for the solubilized form of the enzymes was calculated to be 8.08 ± 0 U mg_{GOx}^{-1}, while 6.65 ± 0.62 U mg_{GOx}^{-1} was determined for the immobilized glucose oxidase with the free form of catalase at a substrate glucose concentration of 600 mM, confirming that the immobilization approach limits the reaction rate. The effectiveness factor was calculated as 0.82 for the system ($c_s > K_m$), indicating the presence of internal (substrate) diffusion limitation, which is confirmed by the evaluation of the kinetic parameters of glucose oxidase for its substrate glucose in the immobilized and free form.

4.8.2. Modelling of the reaction rate

The kinetic parameters in Table 13 are implemented in Equation 12 with considering the deactivation constant k_{deac} = 0.035 ± 0.07 h^{-1} and the effectiveness factor η = 0.82 to reflect the effect of diffusion limitation in the reaction rate equation v in µmol min^{-1} mg_{GOx}^{-1}, yielding Equation 26. The reaction rate was modelled using Equation 26 for the substrate concentration at 25 mM and 300 mM considering the glucose oxidase concentration c_{G0x} in mg_{GOx} mL^{-1}, with the differential equations (Equation 27 and 28) for the substrate glucose consumption and gluconic acid production. The experimental results were compared with the simulation results (Figure 44).

$$v = \frac{v_{max} \cdot c_{glucose} \cdot c_{O_2} \cdot e^{k_{deac} \cdot t} \cdot \eta}{K_{m,glucose} \cdot c_{O_2} + K_{m,O_2} \cdot c_{glucose} + c_{glucose} \cdot c_{O_2}} \qquad (26)$$

where v_{max} in µmol min^{-1} mg$_{GOx}^{-1}$ is the glucose oxidase mass-specific reaction rate, $c_{glucose}$ in mM and c_{O_2} in mM are the glucose and oxygen concentrations, K_m in mM is the Michaelis-Menten constant, k_{deac} in min^{-1} is the deactivation constant, η is the effectiveness factor.

$$\frac{dc_{glucose}}{dt} = - v \cdot c_{GOx} \qquad (27) \qquad \frac{dc_{gluconic\ acid}}{dt} = + v \cdot c_{GOx} \qquad (28)$$

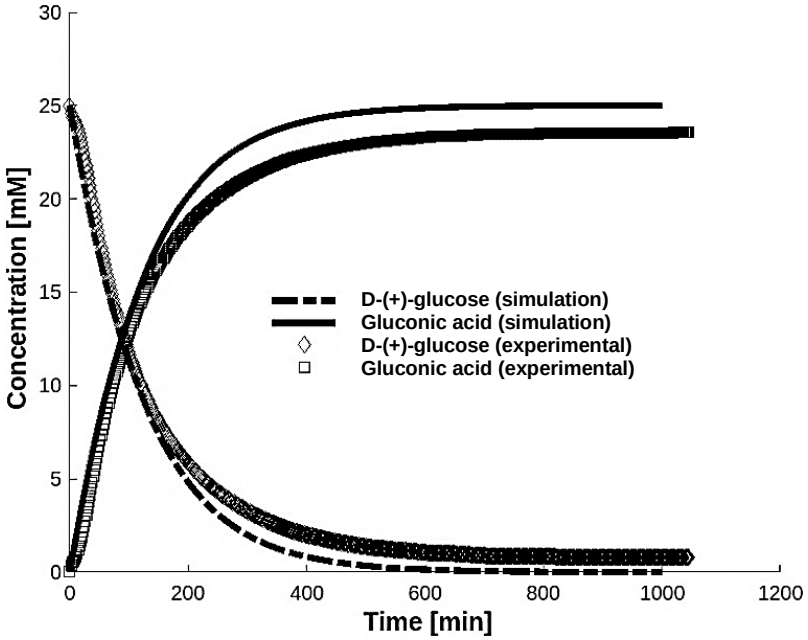

Figure 44. Comparison of the simulation results (dashed lines) with the experimental results (symbols). Biocatalytic oxidation of glucose in the rotating bed reactor under fine bubble aeration with 2 µm sintered frit. Measurement conditions: 8.2 g carriers, 1000 rpm, 35 ± 1°C, enzyme loading on carriers: 1.07 mg$_{GOx}$ g$_{carrier}^{-1}$, catalase (free) / calculated activity of glucose oxidase (immobilized): 1.38, 25 mM glucose solution in 10 mM sodium acetate buffer at a pH of 5.5 ± 0.2, initial volume 200 mL, 1 vvm, k_La = 67.3 ± 3.7 h^{-1}. Simulations were performed using the Matlab R2024a software.

The reaction volume was considered as the volume reactor (28 mL) of the rotating packed bed in the simulation results, where the rotating bed reactor was fully packed with carriers and the volume of void-space is negligible (see Scheme 1). The simulation was run for the conditions under fine bubble and macrobubble aeration at the substrate concentration of 300 mM to verify the effect of the volumetric mass transfer coefficient k_La (Figure 45) on the reaction rate with simulation results.

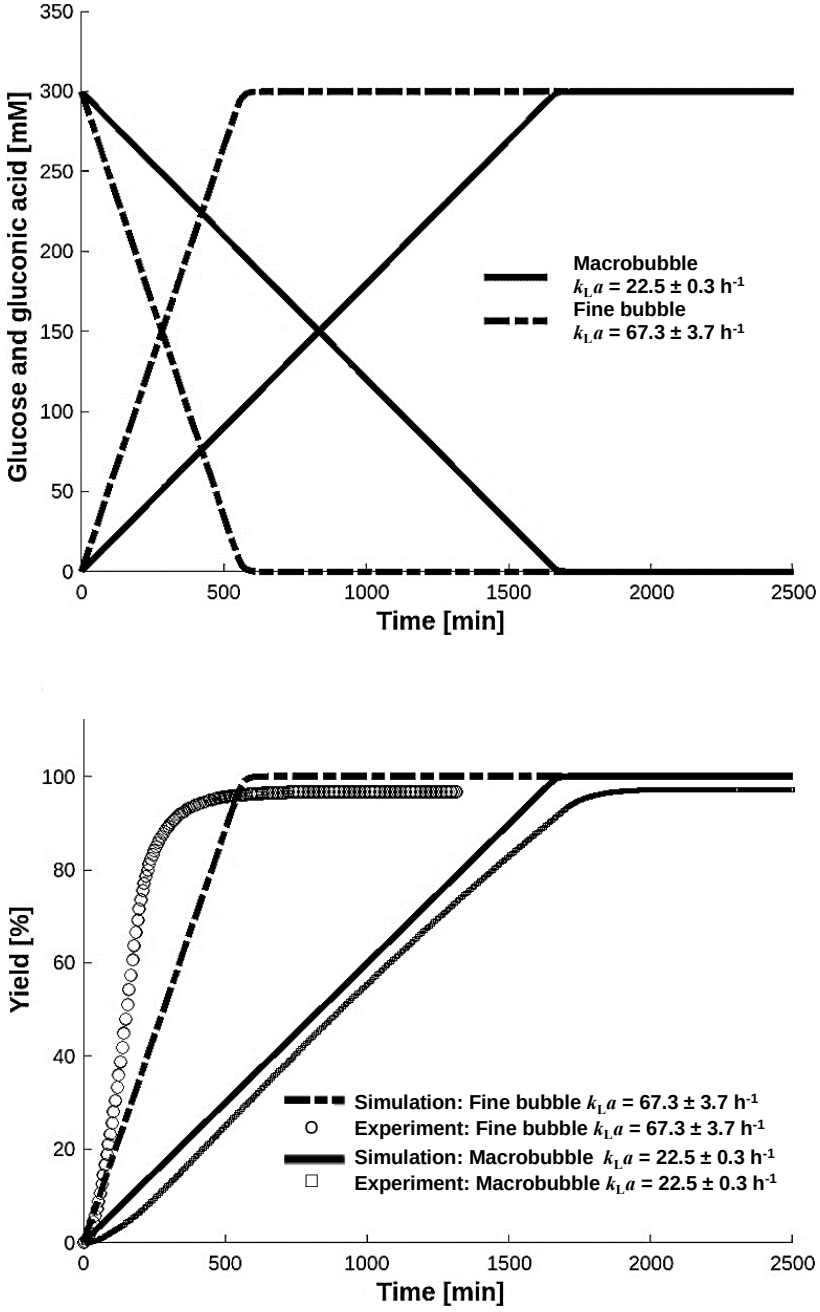

Figure 45. Validation of simulation results with experimental results. Top: Investigation of the influence of the volumetric mass transfer coefficient k_La on the reaction rate with simulation results. Down: Experimental results for fine bubble (2 µm sintered frit) and macrobubble aeration open tube (orifice diameter: 2 mm). Measurement conditions: 8.2 g carriers, 1000 rpm, 35 ± 1°C, catalase (free) / calculated activity of glucose oxidase (immobilized):1.70, enzyme loading on carriers: 7.52 mg_{GOx} $g_{carrier}^{-1}$, initial volume 200 mL, 1 vvm, 300 mM glucose solution in 10 mM sodium acetate buffer at a pH of 5.5 ± 0.2, 0.28 ± 0.06 mg mL^{-1} antifoam 204. Simulations were performed using the Matlab R2024a software.

In Figure 45 (top), the effect of the volumetric mass transfer coefficient k_La for fine bubble aeration 67.3 ± 3.7 h^{-1} and macrobubble aeration 22.5 ± 3.7 h^{-1} on the simulated reaction rate was compared. The simulation results demonstrate a higher value of the

$k_L a$ coefficient resulted in a higher reaction rate. The outcome is confirmed by the experimental results in Figure 45 (down), which were obtained for fine bubble and macrobubble aeration at the substrate concentration (300 mM) and volume-specific aeration rate (1 vvm). A comparison of the simulation results with the experimental results was based on the final yield value achieved during the experiments and the corresponding process time in the simulations (Table 14).

Table 14. Comparison of simulation results with experimental results. 1000 rpm, 35 ± 1°C, 8.2 g carriers, 7.52 mg_{GOx} $g_{carrier}^{-1}$, 300 mM glucose solution in 10 mM sodium acetate buffer pH 5.5 ± 0.2, catalase (free) / calculated activity of glucose oxidase (immobilized): 1.70, initial volume before titration 200 mL, 0.28 ± 0.06 mg mL^{-1} antifoam 204. Simulations were performed using the Matlab R2023a software.

Parameter	Yield [%]	Process time [min]	Yield [%]	Process time [min]	Yield [%]	Process time [min]
Macrobubble aeration with open tube (orifice diameter: 2 mm)						
Simulation	90	1572	97.3	1749	100	3062
Experiment		1642		2146	-	-
Fine bubble aeration with 2 µm sintered frit						
Simulation	90	668	96.8	809	100	2142
Experiment		311		910	-	-

The modelled reaction rate (Equation 26) using the kinetic parameters in Table 13 estimates the reactor performance for the biocatalytic oxidation in an agreement with the experimental results in respect to process time. A prediction of the reactor performance for the condition under the macrobubble aeration gives a close fit with experimental results, thus the modelled reaction rate is verified for macrobubble aeration (Figure 45, down). For the fine bubble aeration condition, the final process time was estimated with a reasonable agreement, however, the experimental reaction rate is higher than the simulated results (Figure 45, down). The predicted model considers the improvement of the volumetric mass transfer coefficient for fine bubble and macrobubble aeration, however, it could not estimate the advantage of smaller bubbles if they enter the rotating packed bed reactor and bring the additional advantage for the reaction rate acceleration during the experimental studies. Further investigation is needed to verify the condition under fine bubble aeration. To determine the optimal substrate concentration for the highest reactor performance, the effectiveness factor and operational effectiveness factor were calculated for each substrate concentration in the following section.

4.8.3. Effectiveness and operational effectiveness factor

The optimal substrate concentration for efficient operation of a rotating packed bed reactor was determined using the dimensionless operational effectiveness factor η_0 (Equation 29), where 90% yield was achieved in both conditions:

- immobilized: immobilized glucose oxidase together with free-form catalase.
- free: free forms of glucose oxidase and catalase

$$\eta_0 = \frac{t_{90\%\text{immobilized}}}{t_{90\%\text{free}}} \qquad (29)$$

where t is the operational process time in h.

The effectiveness factor and the operational effectiveness factor for each substrate concentration (100 mM, 300 mM and 600 mM) were determined for the substrate concentration below and above the Michaelis-Menten constant of 187 ± 54 mM of the immobilized glucose oxidase (Figure 46).

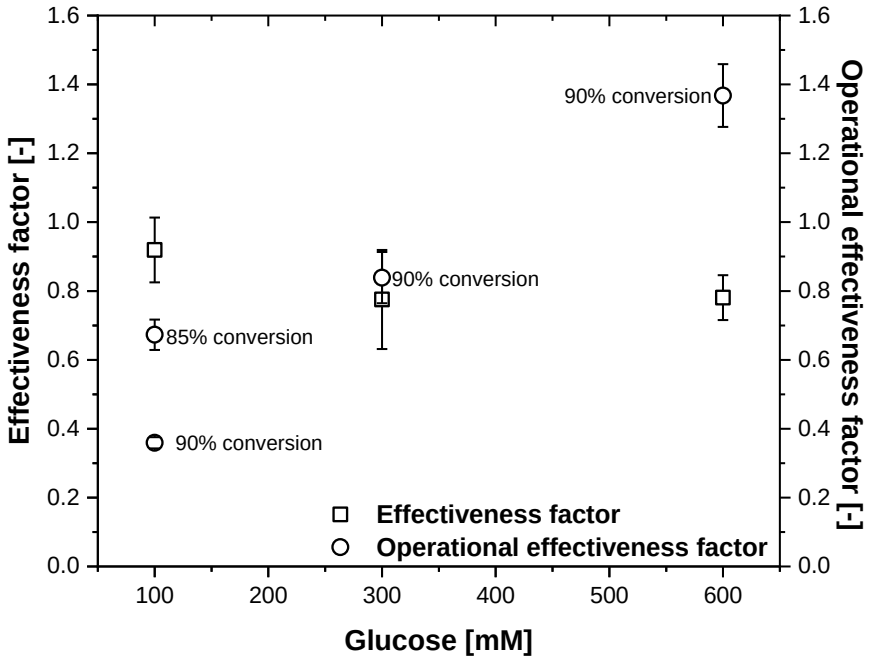

Figure 46. Comparison of effectiveness and operational effectiveness factors. Fine bubble aeration (2 µm sintered frit). 8.2 g carriers, 1000 rpm, 35 ± 1°C, initial volume 200 mL, 1 vvm, pH 5.5 ± 0.2. Glucose solutions were prepared in 10 mM sodium acetate buffer at pH 5.3, enzyme loading on carriers: 7.52 mg_{GOx} $g_{carrier}^{-1}$, antifoam 204: 0.28 ± 0.06 mg mL^{-1}, calculated activity of catalase (free) / calculated activity of glucose oxidase at immobilization and free enzyme: 1.70 and 4.79, respectively. Error bars show the standard deviation obtained from duplicate measurements. The graph is generated by additionally integrating the results of the supervised B.Sc. thesis [118] and the project work [127].

For the substrate concentration 100 mM below the Michaelis-Menten constant of immobilized glucose oxidase $K_{m,imm}$ 187 ± 54 mM, the operational effectiveness factor η_0 was far below one (0.36 ± 0.02) for 90% yield, since the reaction took longer to reach

90% due to the presence of less substrate in the reaction medium. Therefore, the value of η_0 for reaching 85% yield was calculated as 0.67 ± 0.04 that the reaction was almost complete and the residual substrate in the bulk phase was quite low, resulting in a longer time to increase the reaction yield for 5%.

The effectiveness factor was calculated as close to 1 (0.92 ± 0.09) at 100 mM substrate concentration, indicating that 8% loss of activity occurs in the case of immobilization, confirming that no significant difference was observed between the reaction rate determined for immobilized glucose oxidase with free catalase and the free form of both enzymes. As more hydrogen peroxide was generated within the carriers at a higher glucose concentration, a decrease in the effectiveness factor (0.78) was observed and the time to reach 90% yield became longer (Figure 47). Although the equal effectiveness factor was obtained at 300 mM (0.78 ± 0.14) and 600 mM (0.78 ± 0.07) substrate concentration, the operational effectiveness factor η_0 (1.37 ± 0.09) was increased by 63% at 600 mM glucose compared to the conditions using 300 mM (0.84 ± 0.07). This result confirms the severe deactivation of the immobilized glucose oxidase by the accumulated hydrogen peroxide, which causes a decrease in the conversion rate and an increase in the process time, as shown in Figure 47.

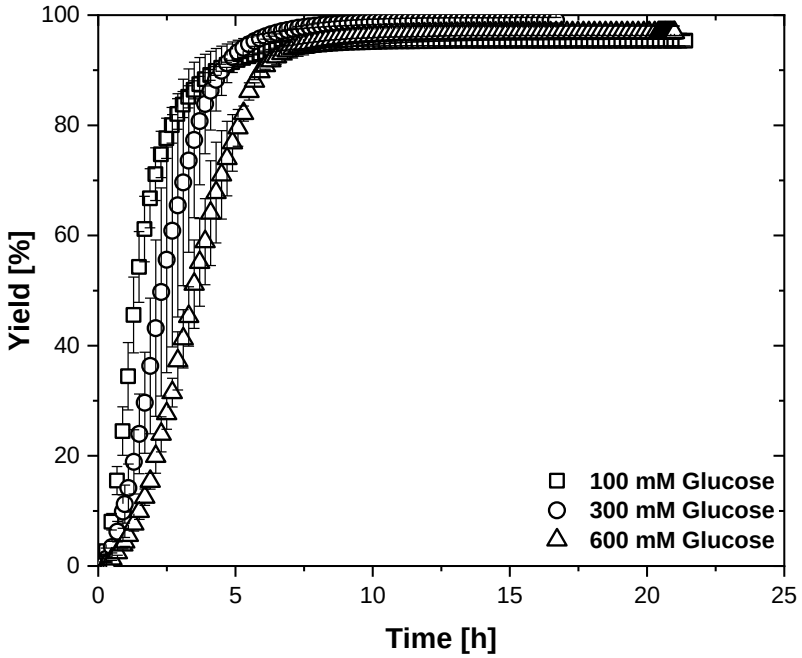

Figure 47. Comparison of conversion rate at different substrate concentrations under fine bubble aeration: 2 µm sintered frit sparger. 8.2 g carriers, 1000 rpm, 35 ± 1°C, 1 vvm, pH 5.5 ± 0.2, initial volume 200 mL. Glucose solutions were prepared in 10 mM sodium acetate buffer at pH 5.3, enzyme loading on carriers: 7.52 mg_{GOx} $g_{carrier}^{-1}$, catalase (free) / calculated activity of glucose oxidase (immobilized): 1.70, antifoam 204: 0.28 ± 0.06 mg mL^{-1}. For 600 mM the duplicate experiment was performed with the ratio of catalase (free) to the calculated activity of glucose oxidase (immobilized) is 4.79, not obtaining an enhancement in the conversion rate. Error bars show the standard deviation obtained from duplicate measurements. The graph is generated by additionally integrating the results of the supervised B.Sc. thesis [118] and the project work [127].

To determine the optimal operating substrate concentration, productivity for glucose oxidase, yield, and process time were calculated at three different substrate concentrations and are listed in Table 15. For a 300 mM substrate concentration, the same immobilized glucose oxidase was employed for batch 2 of the repetitive batches following the completion of the first batch. In the case of substrate concentrations of 100 mM and 600 mM, the use of fresh immobilisates was applied during duplicated experiments, and no repetitive batches were conducted.

Table 15. Comparison of the performance of fine bubble aeration at different substrate concentrations. 8.2 g carriers, 35 ± 1°C, 1000 rpm, 7.52 mg_{GOx} $g_{carrier}^{-1}$, glucose solutions in 10 mM sodium acetate buffer pH 5.5 ± 0.2, initial volume before titration 200 mL, 1 vvm, 0.28 ± 0.06 mg mL^{-1} antifoam 204. The experiments were conducted in duplicate.

Catalyst productivity [$g_{product}$ $g_{immobilizedGOx}^{-1}$]	**Yield** [%]	**Product** [g]	**Process time** [h]	**Glucose oxidase-specific activity** [U mg_{GOx}^{-1}]
Fine bubble aeration with 2 µm sintered frit				
100 mM Glucose in a single batch				
Batch 1: 58 ± 0	90.1	3.5 ± 0.0	4.3 ± 0.3	2.47 ± 0.13
300 mM Glucose used in repetitive batches				
Batch 1: 173 ± 0 Batch 2: 174 ± 0	90	10.6 ± 0.0 10.6 ± 0.0	4.5 ± 0.9 8.8 ± 0.9	4.25 ± 1.15 2.28 ± 0.27
Sum of repetitive batches				
	90	21.2	13.3	
600 mM Glucose in a single batch				
Batch 1: 347.0 ± 0.2	90	21.2 ± 0.0	6.0 ± 0.0	

When comparing productivity for glucose oxidase and process time for all three glucose concentrations, the productivity for glucose oxidase is lower at 100 mM substrate concentration. It was optimal to run the reactor at 600 mM substrate concentration, since the process time reduced by a factor of 2.2 when compared to the sum of operation time for repetitive batches at 300 mM substrate concentration to reach the equal amount of product (Table 15).

4.9. Statistical analysis using the ANOVA method

In this section, the differences in the yield values for the biocatalytic oxidation of glucose were investigated by the method analysis of variance ANOVA (F-test). It is a one-way analysis of variance method used to examine the intergroup and the intragroup for more than two groups [137]. The significance probability value (P) of 0.05 was considered, while investigating the differences in the final yield values of biocatalytic oxidation. T. K. Kim [138] reported the relationship between the significance probability value (P) and the F distribution, which is the ratio of the intergroup variance to the intragroup variance, as shown in Equation 30. The maximum

conversion that is possible was determined by the thermodynamics of the process and the final yield values for all experiments are listed in Table 16.

$$F = \frac{\sum_{i=1}^{G} n_i \cdot (\overline{Y_i} - \overline{Y})^2/(G-1)}{\sum_{ij=1}^{n} n_i \cdot (Y_{ij} - \overline{Y_i})^2/(A_t - G)} \qquad (30)$$

where G is the number of groups, n is the number of observations of the group i, $\overline{Y}$ is the overall mean, Y_{ij} is the j^{th} observational value of a group i, A_t is the total number of measurements

Table 16. Summary of the final yield values. 8.2 g carriers, 35 ± 1°C, 10 mM sodium acetate buffer at pH 5.5 ± 0.2, initial volume before titration 200 mL. One-way Anova analysis was performed in Microsoft Excel 2016. Further details regarding group numbers are provided in the Appendix A.2.2.

Group								
n	**1**	**2**	**3**	**4**	**5**	**6**	**7**	**8**
1	93.6	94.7	92.8	99.4	96.0	98.3	97.3	91.7
2	91.3	98.8	97.6	98.7	97.7	96.6		96.3
3		99.5						
n	**9**	**10**	**11**	**12**	**13**	**14**	**15**	**16**
1	96.1	95.6	96.9	95.0	94.6	99.3	97.9	90.1
2	96.1	95.3	97.5		98.7			

Source of variation	**Sum of squares**	**Degree of freedom**	**Mean sum of squares**	**F**	**p**
Intergroup variance	121.9 $\sum_{i=1}^{G} n_i \cdot (\overline{Y_i} - \overline{Y})^2$	15.0 $G-1$	8.1 $\sum_{i=1}^{G} n_i \cdot (\overline{Y_i} - \overline{Y})^2/(G-1)$	2.0	0.1
Intragroup variance	50.0 $\sum_{ij=1}^{n} n_i \cdot (Y_{ij} - \overline{Y_i})^2$	12.0 $A-G$	4.2 $\sum_{ij=1}^{n} n_i \cdot (Y_{ij} - \overline{Y_i})^2/(A_t - G))$		
Total	171.8	27.0 A			

The F value was calculated as 2.0 as the ratio of the mean sum of squares of the intergroup to the intragroup. Based on the F distribution graph published by T. K. Kim [138], the significance probability value (P) was calculated as 0.1. The F-distribution having values above the significance level of 0.05 means that the null hypothesis stated above can be rejected. This result indicates that there was no significant variation between the final values of yield for all biotransformation reactions (average yield: 96.2 ± 2.5%) at the 95% (p = 0.1 > 0.05) confidence level.

4.10. Interim summary

In this section, an overview of the approaches to overcome the internal diffusion limitations is given. To describe the effect of immobilization on the glucose oxidase mass-specific reaction rate, the kinetic parameters for immobilized and free enzymes were determined.

- Comparable glucose oxidase mass-specific reaction rates were obtained for immobilized 2.27 ± 0.33 U mg_{GOx}^{-1} and free glucose oxidase 2.47 U mg_{GOx}^{-1} when the enzyme was not saturated with its substrate glucose (100 mM).
- The use of enzymes in their free form increased the glucose oxidase-specific activity when the substrate glucose concentration (300 mM, 600 mM and 1000 mM) was higher than the Michaelis-Menten constants of free and immobilized glucose oxidase for the substrate glucose (164 ± 34 mM and 187 ± 54 mM, respectively). Consequently, a higher glucose oxidase-specific activity of 8.08 U mg_{GOx}^{-1} was obtained with free glucose oxidase compared to immobilized glucose oxidase of 6.65 ± 0.62 U mg_{GOx}^{-1}.
- The reaction rate equation was modified to account for the deactivation of glucose oxidase and the effectiveness factor. The reaction model was used to estimate the reaction performance.
- However, at a higher substrate concentration, a higher amount of by-product hydrogen peroxide was produced within the carriers. The application of threefold the amount of co-immobilized catalase at 300 mM and the tripled amount of free catalase at 600 mM glucose concentration, separately, did not increase the glucose oxidase mass-specific reaction rate, which is one of the major limitations of this study.
- The optimal substrate concentration was investigated within the investigations of the diffusion limitations and the effectiveness factor for the application of the immobilized glucose oxidase in a rotating packed bed reactor was determined.
- The stability of the immobilized glucose oxidase was higher at the substrate concentration of 25 mM. However, the productivity for the enzyme glucose oxidase was lower at 25 mM and 100 mM substrate concentration. To achieve enhanced productivity for glucose oxidase, the reactor should be operated at a substrate glucose concentration of 600 mM. This approach resulted in a process time that was 2.2 times shorter than the sum of the running times of repetitive batches operated at a substrate concentration of 300 mM, which yielded an equivalent amount of product.
- For all biotransformation reactions, there was no significant difference between the final yield values.

5. Discussion and outlook: A process engineering perspective

In oxidative biocatalytic reactions, in which molecular oxygen is utilized as a secondary substrate, the reaction rate is constrained by the inadequate oxygen mass transfer rate and its solubility in the reaction medium. During the course of project development, the issue was addressed by implementing a higher volume-specific surface area, which enabled a higher mass transfer rate of molecular oxygen as well as increased local oxygen concentrations in the liquid medium through the use of fine bubble technology. The use of fine bubble technology in previous studies has demonstrated its potential benefit in enhancing mass transfer rates and maintaining enzyme stability in conventional stirred tank and bubble column reactors [24, 61-63, 139-140]. Nevertheless, the question of the applicability of fine bubbles in practical applications remained unanswered.

The objective of the second phase of the project was to conduct studies with the aim of providing answers to the question of the applicability of the fine bubble technology in different reactor concepts, thereby expanding the scope of fine bubbles. Packed bed bioreactors offer several advantages, including the ability to achieve a high conversion to volume ratio. This is due to the fact that the reactor volume is mostly filled with enzymes, immobilized on carriers. This advantage was utilized in the second phase of the study, where a rotating packed bed reactor was employed. The SpinChem® vessel V2 with a rotating packed bed basket S2 was selected for this study due to its promising intensification potential in biocatalytic reactions. A cooperation with the stakeholder SpinChem AB was established to effectively explore the research gaps in this project in collaboration of the Institute of Technical Biocatalysis and the Institute of Multiphase Flows [41,141].

The limitations of mass transfer (oxygen mass transfer and diffusion limitations in the rotating packed bed reactor) and the associated challenges were addressed through the presentation of experimental results, which were supported by reaction rate modeling (Equation 26) and simulations (Figure 44 and Figure 45). This research demonstrates exemplary the efficient utilization of oxidases that suffer from limited oxygen availability, which represents a significant challenge in oxidative biocatalytic processes. The next section will present the techno-economic performance of immobilized glucose oxidase packed in a rotating bed basket in the modified SpinChem® vessel to clearly state the benefit of the fine bubble technology in the innovative SpinChem® rotating bed reactor.

5.1. Process considerations

To evaluate the performance of the SpinChem® vessel V2 with a rotating packed bed basket S2, which was aerated with fine bubbles, the success factors listed by P. Tufvesson [112] were considered for this study. Table 17 presents a comparison of the success factors calculated from the outcome of Figure 35 for fine bubble aeration and macrobubble aeration.

$$Productivity\ [g\,L^{-1}h^{-1}] = \frac{mass\ of\ product}{reaction\ volume \cdot process\ time} \quad (31)$$

$$Productivity\ of\ GOx\ [g_{product}\,g^{-1}_{GOximmobilized}] = \frac{mass\ of\ product}{mass\ of\ glucose\ oxidase} \quad (32)$$

Table 17. Process considerations. 8.2 g carriers, 35 ± 1°C, 1000 rpm, 7.52 $mg_{GOx}\ g_{carrier}^{-1}$, 600 mM glucose in 10 mM sodium acetate buffer pH 5.5 ± 0.2, initial volume before titration 200 mL, 1 vvm, 0.28 ± 0.06 mg mL^{-1} antifoam 204.

Catalyst productivity [$g_{product}\ g_{immobilizedGOx}^{-1}$]	**Yield** [%]	**Product** [g]	**Process time** [h]	**Product concentration** [$g\ L^{-1}$]
Macrobubble aeration with open tube (orifice diameter: 2 mm)				
107 ± 8	27.8 ± 2.3	6.6 ± 0.3	21	28.2 ± 0
49.6 ± 3.5	12.9 ± 0.9	3.0 ± 0.1	10	14.1 ± 0.9
Fine bubble aeration with 2 µm sintered frit				
373 ± 5	96.8 ± 1.2	22.8 ± 0.3	21	71.7 ± 0.0
371 ± 6	96.2 ± 1.6	22.7 ± 0.4	10	71.4 ± 0.2
Factors for economically acceptable biocatalytic processes applying immobilized biocatalysts [112]				
50-100	>90	-	-	> 50

A final yield of 96.8 ± 1.2% was measured after 21 h for fine bubble aeration (2 µm sintered frit), while the yield measured for macrobubble aeration (open tube: 2mm orifice diameter) at the equal process time was 27.8 ± 2.3%. For the process under fine bubble aeration the operating time was determined to be 10 h, as no significant increase in product concentration was observed for the remaining 11 h. 22.7 ± 0.4 gram (calculated) of product was produced after 10 h and the final product amount at 21 h was calculated to be 22.8 ± 0.3 g of product. For the process under macrobubble aeration, a yield of 27.8 ± 2.3% (6.55 ± 0.27 g product calculated) was measured at the identical operation time of 21 h. The enhanced reaction rate achieved through the utilization of fine bubble aeration led to a significant increase in productivity for glucose oxidase (373 ± 5 $g_{product}\ g_{immobilisedGOx}^{-1}$), with a 3.5-fold improvement observed at an identical operational duration of 21 hours in comparison to macrobubble aeration, where a productivity of 107 ± 8 $g_{product}\ g_{immobilisedGOx}^{-1}$ was obtained.

The determined success factors are within the range of the parameters determined for economically feasible biocatalytic processes. The established biocatalytic oxidation process under fine bubble aeration with the SpinChem® vessel V2 with a rotating packed bed basket S2 meets the industrial process requirements in terms of productivity for glucose oxidase, yield and product concentration.

5.2. Techno-economic analysis

The focus of this section is to evaluate the techno-economic analysis of a lab-scale SpinChem® vessel V2 with a rotating packed bed basket S2 with immobilized glucose oxidase. Its performance under fine bubble aeration (2 µm sintered frit) was compared to macrobubble aeration (open tube with a 2 mm orifice diameter) at 300 mM substrate concentration, where the stability of the immobilized glucose oxidase was investigated in section 4.6. The results of two repetitive batches under fine bubble aeration were compared to a single batch under macrobubble aeration, as shown in Figure 48.

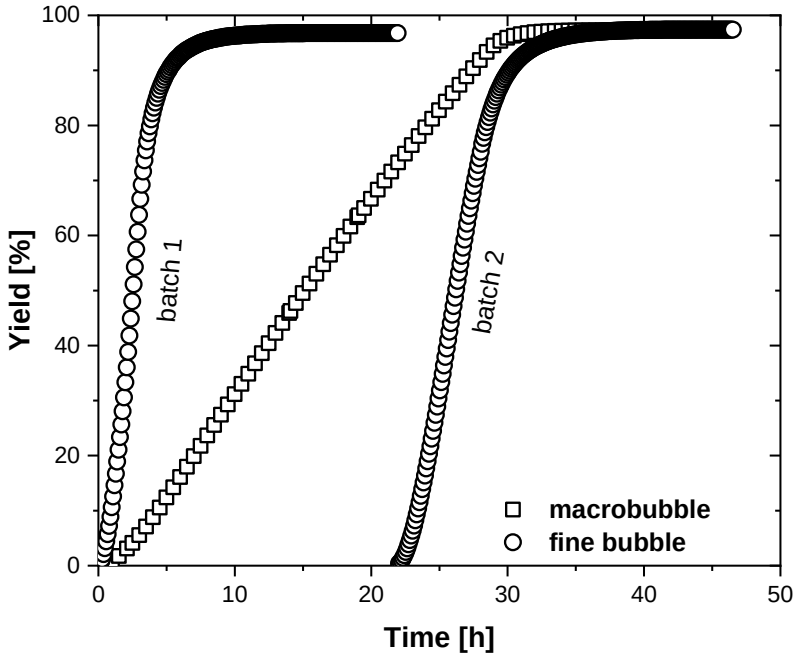

Figure 48. Comparison of the performance immobilized glucose oxidase with repetitive batches. Fine bubble (2 µm sintered frit) and macrobubble aeration (open tube: orifice diameter: 2 mm) in SpinChem® vessel V2 with a rotating packed bed basket S2. 8.2 g carriers, 1000 rpm, 35 ± 1°C, 1 vvm, initial volume 200 mL, pH 5.5 ± 0.2, 300 mM glucose solution in 10 mM sodium acetate buffer at pH 5.3, enzyme loading on carriers: 7.52 mg_{GOx} $g_{carrier}^{-1}$, catalase (free) / calculated activity of glucose oxidase (immobilized): 1.70, antifoam 204: 0.28 ± 0.06 mg mL^{-1}. The graph is generated by integrating the results of the supervised B.Sc. thesis [118].

For the process under fine bubble aeration, 7.5 h are required to reach 95.0% yield and to produce 11.2 g (calculated) product for batch 1, while the process time was increased by a factor of 3.9 for macrobubble aeration to produce the equal amount of product under identical operating conditions (Table 18). Since the final yield value of 96.8% was achieved in the first batch under fine bubble aeration, the second batch was carried out using the same carriers with immobilized glucose oxidase. The immobilized glucose oxidase showed the performance of the final yield value of 97.4% for batch 2 of the repetitive batches under fine bubble aeration.

Table 18. Performance of the immobilized glucose oxidase in a rotating packed bed reactor. 8.2 g carriers, 1000 rpm, 35 ± 1°C, initial volume 200 mL, 1 vvm, pH 5.5 ± 0.2. Glucose solution 300 mM was prepared in 10 mM sodium acetate buffer at pH 5.3, enzyme loading on carriers: 7.52 mg_{GOx} $g_{carrier}^{-1}$, catalase (free) / calculated activity of glucose oxidase (immobilized): 1.70, antifoam 204: 0.28 ± 0.06 mg mL^{-1}. The graph is generated by integrating the results of the supervised B.Sc. thesis [118].

Batch	Productivity for glucose oxidase [$g_{product}$ $g_{immobilizedGOx}^{-1}$]	Yield [%]	Product [g]	Process time [h]
	Macrobubble aeration with open tube (orifice diameter: 2 mm)			
1	183.1	95.0	11.2	29.2
1	187.4	97.3	11.4	35.7
Repetitive batches	**Fine bubble aeration with 2 µm sintered frit**			
1	183.0	95.0	11.2	7.5
1	186.5	96.8	11.4	15.1
2	184.9	95.0	11.2	10.7
2	189.6	97.4	11.5	20.6
	Sum of repetitive batches under fine bubble aeration			
	(186.5+189.6) 376.1		(11.4+11.5) 22.9	(15.1+20.6) 35.7

The total amount of product from the repetitive batches (batch 1 and batch 2) was calculated as 22.9 g at 35.7 h, while for macrobubble aeration, the amount of product produced was calculated to be 11.4 g at 35.7 h, demonstrating the enhanced performance of the immobilized glucose oxidase under fine bubble aeration, where the product amount was doubled using the advantage of biocatalyst reuse. The results obtained with fine bubble aeration are promising for further biocatalytic reactions utilizing oxygen, and therefore, the approach of the economic evaluation of the innovative reactor concept SpinChem® vessel V2 with a rotating packed bed basket S2 under fine bubble aeration with immobilized glucose oxidase is described by the following parameters [142,143]:

- Capital expenditure (CapEx) was determined for the cost drivers of the process, which are determined as the enzymes (glucose oxidase and catalase) and the ReliZyme™ HFA 403 M-grade carrier for this study (Figure 49).

$$CapEx = m_{\mathrm{GOx}} \cdot price_{\mathrm{GOx}} + m_{\mathrm{catalase}} \cdot price_{\mathrm{catalase}} + m_{\mathrm{carriers}} \cdot price_{\mathrm{carriers,\ GOx}} \qquad (33)$$

where m_{GOx} , m_{catalase} and m_{carriers} are the masses of the enzymes glucose oxidase, catalase and carriers in g, $price$ denotes the unit price of the component in Euro per gram.

Operating expenditure (OpEx) was calculated for the components added to the reaction medium without incorporating the cost of deionized water and oxygen supplied as compressed air.

$$OPEx = \sum_{i=1}^{n} m_i \cdot price_i \qquad (34)$$

where m_i is the mass of component i in g and $price$ denotes the unit price of the component i.

The unit price of the enzymes, carriers and feed components in the reaction medium are summarized in Table 19. A graphical representation of the cost-percent distribution of the components required for the biocatalytic oxidation of glucose is presented in Figure 49, where the glucose oxidase was determined to be the cost-driven biocatalysis.

Table 19. Cost of the components used for the biocatalytic oxidation of glucose.

	Unit	Consumed	Price [Euro per unit]	Price [Euro]
CapEx				
Glucose oxidase, GOx (EC Number: 1.1.3.4)	g	0.08	624.00[86]	47.17
ReliZyme™ HFA 403 M grade carriers	g	8.20	0.78[87]	6.40
Catalase (EC Number: 1.11.1.6)	g	0.01	91.00[88]	1.16
OpEx				
D-(+)-glucose	g	10.81	0.03[144]	0.36
Sodium acetate	g	0.13	0.11[145]	0.01
Acetic acid	L	0.00	33.50[146]	0.001
1 M NaOH Sodium hydroxide	g	2.3	0.02[147]	0.05
Oxygen as compressed air	mL min^{-1}	200	0	0
Deionized water in reaction volume	mL	200	0	0

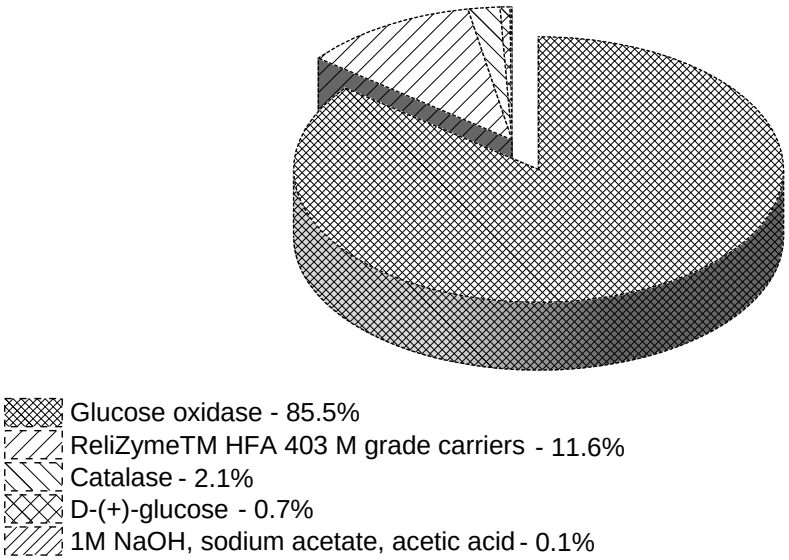

Figure 49. A cost-percent distribution of the components utilized in the biocatalytic oxidation of glucose.

- *Total expenditure* (TotEx) was calculated as the ratio of the sum of capital and operating expenditure per gram of product.

$$Total\ expenditure\ =\ \frac{CapEx + OpEx}{mass\ of\ product} \qquad (35)$$

- Techno-economic performance (TEP) was calculated to evaluate the performance of the SpinChem® vessel V2 with a rotating packed bed basket S2 with a focus on the production rate, productivity for glucose oxidase, and the total expenditure costs.

$$TEP\ =\ \frac{mass\ of\ product \cdot productivity\ of\ glucose\ oxidase}{process\ time \cdot total\ expenditure} \qquad (36)$$

- Relative techno-economic performance (TEP_{relative}) indicates the enhancement factor by the ratio of techno-economic performance (TEP) obtained under fine bubble (2 µm sintered frit) and macrobubble aeration (open tube with a 2 mm orifice diameter). The techno-economic performance (TEP) of the immobilized glucose oxidase under fine bubble aeration was compared with the reference condition: macrobubble aeration (Table 20).

$$TEP_{\text{relative}} = \frac{TEP_{\text{fine bubble}}}{TEP_{\text{macrobubble}}} \qquad (37)$$

Table 20. Comparison of the techno-economic performance (TEP) of the immobilized glucose oxidase (GOx) in a rotating packed bed reactor. 8.2 g carriers, enzyme loading on carriers: 7.52 mgGOx $g_{carrier}^{-1}$, catalase (free) / calculated activity of glucose oxidase (immobilized): 1.70, antifoam 204: 0.28 ± 0.06 mg mL^{-1}, 1000 rpm, 35 ± 1°C, 1 vvm, initial volume 200 mL, pH 5.5 ± 0.2. Glucose solution (300 mM) was prepared in 10 mM sodium acetate buffer at pH 5.3. The graph is generated by integrating the results of the supervised B.Sc. thesis [118].

CapEX [Euro]	OpEX [Euro]	TotEx [Euro per gram product]	Production rate [g h^{-1}]	Product concentration [$g_{product}$ L^{-1}]	Productivity [$g_{product}$ L^{-1} h^{-1}]	Productivity for glucose oxidase [$g_{product}$ $g_{immobilizedGOx}^{-1}$]	TEP	$TEP_{relative}$
Batch 1: Macrobubble aeration with open tube (orifice diameter: 2 mm)								
55	0.4	4.8	0.3	44.3	1.2	187.4	12.5	1
Repetitive batches: Fine bubble aeration with 2 µm sintered frit								
Batch 1								
55	0.4	4.8	0.8	44.1	2.9	186.5	29	
Batch 2								
1.2	0.4	0.1	0.6	44.4	2.2	189.6	760.6	
Overall: Fine bubble aeration with repetitive batches								
56	0.8	2.5	0.6			376.1	96.9	7.8

The capital and operating costs of the oxidative biocatalytic process under macrobubble (open tube with a 2 mm orifice diameter) aeration were calculated as 55 Euro and 0.4 Euro for one batch, respectively, and the values are identical for batch 1 under fine bubble aeration (2 µm sintered frit), since the equal amount of enzymes, carriers and buffers were used. However, due to the enhanced reaction rate (Figure 48), the production rate (Table 20) was increased by a factor of 2.7 for fine bubble aeration (0.3 g h^{-1}: macrobubble, 0.8 g h^{-1}: fine bubble) as demonstrated in Figure 50.

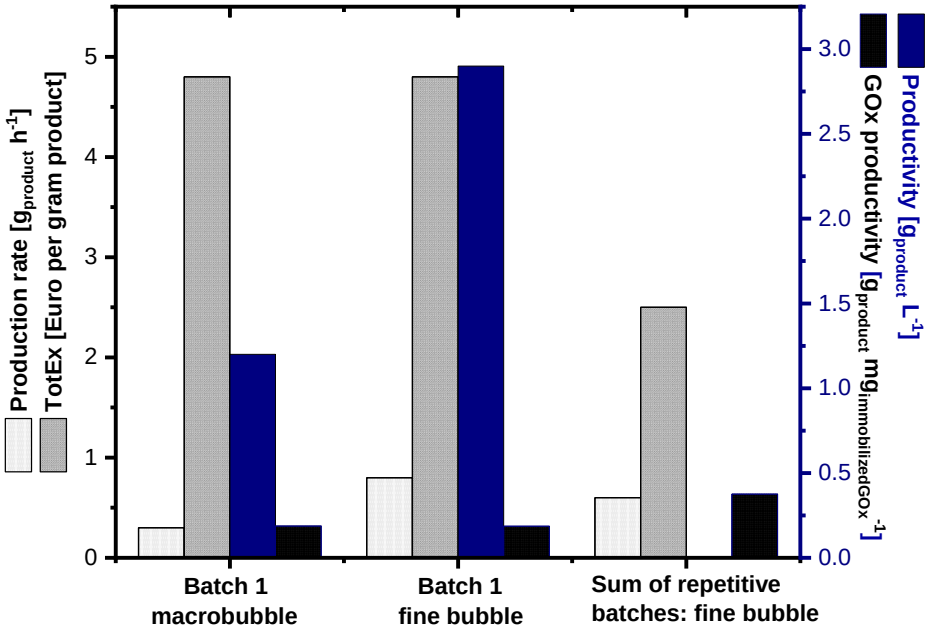

Figure 50. Comparison of performance indicators and the relative TEP for macrobubble (open tube) and fine bubble (2 µm sintered frit) aeration. Performance indicators: (production rate, productivity and total expenditure).

All reactions in Figure 50 reach a final yield value above 96% with the same amount of immobilized glucose oxidase. The comparable productivities for glucose oxidase were measured for the single batch reaction under macrobubble aeration (open tube with 2mm orifice diameter:187.4 $g_{product}$ $g_{immobilizedGOx}^{-1}$) and for each batch of repetitive batches under fine bubble aeration (2 µm sintered frit sparger - batch 1: 186.5 $g_{product}$ $g_{immobilizedGOx}^{-1}$ and batch 2: 189.6 $g_{product}$ $g_{immobilizedGOx}^{-1}$).

The total expenditure was diminished by 48% with the application of the second batch under fine bubble aeration because the immobilized glucose oxidase was reused, which is the cost driver of the process (see Figure 49). The techno-economic performance of immobilized glucose oxidase with a rotating packed bed reactor under fine bubble aeration was calculated using Equation 36 and compared with macrobubble aeration with Equation 37. Taking advantage of the doubled production rate and productivity for glucose oxidase, the fine bubble aeration led to a 7.8 TEP - improvement of the SpinChem® vessel V2 with a rotating packed bed basket S2.

5.3. Challenges of the application of the SpinChem® rotating packed bed reactor

In the field of oxidative biocatalysis, oxidases function by oxidizing low-value compounds into high-value or intermediate molecules, a process that requires molecular oxygen as a substrate. The most significant constraints are related to the mass transfer and solubility of oxygen, as well as the potential for enzyme deactivation in multiphase systems when the biocatalyst interacts with the hydrophobic gas-liquid interface [23, 24]. To achieve an effective reactor design, it is essential to consider the approaches that can be applied to overcome the limitations, as well as the potential drawbacks associated with the implementation of these approaches [23].

The novelty of this work is the use of fine bubble aeration for a biocatalytic reaction in the SpinChem® vessel with a rotating packed bed basket, where the mass transfer of oxygen was improved. The biocatalytic oxidation process as well as the productivity for glucose oxidase were significantly intensified. The findings of this study contribute to the sustainability of biotransformation processes by reducing the required aeration rate and enhancing the techno-economic performance of immobilized glucose oxidase packed in a rotating bed basket in a SpinChem® vessel, where the enzyme glucose oxidase was effectively reused.

One of the key challenges in this research was to overcome diffusion limitations in the rotating packed bed reactor. The kinetic investigations were conducted using the enzyme glucose oxidase in both its free and immobilized forms to determine the affinity of the enzyme glucose oxidase for its substrate glucose. The Michaelis-Menten constant for free glucose oxidase in SpinChem® reactor was determined to be 164 ± 34 mM, which is higher than 73.1 ± 6.87 mM in a standard configuration of a batch reactor [122]. The affinity of glucose oxidase for its immobilized form in the SpinChem® rotating packed bed reactor was found to be close to that of its free form, with a value of 187 ± 54 mM. Given that the Michaelis-Menten constants for free and immobilized glucose oxidase are similar in value and fall within the standard deviation range, the question arises as to whether the observed reaction was limited by the oxygen provided to the reaction medium. This could restrict the achievement of a higher substrate affinity. As illustrated in Figure 33, the reaction rate is not oxygen-limited at a lower substrate concentration of 25 mM, and similar reaction rates for the substrate concentration of 25 mM were achieved for immobilized and free glucose oxidase application (Figure 36). It was demonstrated that the reaction rate was limited by oxygen availability at higher substrate concentrations of 300 mM (Figure 31).

Another challenge is to maintain the biocatalytic performance in the rotating packed bed reactor for repetitive batches. Severe deactivation k_{deac} = 0.035 ± 0.07 h^{-1} of immobilized glucose oxidase was observed at a substrate concentration of 300 mM. The deactivation of the immobilized glucose oxidase was determined to be caused by the by-product hydrogen peroxide, as the deactivation of the enzyme glucose oxidase was lower at a lower substrate concentration (Table 12). It was unexpected that the co-immobilization of catalase, which decomposes the by-product hydrogen peroxide

within the carriers, did not improve the reaction rate. The reaction rate was observed to be enhanced when both enzymes were used in their free form, with a tripled catalase concentration.

Visualization of the interior of the stainless-steel rotating packed bed basket was challenging, which could enable to investigate the internal fluid flow. The answer to the question of whether fine bubbles can enter the rotating packed bed reactor, and the pores of the carriers is open. The outcome of this investigation would help to understand the mechanism of biocatalytic intensification. Since the polymer optical fiber is very sensitive to bending, further investigation of the oxygen concentration in a rotating packed bed reactor could not be performed. The relative flow in the packed bed reactor could be increased by using carriers with larger diameters. To increase the relative flow, alginate beads were prepared as shown in Figure 51.

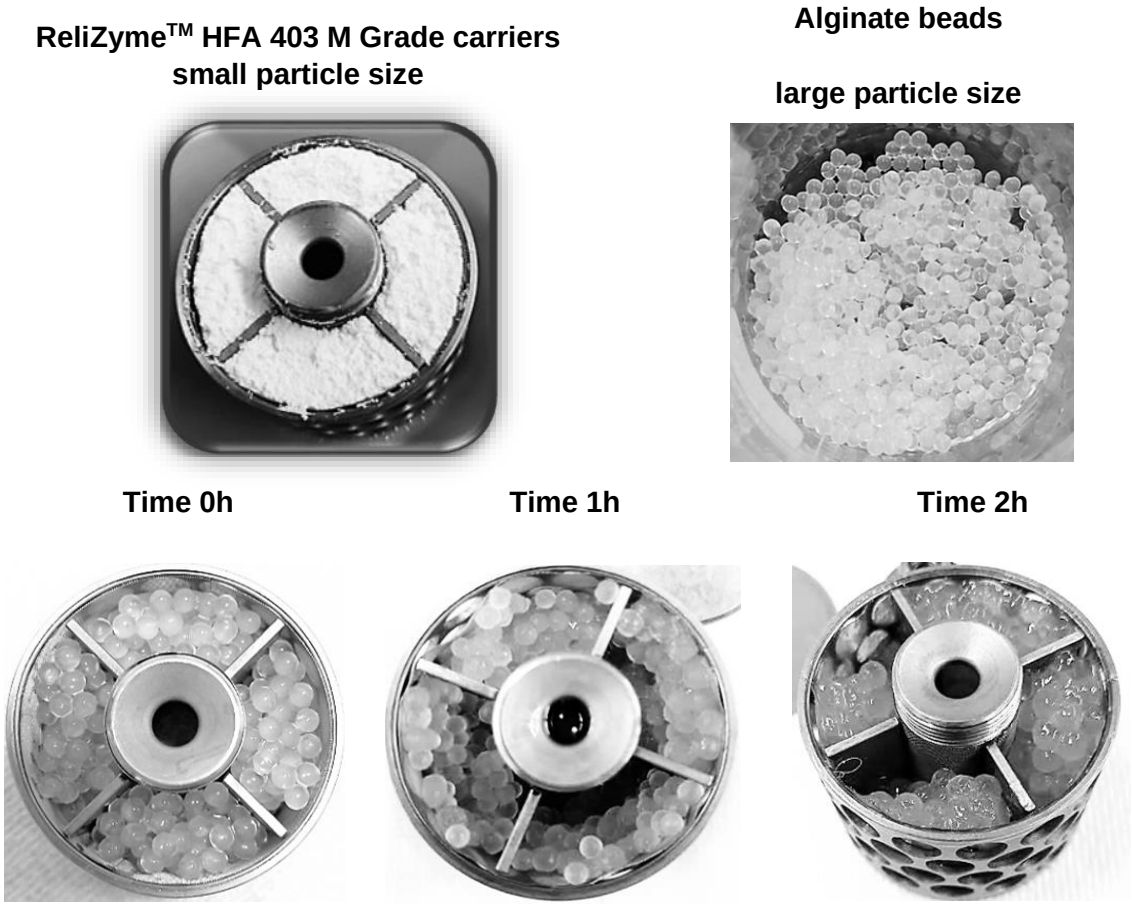

Figure 51. Qualitative investigation of the alginate beads with a larger carrier diameter in a rotating packed bed reactor.

The alginate beads were melted at 37°C after 2 h. Therefore, no further quantitative investigations were performed. Furthermore, carriers with larger diameters than the ReliZyme™ HFA 403 M grade carriers are not available on the market. Stable carriers with larger diameters and appropriate functional groups could be manufactured in cooperation with commercial suppliers for further investigations.

5.4. Further works

This thesis presents an analysis and characterization of an innovative reactor concept: a SpinChem® vessel V2 with a rotating packed bed basket S2 through the use of a sintered frit sparger with a pore size of 2 µm. The superiority of fine bubble aeration (2 µm sintered frit) over macrobubble aeration (open tube with a 2 mm orifice diameter) in this novel reactor setup was demonstrated. Further investigations are necessary to characterize the superficial velocity through the rotating packed bed reactor for the characterization of the pressure drop according to the Ergun Equation [148]. The pressure drop inside the packed bed depends on the carrier diameter. As the carrier diameter decreases, the pressure drop increases, resulting in lower conversion at time t. By increasing the superficial velocity inside the rotating packed bed reactor, the pressure drop could be minimized, allowing a higher conversion at time t [149].

Magnetic resonance imaging (MRI) is a promising alternative for the characterization of the superficial velocity inside the packed bed reactor and is applied at the Technical University of Hamburg, where process imaging techniques are used for the determination of the local phase distributions in multiphase flows [150]. The technique could be applied to the study of the oxygen concentration profile and the flow field of fine bubbles in the rotating packed bed reactor, which is the challenge in this work due to the limitations in the technical applicability of the visualization of the stainless-steel rotating packed bed basket. In addition to the oxygen concentration profile in the rotating packed bed reactor, it is critical to investigate the local oxygen transfer rate as well as fields around fine bubbles and the oxygen consumption by the immobilized glucose oxidase, considering the boundary layer conditions. An alternative oxidase could be used in a rotating bed reactor to facilitate the application of fine bubble technology and to extend the use of oxidases in a rotating bed reactor.

5.5. Most important advances

The intensification of bioprocesses in multiphase systems, particularly gas-liquid ones, is a highly desirable objective, not only in aerobic fermentation, but also in oxygen-dependent biocatalytic transformation reactions. Previously published studies have demonstrated the performance of fine bubble technology for the intensification of biocatalytic processes in a stirred tank reactor. This approach involves the use of fine bubbles, which increases the surface area per volume of gas, available for mass transfer at the gas-liquid interphase [24, 61-63].

The primary objective of this work is the integration of fine bubble technology with 2 µm sintered frit sparger into a modified SpinChem® vessel. The subject of the work is of significant practical relevance, and the findings have the potential for practical application in biotechnology. The most significant advancements are presented as follows:

- The results of this study demonstrate, for the first time, the successful implementation of fine bubble technology in conjunction with immobilized glucose oxidase in a modified SpinChem® vessel V2 with a rotating packed bed basket S2.

- The oxygen concentration was monitored in real-time using an immersed Presens oxygen sensor from PreSens Precision Sensing GmbH (Regensburg, Germany) in a modified SpinChem® vessel throughout the course of the oxygen-dependent biocatalytic oxidation reaction. The data was subjected to analysis with the objective of identifying the limitations in the mass transfer of oxygen, while the molecular oxygen was consumed by the immobilized glucose oxidase.
- The application of repetitive batches using the immobilized glucose oxidase in the rotating packed bed reactor was demonstrated under fine bubble aeration.
- The kinetic parameters were determined in the laboratory-scale reactor, with a volume of 200 mL, rather than in a smaller volume, such as that in a 1.5 mL plastic Eppendorf (Safe-Lock) tube. This approach was applied to reflect the real process conditions, with the understanding that kinetic parameters are specific to the reactor geometry.
- Matlab simulations were conducted for the biocatalytic oxidation process in the novel reactor set-up. The lab-scale techno-economic performance for immobilized glucose oxidase packed in a rotating bed reactor under fine bubble aeration was investigated.

6. Conclusion

The focus of this study is to demonstrate the applicability of fine bubble technology in a novel reactor design: SpinChem® vessel V2 with a rotating packed bed basket S2 integrated with fine bubble aeration. The following findings indicate that fine bubble aeration enabled an efficient biotransformation process, where the techno-economic performance of immobilized glucose oxidase was improved in this modified reactor concept:

- Covalently immobilized glucose oxidase on epoxy-functionalized carriers was utilized in the rotating packed bed reactor with an activity yield of the immobilization of over 98%.
- At the equal volume-specific aeration rate, the volumetric mass transfer was increased by a factor of 3 by changing from macrobubble (22.5 h^{-1}) aeration to fine bubble (67.3 h^{-1}) aeration.
- The oxidative biotransformation reaction was catalyzed by the immobilized glucose oxidase with a yield of 96.2 ± 2.5% using an established enzyme carrier system in the SpinChem® rotating packed bed reactor.
- The highest achievable glucose oxidase-specific activity under fine bubble aeration was found to be 5.82 ± 0.23 U mg_{GOx}^{-1}. The reaction rate was improved by a factor of 12.9 compared to macrobubble aeration under identical conditions at 600 mM substrate concentration, taking advantage of the higher volumetric mass transfer coefficient of fine bubble aeration at 1 vvm. The productivity for immobilized glucose oxidase increased by a factor of 3.5 at the identical operating time of 21 h (373 ± 5 $g_{product}$ $g_{immobilizedGOx}^{-1}$) compared to macrobubble aeration (107 ± 8 g product $g_{immobilizedGOx}^{-1}$).
- At comparable volumetric mass transfer coefficients, fine bubble aeration (1 vvm) reduced the oxygen consumption by 87.5% compared to macrobubble aeration (0.125 vvm), while maintaining similar glucose oxidase mass-specific reaction rates.
- Validation of the reactor design (SpinChem® vessel V2 with a rotating packed bed basket S2 and integrated fine bubble aeration) was carried out in repetitive batches. The process time was reduced by half as a result of the increased reaction rate observed under fine bubble aeration.
- The stability of the immobilized glucose oxidase was longer at the substrate concentration (8.8 mM < $K_{m,immob}$ and 25 mM < $K_{m,immob}$) than in the presence of excess substrate saturation (300 mM > $K_{m,immob}$ and 600 mM > $K_{m,immob}$). The cause of the decrease in enzyme stability was investigated in relation to diffusion limitations.
- Kinetic parameters for free and immobilized glucose oxidase were measured and used in the reaction rate modeling. The Michaelis-Menten constants of the free and immobilized glucose oxidase were determined to be 164 ± 34 mM and

187 ± 54 mM, respectively. The use of the free form of the enzymes increased the reaction rate when the substrate glucose concentration was higher than the Michaelis-Menten constant. Compared to the mass-specific activity of immobilized glucose oxidase of 6.65 ± 0.62 U mg_{GOx}^{-1}, the free form of glucose oxidase yielded a higher glucose oxidase mass-specific activity of 8.08 U mg_{GOx}^{-1}, indicating the presence of diffusion limitations.

- The reaction rate equation was modified by implementing the biocatalyst deactivation constant as well as the effectiveness factor and used to estimate the reaction performance. The reaction rate catalyzed by immobilized glucose oxidase using fine bubbles and macrobubbles was modeled using Matlab simulations. The findings of the simulation were found to be comparable with the experimental results obtained with fine bubbles and demonstrated a satisfactory level of agreement with the experimental results achieved under macrobubble aeration.
- The main challenge in this study was the production of the by-product hydrogen peroxide within the carriers. A tripled amount of co-immobilized catalase at 300 mM and a tripled amount of free form at 600 mM glucose concentration did not increase the glucose oxidase-specific activity to degrade this by-product.
- Compared to macrobubble aeration (187.4 $g_{product}$ $g_{immobilizedGOx}^{-1}$), productivity for glucose oxidase (376.1 $g_{product}$ $g_{immobilizedGOx}^{-1}$) was doubled by applying one batch under fine bubble aeration at 300 mM substrate concentration.
- To increase the productivity for glucose oxidase, it would be ideal to run the reactor at a substrate concentration of 600 mM, as this reduced the process time by a factor of 2.2 compared to repetitive batches at 300 mM substrate concentration for the equal amount of product.
- According to the results of the lab-scale techno-economic performance for immobilized glucose oxidase with a rotating packed bed reactor under fine bubble aeration, glucose oxidase was identified as the cost driver of the process. By using repetitive batches under fine bubble aeration, the total cost was reduced by half. Fine bubble aeration improved the TEP-performance for the SpinChem® rotating packed bed reactor by 7.8 times by doubling the production rate and productivity for glucose oxidase.

This research is an exemplary application of efficient utilization of oxidases that suffer from limited oxygen availability, which is a major challenge in oxidative biocatalytic processes. The biocatalytic oxidation was intensified, the productivity for immobilized glucose oxidase was enhanced, the required aeration rate was reduced, and the techno-economic performance for the immobilized glucose oxidase packed in a rotating bed reactor in the modified SpinChem® vessel was improved, thus addressing the sustainability of biotransformation processes.

Appendix

A.1. Matlab codes

Code 1

```
function [dc] = rate_exp(t,c)

dc=zeros(size(c));

v_max=6.65;          %U/mg
K_oxygen=0.084;      %mM
K_glucose=187;       %mM
c_gox=0.308448;      %mg/ml, %volume of rotating bed reactor = 28 ml)
                      %for a 1.07 gGOX per gram carrier load, 98% immob yield
Csat=0.24042;         %mM @35°C
kla=67.3/60;         %min^-1 @35°C
n=0.82               %effectiveness factor
kdeac= 0.035/60      %min^-1
vforward=(v_max*c(1)*c(2)*(exp(kdeac))/(K_oxygen*c(1)+K_glucose*c(2)+c(1)*c(2)))*n
;
OTR=kla*(Csat-c(2));
dc(1)=-vforward*c_gox;
dc(2)=(-1/2)*vforward*c_gox+OTR;
dc(3)=+vforward*c_gox;
end
```

Code 2

```
inicond=[25, 0.24042, 0]            %mM
t=[0 1000];                          %min
[t_solution,C]=ode45(@rate_exp,t,inicond);
hold on
ylim([0 30]);
plot(t_solution,C(:,1),'-.','Color',[0 0 0],'LineWidth',3);
plot(t_solution,C(:,3),'-','Color',[0 0 0],'LineWidth',3);
legend
xlabel('\fontname{Arial} Time [min]','FontSize',12,'FontWeight','bold','Color',[0
0 0])
ylabel('\fontname{Arial} Concentration
[mM]','FontSize',12,'FontWeight','bold','Color',[0 0 0])
Csat=0.24042;                       %saturationconcinwater @ 35 °C
hold on
meas_time=[];                        %enter the sampling times
glucoseconc=[];                      %enter the substrate concentration measured
hold on
plot (meas_time, glucoseconc,'diamondk','LineWidth',0.5);
gluconicacidconc=[];                  %enter the product concentration measured
hold on
plot (meas_time, gluconicacidconc,'squarek','LineWidth',0.5);
```

Code 3

```
inicond=[300, 0.24042, 0]      L %mM
t=[0 2500];                    %min
[t_solution,C]=ode45(@rate_exp,t,inicond);
hold on
yield=(C(:,3)/300)*100
plot(t_solution,yield,'-.','Color',[0 0 0],'LineWidth',3);
xlabel('\fontname{Arial} Time [min]','FontSize',12,'FontWeight','bold','Color',[0
0 0])
ylabel('\fontname{Arial} Yield [%]','FontSize',12,'FontWeight','bold','Color',[0 0
0])
Csat=0.24042;                  %saturationconcinwater @35°C
hold on
M = readmatrix('datayieldsimulation.xlsx');
fbtime= M(1:221,5);
fbyield= M(1:221,6);
plot(fbtime,fbyield,'o','Color',[0 0 0],'LineWidth',0.5);
hold on
```

Code 4

```
inicond=[300, 0.24042, 0]       %mM
t=[0 2500];                     %min
[t_solution,C]=ode45(@rate_exp,t,inicond);
hold on
yield=(C(:,3)/300)*100
plot(t_solution,yield,'-','Color',[0 0 0],'LineWidth',3);
xlabel('\fontname{Arial} Time [min]','FontSize',12,'FontWeight','bold','Color',[0
0 0])
ylabel('\fontname{Arial} Yield [%]','FontSize',12,'FontWeight','bold','Color',[0 0
0])
Csat=0.24042;                   %saturationconcinwater @35°C
hold on
M = readmatrix('datayieldsimulation.xlsx');
macrobubbletime= M(1:418,2);
macrobubbleyield= M(1:418,3);
plot(macrobubbletime,macrobubbleyield,'square','Color',[0 0 0],'MarkerSize',3);
hold on
```

A.2. Experimental details

A.2.2. Group numbers in Table 16

1. Fine bubble aeration: 1000 rpm, 0.125 vvm, 25 mM substrate glucose, applied enzyme loading on carriers: 1.07 $mg_{GOx}g^{-1}_{carrier}$, calculated activity of catalase / calculated activity of glucose oxidase:1.38. Catalase: free, GOx: immobilized
2. Fine bubble aeration: 1000 rpm, 1 vvm, 25 mM substrate glucose, applied enzyme loading on carriers: 1.07 $mg_{GOx}g^{-1}_{carrier}$, calculated activity of catalase / calculated activity of glucose oxidase:1.38. Catalase: free, GOx: immobilized
3. Fine bubble aeration: 1000 rpm, 1 vvm, 25 mM substrate glucose, applied enzyme loading on carriers: 7.52 $mg_{GOx}g^{-1}_{carrier}$, calculated activity of catalase / calculated activity of glucose oxidase:1.70, antifoam 204: 0.28 ± 0.06 mg mL^{-1}. Catalase: free, GOx: immobilized
4. Fine bubble aeration: 1000 rpm, 1 vvm, 300 mM substrate glucose, applied enzyme loading on carriers: 7.52 $mg_{GOx}g^{-1}_{carrier}$, calculated activity of catalase / calculated activity of glucose oxidase:1.70, antifoam 204: 0.28 ± 0.06 mg mL^{-1}. Catalase: free, GOx: immobilized
5. Fine bubble aeration: 1000 rpm, 1 vvm, 600 mM substrate glucose, applied enzyme loading on carriers: 7.52 $mg_{GOx}g^{-1}_{carrier}$, calculated activity of catalase / calculated activity of glucose oxidase:1.70, antifoam 204: 0.28 ± 0.06 mg mL^{-1}. Catalase: free, GOx: immobilized
6.: Macrobubble aeration: 1000 rpm, 1 vvm, 25 mM substrate glucose, applied enzyme loading on carriers: 1.07 $mg_{GOx}g^{-1}_{carrier}$, calculated activity of catalase / calculated activity of glucose oxidase:1.38. Catalase: free, GOx: immobilized
7. Macrobubble aeration: 1000 rpm, 1 vvm, 300 mM substrate glucose, applied enzyme loading on carriers: 7.52 $mg_{GOx}g^{-1}_{carrier}$, calculated activity of catalase / calculated activity of glucose oxidase:1.70, antifoam 204: 0.28 ± 0.06 m. Catalase: free, glucose oxidase: immobilized
8. Fine bubble aeration: 1000 rpm, 1 vvm, 300 mM substrate glucose, applied enzyme loading on carriers: 7.52 $mg_{GOx}g^{-1}_{carrier}$, calculated activity of catalase / calculated activity of glucose oxidase:4.79, antifoam 204: 0.28 ± 0.06 mg mL^{-1}. Catalase: free, glucose oxidase: free
9. Fine bubble aeration: 1000 rpm, 1 vvm, 600 mM substrate glucose, applied enzyme loading on carriers: 7.52 $mg_{GOx}g^{-1}_{carrier}$, calculated activity of catalase / calculated activity of glucose oxidase:4.79, antifoam 204: 0.28 ± 0.06 mg mL^{-1}. Catalase: free, glucose oxidase: free
10. Fine bubble aeration: 1000 rpm, 1 vvm, 1000 mM substrate glucose, applied enzyme loading on carriers: 7.52 $mg_{GOx}g^{-1}_{carrier}$, calculated activity of catalase / calculated activity of glucose oxidase:4.79, antifoam 204: 0.28 ± 0.06 mg mL^{-1}. Catalase: free, glucose oxidase: free
11. Fine bubble aeration: 1000 rpm, 1 vvm, 300 mM substrate glucose, applied enzyme loading on carriers: 7.52 $mg_{GOx}g^{-1}_{carrier}$, calculated activity of catalase / calculated activity of glucose oxidase:1.70, antifoam 204: 0.28 ± 0.06 mg mL^{-1}. Catalase: immobilized, glucose oxidase: immobilized
12. Macrobubble aeration: 500 rpm, 0.5 vvm, 125 mM substrate glucose, applied enzyme loading on carriers: 7.33 $mg_{GOx}g^{-1}_{carrier}$, calculated activity of catalase / calculated activity of glucose oxidase:1.38. Catalase: free, glucose oxidase: immobilized
13. Fine bubble aeration: 500 rpm, 0.67 vvm, 8.8 mM substrate glucose, applied enzyme loading on carriers: 1.07 $mg_{GOx}g^{-1}_{carrier}$, calculated activity of catalase / calculated activity of glucose oxidase:1.38. Catalase: free, glucose oxidase: immobilized
14. Fine bubble aeration: 500 rpm, 0.67 vvm, 25 mM substrate glucose, applied enzyme loading on carriers: 1.07 $mg_{GOx}g^{-1}_{carrier}$, calculated activity of catalase / calculated activity of glucose oxidase:1.38. Catalase: free, glucose oxidase: immobilized
15. Fine bubble aeration: 1000 rpm, 0.75 vvm, 300 mM substrate glucose, applied enzyme loading on carriers: 7.52 $mg_{GOx}g^{-1}_{carrier}$, calculated activity of catalase / calculated activity of glucose oxidase:1.70, antifoam 204: 0.28 ± 0.06 mg mL^{-1}. Catalase: free, glucose oxidase: immobilized
16. Fine bubble aeration: 1000 rpm, 1 vvm, 100 mM substrate glucose, applied enzyme loading on carriers: 7.52 $mg_{GOx}g^{-1}_{carrier}$, calculated activity of catalase / calculated activity of glucose oxidase:4.79, antifoam 204: 0.28 ± 0.06 mg mL^{-1}. Catalase: free, glucose oxidase: free

A.3. List of figures

A.4. List of tables

A.5. List of symbols

Symbol	Unit	Meaning
d_B	µm	Bubble diameter
Δp	mN µm^{-2}	Laplace pressure
H	atm m^3 kmol^{-1}	Henry's constant
p_i	atm	Partial pressure of the component i in the bubble
c_L^*	kmol m^{-3}	Saturation concentration of the gas molecule in the liquid phase
N_d	mol s^{-1}	Dissolution rate
k_L	m s^{-1}	Liquid phase mass transfer coefficient
A	m^2	Bubble surface area
A_c	m^2	Surface area of carriers
p^*	atm	Partial pressure of the gas component i in equilibrium with the dissolved gas molecule in the liquid phase
$k_L a$	h^{-1}	Volumetric mass transfer coefficient
c_{enzyme}	mg mL^{-1}	Enzyme concentration
c_{sp}	mg mL^{-1}	Mass concentration of the substrate at the accumulation layer of the carriers
V	mL	Volume
$\dot{V}$	mL min^{-1}	Volume flow rate
m	g	Mass
vvm	min^{-1}	Volumetric flow rate of air given per unit volume of liquid
K	-	Equilibrium constant
R	J K^{-1} mol^{-1}	Molar gas constant
ΔG	J mol^{-1}	Gibbs free energy
n	mol	Mole
OTR	mM min^{-1}	Oxygen transfer rate
t	min	Time
c	mmol L^{-1}	Concentration
$Re_{impeller}$	-	Impeller Reynolds number
N	s^{-1}	Rotational rate
D	m	Diameter of the rotating packed bed basket
r	mg mL^{-1} min^{-1}	Reaction rate on the layer of carriers
K_m	mM	Michaelis-Menten constant
OCR	mM min^{-1}	Oxygen consumption rate
OPR	mM min^{-1}	Reaction rate of hydrogen peroxide decomposition
k_{deac}	h^{-1}	Deactivation constant
$t_{1/2}$	h	Half-life
$\dot{N}$	mol m^{-2} s^{-1}	Molar flow density
D	m^2 s^{-1}	Diffusion coefficient

A.6. List of Greek symbols

Symbol	Unit	Meaning
σ	mN µm^{-1}	Surface tension
ρ	kg m^{-3}	Liquid density
g	m s^{-2}	Gravitational acceleration
μ	kg m^{-1} s^{-1}	Liquid dynamic viscosity
v	U mL^{-1}	Activity of glucose oxidase in the supernatant
v_R	U mg$_{GOx}^{-1}$	Glucose oxidase-specific activity
ϑ_B	m s^{-1}	Bubble rising velocity
η	-	Effectiveness factor
η_0	-	Dimensionless operational effectiveness factor
β	m s^{-1}	Mass transfer coefficient
δ_c	m	Concentration boundary layer thickness
$\beta_{substrate}$	m	A constant of the substrate on the layer

A.7. List of abbreviations

Abbreviation	Meaning
CYP	Cytochrome P450 monooxygenase
XOR	Xanthine oxidoreductase
FMO	Flavin monooxygenase
GOx	Glucose oxidase
Cat	Catalase
AMB3	Fine bubble generator
BSA	Bovine serum albumin
POD	Peroxidase
PID	Piping and instrumentation diagram
HPLC	High performance liquid chromatography
DFG	Deutsche Forschungsgemeinschaft
ANOVA	Analysis of variance
CapEx	Capital expenditure
OpEx	Operating expenditure
TotEx	Total expenditure
TEP	Techno-economic performance
MRI	Magnetic resonance imaging

Bibliography

[1] Enzymes Market Size, Share, Competitive Landscape and Trend Analysis Report by Type, by Source, by Reaction Type, by Application: Global Opportunity Analysis and Industry Forecast, 2021-2031, Allied Market Research Diagnostics and Biotech Industry Research Reports 2022, Report Code: A00579, reached on 3rd of May 2024. https://www.alliedmarketresearch.com/enzymes-market

[2] P. Tripathi, S. Sinha, Industrial Biocatalysis: an Insight into Trends and Future Direction, Curr Sustainable Renewable Energy Rep 2020, 7, 66. https://doi.org/10.1007/s40518-020-00150-8

[3] R. Radtke, Weltweite Ausgaben für Biotechnologie in den Jahren 2012 bis 2028, Ausgaben für Biotech weltweit bis 2028, Statista Research Department 2024, reached on 8th of August 2024. https://de.statista.com/statistik/daten/studie/1368790/umfrage/weltweite-ausgaben-fuer-biotech/

[4] S. Wu, R. Snajdrova, J.C. Moore, K. Baldenius, U.T. Bornscheuer, Biocatalysis: Enzymatic Synthesis for Industrial Applications, Angew Chem Int Ed 2020, 60, 88. https://doi.org/10.1002/anie.202006648

[5] E.L. Bell, W. Finnigan, S.P. France, A.P. Green, M.A. Hayes, L.J. Hepworth, S.L. Lovelock, H. Niikura, S. Osuna, E. Romero, K.S. Ryan, N.J. Turner, S.L. Flitsch, Biocatalysis, Nat Rev Methods Primers 2021, 1. https://doi.org/10.1038/s43586-021-00044-z

[6] N. Guajardo, P. Domínguez de María, Production of Bulk Chemicals with Biocatalysis: Drivers and Challenges Reflected in Recent Industrial Granted Patents (2015–2020), Molecules 2021, 26, 736. https://doi.org/10.3390/molecules26030736

[7] J. Schwarz, J. Volmer, S. Lütz, Enzymes in the Chemical and Pharmaceutical Industry, Editors: K.E. Jaeger, A. Liese, C. Syldatk, Introduction to Enzyme Technology 2024, 289. https://doi.org/10.1007/978-3-031-42999-6_14

[8] T. Reichstein, A. Grüssner A., Eine ergiebige Synthese der l-Ascorbinsäure (C-Vitamin). Helvetica Chimica Acta 1934, 17, 311.

[9] J.M. Nelson, E.G. Griffin, Adsorption of Invertase, J. Am. Chem. Soc. 1916, 38, 1109. https://doi.org/10.1021/ja02262a018

[10] Grubhofer N., Schleith L., Modifizierte ionenaustauscher als spezifische adsorbentien, Naturwissenschaften 1953, 40, 508.

[11] K. Rodríguez-Núñez, C. Bernal, R. Martínez, Immobilized Biocatalyst Engineering: High throughput enzyme immobilization for the integration of biocatalyst improvement strategies, International Journal of Biological Macromolecules 2021, 170, 61. https://doi.org/10.1016/j.ijbiomac.2020.12.097

[12] S.P. France, R.D. Lewis, C.A. Martinez, The Evolving Nature of Biocatalysis in Pharmaceutical Research and Development, JACS Au 2023, 3, 715. https://doi.org/10.1021/jacsau.2c00712

[13] F. Gallou, H. Gröger, B.H. Lipshutz, Status check: biocatalysis; its use with and without chemocatalysis. How does the fine chemicals industry view this area?, Green Chem. 2023, 25, 6092. https://doi.org/10.1039/D3GC01931D

[14] G. Espina, J. Atalah, J.M. Blamey, Extremophilic Oxidoreductases for the Industry: Five Successful Examples With Promising Projections, Front. Bioeng. Biotechnol. 2021, 9. https://doi.org/10.3389/fbioe.2021.710035

[15] A.J.C. Wahart, J. Staniland, G.J. Miller, S.C. Cosgrove, Oxidase enzymes as sustainable oxidation catalysts, R. Soc. Open Sci. 2022, 9. http://doi.org/10.1098/rsos.211572

[16] J. Dong, E. Fernández-Fueyo, F. Hollmann, C.E. Paul, M. Pesic, S. Schmidt, Y. Wang, S. Younes, W. Zhang, Biocatalytic Oxidation Reactions: A Chemist's Perspective, Angew Chem Int Ed 2018, 57, 9238. https://doi.org/10.1002/anie.201800343

[17] J. Schwarz, K. Rosenthal, R. Snajdrova, M. Kittelmann, S. Lütz, The Development of Biocatalysis as a Tool for Drug Discovery, Chimia 2020, 74, 368. https://doi.org/10.2533/chimia.2020.368

[18] M. Burns, W. Bi, H. Kim, M.S. Lall, C. Li, B.T. O'Neill, Ketoreductase/Transaminase, One-Pot, Multikilogram Biocatalytic Cascade Reaction, Org. Process Res. Dev. 2021, 25, 941. https://doi.org/10.1021/acs.oprd.0c00557

[19] M.A. Huffman, A. Fryszkowska, O. Alvizo, M. Borra-Garske, K.R. Campos, K.A. Canada, P.N. Devine, D. Duan, J.H. Forstater, S.T. Grosser, H.M. Halsey, G.J. Hughes, J. Jo, L.A. Joyce, J.N. Kolev, J. Liang, K.M. Maloney, B.F. Mann, N.M. Marshall, M. McLaughlin, J.C. Moore, G.S. Murphy, C.C. Nawrat, J. Nazor, S. Novick, N.R. Patel, A. Rodriguez-Granillo, S.A. Robaire, E.C. Sherer, M.D. Truppo, A.M. Whittaker, D. Verma, L. Xiao, Y. Xu, H. Yang, Design of an in vitro biocatalytic cascade for the manufacture of islatravir, Science 2019, 366, 1255. https://doi.org/10.1126/science.aay8484

[20] J.A. McIntosh, T. Benkovics, S.M. Silverman, M.A. Huffman, J. Kong, P.E. Maligres, T. Itoh, H. Yang, D. Verma, W. Pan, H.-I. Ho, J. Vroom, A.M. Knight, J.A. Hurtak, A. Klapars, A. Fryszkowska, W.J. Morris, N.A. Strotman, G.S. Murphy, K.M. Maloney, P.S. Fier, Engineered Ribosyl-1-Kinase Enables Concise Synthesis of Molnupiravir, an Antiviral for COVID-19, ACS Cent. Sci. 2021, 7, 1980. https://doi.org/10.1021/acscentsci.1c00608

[21] G. A. Truesdale, A. Downing, Solubility of Oxygen in Water, Nature, 1954, 173, 1236.

[22] G. Vernet, M. Hobisch, S. Kara, Process intensification in oxidative biocatalysis, Current Opinion in Green and Sustainable Chemistry 2022, 38, 100692. https://doi.org/10.1016/j.cogsc.2022.100692

[23] E. Erdem, J.M. Woodley, Industrially useful enzymology: Translating biocatalysis from laboratory to process, Chem Catalysis 2022, 2, 2499. https://doi.org/10.1016/j.checat.2022.09.037

[24] B. Thomas, D. Ohde, S. Matthes, P. Bubenheim, K. Terasaka, M. Schlüter, A. Liese, Enhanced enzyme stability and gas utilization by microbubble aeration applying microporous aerators, Catal. Sci. Technol. 2023, 13, 1098. http://dx.doi.org/10.1039/D2CY01761J

[25] A. Lorente-Arevalo, M. Ladero, J.M. Bolivar, Intensification of oxygen-dependent biotransformations catalyzed by immobilized enzymes, Current Opinion in Green and Sustainable Chemistry 2021, 32, 100544.https://doi.org/10.1016/j.cogsc.2021.100544

[26] B.O. Burek, A.W.H. Dawood, F. Hollmann, A. Liese, D. Holtmann, Process Intensification as Game Changer in Enzyme Catalysis, Front. Catal. 2022, 2. https://doi.org/10.3389/fctls.2022.858706

[27] M. Crotti, M.S. Robescu, J.M. Bolivar, D. Ubiali, L. Wilson, M.L. Contente, What's new in flow biocatalysis? A snapshot of 2020–2022, Front. Catal. 2023, 3. https://doi.org/10.3389/fctls.2023.1154452

[28] M.R. Chapman, S.C. Cosgrove, N.J. Turner, N. Kapur, A.J. Blacker, Highly Productive Oxidative Biocatalysis in Continuous Flow by Enhancing the Aqueous Equilibrium Solubility of Oxygen, Angew Chem Int Ed 2018, 57, 10535. https://doi.org/10.1002/anie.201803675

[29] J.M. Bolivar, A. Mannsberger, M.S. Thomsen, G. Tekautz, B. Nidetzky, Process intensification for O2-dependent enzymatic transformations in continuous single-phase pressurized flow, Biotech & Bioengineering 2019, 116, 503. https://doi.org/10.1002/bit.26886

[30] A. Toftgaard Pedersen, T.M. de Carvalho, E. Sutherland, G. Rehn, R. Ashe, J.M. Woodley, Characterization of a continuous agitated cell reactor for oxygen dependent biocatalysis, Biotech & Bioengineering 2017, 114, 1222. https://doi.org/10.1002/bit.26267

[31] K. Ganesh, J.B. Joshi, S.B. Sawant, Cellulase deactivation in a stirred reactor, Biochemical Engineering Journal 2000, 4, 137.https://doi.org/10.1016/S1369-703X(99)00045-5

[32] M.J. Osiecki, T.D. Michl, B. Kul Babur, M. Kabiri, K. Atkinson, W.B. Lott, H.J. Griesser, M.R. Doran, Packed Bed Bioreactor for the Isolation and Expansion of Placental-Derived Mesenchymal Stromal Cells, PLoS ONE 2015, 10, e0144941.https://doi.org/10.1371/journal.pone.0144941

[33] G.T. Vladisavljević, Biocatalytic membrane reactors (BMR), Physical Sciences Reviews 2016, 1. https://doi.org/10.1515/psr-2015-0015

[34] P. Žnidaršič-Plazl, Biocatalytic process intensification via efficient biocatalyst immobilization, miniaturization, and process integration, Current Opinion in Green and Sustainable Chemistry 2021, 32, 100546.https://doi.org/10.1016/j.cogsc.2021.100546

[35] K. M↘rtensson, Choosing an enzyme reactor theoretical background and considerations as illustrated in a case study, Appl Biochem Biotechnol 1982, 7, 11. https://doi.org/10.1007/BF02798612

[36] R. Lindeque, J. Woodley, Reactor Selection for Effective Continuous Biocatalytic Production of Pharmaceuticals, Catalysts 2019, 9, 262. https://doi.org/10.3390/catal9030262

[37] W. Zimmerman, V. Tesar, S. Butler, H. Bandulasena, Microbubble Generation, ENG 2008, 2, 1. http://dx.doi.org/10.2174/187221208783478598

[38] H. Warmeling, A. Behr, A.J. Vorholt, Jet loop reactors as a versatile reactor set up - Intensifying catalytic reactions: A review, Chemical Engineering Science 2016, 149, 229. https://doi.org/10.1016/j.ces.2016.04.032

[39] J.J. Carberry, Designing Laboratory Catalytic Reactors, Ind. Eng. Chem. 1964, 56, 39. https://doi.org/10.1021/ie50659a007

[40] P.T. Wai, P. Jiang, Y. Shen, P. Zhang, Q. Gu, Y. Leng, Catalytic developments in the epoxidation of vegetable oils and the analysis methods of epoxidized products, RSC Adv. 2019, 9, 38119. https://doi.org/10.1039/C9RA05943A

[41] Z. Perçin, L. Kursula, E. Löfgren, E. Byström, F. Kexel, P. Bubenheim, M. Schlüter, A. Liese, Intensification of a biocatalytic oxidation under fine bubble aeration in a rotating bed reactor, Biochemical Engineering Journal 2024, 207, 109333. https://doi.org/10.1016/j.bej.2024.109333

[42] T. Ma, W. Kong, Y. Liu, H. Zhao, Y. Ouyang, J. Gao, L. Zhou, Y. Jiang, Asymmetric Hydrogenation of C=C Bonds in a SpinChem Reactor by Immobilized Old Yellow Enzyme and Glucose Dehydrogenase, Appl Biochem Biotechnol 2022, 194, 4999. https://doi.org/10.1007/s12010-022-03991-9

[43] S. Donzella, C. Compagno, F. Molinari, F. Paradisi, M.L. Contente, Boosting the catalytic performance of a marine yeast in a SpinChem® reactor for the synthesis of perillyl alcohol, React. Chem. Eng. 2023, 8, 2963. https://doi.org/10.1039/D3RE00474K

[44] Reactor design supported by computational fluid dynamics (CFD), reached on 3rd of May 2024. https://www.spinchem.com/media/voop0xv5/application-1020_2.png?width=770&

[45] Mass transfer revolutionized, Biotransformation, Biocatalysis, SpinCHem AB, https://www.youtube.com/watch?v=meG0km4Vn6o, reached on 13th of August 2024

[46] The rotating bed reactor, SpinChem AB, reached on 2nd of May 2024. https://www.spinchem.com/media/r3eazg4q/p1020017_960px.png?anchor=center&mode=crop&quality=90&width=960&height=960&rnd=132639203757630000

[47] N.R. Mohamad, N.H.C. Marzuki, N.A. Buang, F. Huyop, R.A. Wahab, An overview of technologies for immobilization of enzymes and surface analysis techniques for immobilized enzymes, Biotechnology & Biotechnological Equipment 2015, 29, 205. https://doi.org/10.1080/13102818.2015.1008192

[48] Y.R. Maghraby, R.M. El-Shabasy, A.H. Ibrahim, H.M.E.-S. Azzazy, Enzyme Immobilization Technologies and Industrial Applications, ACS Omega 2023, 8, 5184. https://doi.org/10.1021/acsomega.2c07560

[49] T. Jesionowski, J. Zdarta, B. Krajewska, Enzyme immobilization by adsorption: a review, Adsorption 2014, 20, 801. https://doi.org/10.1007/s10450-014-9623-y

[50] H.H. Nguyen, M. Kim, An Overview of Techniques in Enzyme Immobilization, Appl. Sci. Converg. Technol. 2017, 26, 157. https://doi.org/10.5757/ASCT.2017.26.6.157

[51] M.Y. Arica, V. Hasirci, Immobilization of glucose oxidase: A comparison of entrapment and covalent bonding, J of Chemical Tech & Biotech 1993, 58, 287. https://doi.org/10.1002/jctb.280580313

[52] C. Garcia-Galan, Á. Berenguer-Murcia, R. Fernandez-Lafuente, R.C. Rodrigues, Potential of Different Enzyme Immobilization Strategies to Improve Enzyme Performance, Adv Synth Catal 2011, 353, 2885.https://doi.org/10.1002/adsc.201100534

[53] ReliChrom™ Provisory General Documentation English version PDF, Resindion S.r.l., reached on 2nd of May 2024. https://www.resindion.com/resindion/download/RESINDION_ReliZymeSepabeadsEC_PGD_050612.pdf

[54] R. Torres, C. Mateo, G. Fernandez-Lorente, C. Ortiz, M. Fuentes, J.M. Palomo, J.M. Guisan, R. Fernandez-Lafuente, A Novel Heterofunctional Epoxy-Amino Sepabeads for a New Enzyme Immobilization Protocol: Immobilization-Stabilization of β-Galactosidase from Aspergillus oryzae, Biotechnol. Prog. 2003, 19, 1056. https://doi.org/10.1021/bp025771g

[55] C. Mateo, O. Abian, G. Fernández-Lorente, J. Pedroche, R. Fernández-Lafuente, J.M. Guisan, Epoxy Sepabeads: A Novel Epoxy Support for Stabilization of Industrial Enzymes via Very Intense Multipoint Covalent Attachment, Biotechnology Progress 2002, 18, 629. https://doi.org/10.1021/bp010171n

[56] T. Heinks, N. Montua, M. Teune, J. Liedtke, M. Höhne, U.T. Bornscheuer, G. Fischer von Mollard, Comparison of Four Immobilization Methods for Different Transaminases, Catalysts 2023, 13, 300. https://doi.org/10.3390/catal13020300

[57] P. Borza, I.C. Benea, I. Bîtcan, A. Todea, S.G. Muntean, F. Peter, Enzymatic Degradation of Azo Dyes Using Peroxidase Immobilized Onto Commercial Carriers With Epoxy Groups, Studia UBB Chemia 2020, 65, 279. https://doi.org/10.24193/subbchem.2020.1.22

[58] M. Cárdenas-Fernández, E. Khalikova, T. Korpela, C. López, G. Álvaro, Co-immobilised aspartase and transaminase for high-yield synthesis of l-phenylalanine, Biochemical Engineering Journal 2015, 93, 173. https://doi.org/10.1016/j.bej.2014.10.010

[59] L. Babich, A.F. Hartog, L.J.C. van Hemert, F.P.J.T. Rutjes, R. Wever, Synthesis of Carbohydrates in a Continuous Flow Reactor by Immobilized Phosphatase and Aldolase, ChemSusChem 2012, 5, 2348. https://doi.org/10.1002/cssc.201200468

[60] S. Illner, C. Hofmann, P. Löb, U. Kragl, A Falling-Film Microreactor for Enzymatic Oxidation of Glucose, ChemCatChem 2014, 6, 1748. https://doi.org/10.1002/cctc.201400028

[61] D. Ohde, B. Thomas, S. Matthes, Z. Percin, C. Engelmann, P. Bubenheim, K. Terasaka, M. Schlüter, A. Liese, Fine Bubble-based CO2 Capture Mediated by Triethanolamine Coupled to Whole Cell Biotransformation, Chemie Ingenieur Technik 2019, 91, 1822. https://doi.org/10.1002/cite.201900113

[62] S. Matthes, B. Thomas, D. Ohde, M. Hoffmann, P. Bubenheim, A. Liese, S. Tanaka, K. Terasaka, M. Schlueter, Hydrodynamic and Mass Transfer Correlation in a Microbubble Aerated Stirred Tank Reactor, J. Chem. Eng. Japan 2020, 53, 577. https://doi.org/10.1252/jcej.19we181

[63] B. Thomas, D. Ohde, S. Matthes, C. Engelmann, P. Bubenheim, K. Terasaka, M. Schlüter, A. Liese, Comparative investigation of fine bubble and macrobubble aeration on gas utility and biotransformation productivity, Biotech & Bioengineering 2020, 118, 130. https://doi.org/10.1002/bit.27556

[64] ISO 20480-1:2017(E): Fine bubble technology — General principles for usage and measurement of fine bubbles — Part 1: Terminology, ISO Copyright office, 2017

[65] M. Alheshibri, J. Qian, M. Jehannin, V.S.J. Craig, A History of Nanobubbles, Langmuir 2016, 32, 11086. https://doi.org/10.1021/acs.langmuir.6b02489

[66] N.R. Pallas, Y. Harrison, An automated drop shape apparatus and the surface tension of pure water, Colloids and Surfaces 1990, 43, 169. https://doi.org/10.1016/0166-6622(90)80287-E

[67] H. Tsuge, Micro-and Nanobubbles, Pan Stanford Publishing Pte. Ltd., Temasek Blvd, Singapore, 2014, 3-6. ISBN 978-981-4463-10-2

[68] B. Thomas, Anwendung von Feinblasentechnologie in der Biokatalyse, TUHH Universitätsbibliothek, Hamburg, 2021. https://doi.org/10.15480/882.3438

[69]Solvent Filters, TECHLAB GmbH (Braunschweig, Germany), https://techlab.de/web/index.php?WSparam=2&WSdaten=4476, reached on 06th of August 2024

[70] SPG membrane, SPG Technology Co.,Ltd (Higashikaminaka Sadowaracho, Japan), https://www.spg-techno.co.jp/english_top/technology/spg-membrane/, reached on 6th of August 2024

[71] S. Matthes, Fundamentals of microscale bubbles in process engineering, TUHH Universitätsbibliothek, Cuvillier Verlag, Göttingen, 2021. ISBN: 978373697511

[72] X. Liu, M. Lei, Z. Wang, S. Yuan, Q. Li, Z. Wang, Hydrodynamics and mass transfer performance of microbubble flow in the bubble column with a contraction section, Chemical Engineering Research and Design 2024, 205, 91. https://doi.org/10.1016/j.cherd.2024.02.025

[73] Y. Maeda, S. Hosokawa, Y. Baba, A. Tomiyama, Y. Ito, Generation mechanism of micro-bubbles in a pressurized dissolution method, Experimental Thermal and Fluid Science 2015, 60, 201. http://dx.doi.org/10.1016/j.expthermflusci.2014.09.010

[74] D.S. Christen, Praxiswissen der chemischen verfahrenstechnik: handbuch fur chemiker und verfahrensingenieure, Springer Heidelberg Dordrecht London NewYork, 2009, 284. 324. https://doi.org/10.1007/978-3-540-88975-5

[75] M. Kraume, Transportvorgänge in der Verfahrenstechnik Grundlagen und apparative Umsetzungen, Springer-Verlag GmbH Deutschland, 2022, 3rd Edition, 305, https://doi.org/10.1007/978-3-662-60012-2

[76] S. Sulaiman, M. N. Mokhtar, M. Z. M. Nor, K. F. Md. Yunos, M. N. Naim, Mass transfer with reaction kinetics of the biocatalytic membrane reactor using a fouled covalently immobilised enzyme layer (α–CGTase–CNF layer), Biochemical Engineering Journal 2019, 152, 107374, https://doi.org/10.1016/j.bej.2019.107374

[77] D. Vasic-Racki, U. Kragl, A. Liese, Benefits of enzyme kinetics modelling, Chem. Biochem. Eng. Q. 17 (2003) 3–14.

[78] H. Ramesh, T. Mayr, M. Hobisch, S. Borisov, I. Klimant, U. Krühne, J.M. Woodley, Measurement of oxygen transfer from air into organic solvents, J of Chemical Tech & Biotech 2015, 91, 832. https://doi.org/10.1002/jctb.4862

[79] F. Garcia-Ochoa, E. Gomez, Prediction of gas-liquid mass transfer coefficient in sparged stirred tank bioreactors, Biotech & Bioengineering 2005, 92, 761. https://doi.org/10.1002/bit.20638

[80] A.A. Homaei, R. Sariri, F. Vianello, R. Stevanato, Enzyme immobilization: an update, J Chem Biol 2013, 6, 185. https://doi.org/10.1007/s12154-013-0102-9

[81] J.M. Woodley, Accelerating the implementation of biocatalysis in industry, Appl Microbiol Biotechnol 2019, 103, 4733. https://doi.org/10.1007/s00253-019-09796-x

[82] I. Eş, J.D.G. Vieira, A.C. Amaral, Principles, techniques, and applications of biocatalyst immobilization for industrial application, Appl Microbiol Biotechnol 2015, 99, 2065. https://doi.org/10.1007/s00253-015-6390-y

[83] G. Ozyilmaz, S.S. Tukel, O. Alptekin, Activity and storage stability of immobilized glucose oxidase onto magnesium silicate, Journal of Molecular Catalysis B: Enzymatic 2005, 35, 154.https://doi.org/10.1016/j.molcatb.2005.07.001

[84] Micro Nano Bubble Generator, Model: AMB3 Instruction Manual, Asupu Nanobubble Technology (Nagaizumi-cho, Sunto-gun, Shizuoka-ken, Higashino, Japan) https://d3pcsg2wjq9izr.cloudfront.net/files/74427/download/660296/1.pdf, reached on 5th of August 2024.

[85] European Chemicals Agency, Registration Dossier - ECHA (Europa.eu), D-gluconic acid - Endpoint summary, reached on 15th of February 2024. https://echa.europa.eu/registration-dossier/-/registered-dossier/1957/7/9/1

[86] Glucose oxidase (Enzyme Commission Number: 1.1.3.4) GOx type VII (G2133) lyophilized powder from *Aspergillus niger*, Sigma-Aldrich/Merck KGaA, Darmstadt, Germany, reached on 7th of August 2024. https://www.sigmaaldrich.com/DE/en/product/sigma/g2133

[87] ReliZyme™ HFA 403 M grade carrier, Resindion S.r.l., Rome, Italy, Invoice no. 23-000501, 12.12.2023

[88] Catalase (Enzyme Commission Number: 1.11.1.6) (C0052) solid powder from bovine liver, TCI Deutschland GmbH, Eschborn, Germany, reached on 2nd of May 2024. https://www.sigmaaldrich.com/DE/en/product/sigma/c1345

[89] Glucose oxidase (Enzyme Commission Number: 1.1.3.4) GOx type VII (G2133) lyophilized powder from *Aspergillus niger*, Certificate of Analysis (Batch Number: BCCB5681), Sigma-Aldrich/Merck KGaA, Darmstadt, Germany, reached on 7th of August 2024. https://www.sigmaaldrich.com/DE/en/product/sigma/g2133

[90] T. Zor, Z. Selinger, Linearization of the Bradford Protein Assay Increases Its Sensitivity: Theoretical and Experimental Studies, Analytical Biochemistry 1996, 236, 302. https://doi.org/10.1006/abio.1996.0171

[91] A. Liese, L. Hilterhaus, Evaluation of immobilized enzymes for industrial applications, Chem. Soc. Rev. 2013, 42, 6236.https://doi.org/10.1039/C3CS35511J

[92] Purolite™ Lifetech™ ECR Resins for Enzyme Immobilization, ECR8285, reached on 2nd of May 2024. https://www.fishersci.dk/shop/products/lifetech-ecr-resins-enzyme-immobilization-ecr8285-3/p-7214892

[93] Y.-J. Cho, O.-J. Park, H.-J. Shin, Immobilization of thermostable trehalose synthase for the production of trehalose, Enzyme and Microbial Technology 2006, 39, 108. https://doi.org/10.1016/j.enzmictec.2005.10.004

[94] L. Hilterhaus, B. Minow, J. Müller, M. Berheide, H. Quitmann, M. Katzer, O. Thum, G. Antranikian, A.P. Zeng, A. Liese, Practical application of different enzymes immobilized on sepabeads, Bioprocess Biosyst Eng 2008, 31, 163. https://doi.org/10.1007/s00449-008-0199-3

[95] R.C. Bateman Jr., J.A. Evans, Using the Glucose Oxidase/Peroxidase System in Enzyme Kinetics, J. Chem. Educ. 1995, 72, A240. https://doi.org/10.1021/ed072pA240

[96] B. Saha, P. Songe, T.H. Evers, M.W.J. Prins, The influence of covalent immobilization conditions on antibody accessibility on nanoparticles, Analyst 2017, 142, 4247. https://doi.org/10.1039/c7an01424d

[97] K. Ruby, S.K. Majumder, Effect of Salt on the Stability of Microbubbles in the Presence of Micro–Nanoparticles: Substantial Adsorption in the Separation of Particles by Flotation, Ind. Eng. Chem. Res. 2019, 58, 18881. https://doi.org/10.1021/acs.iecr.9b03882

[98] S.M. Peyghambarzadeh, A. Hatami, A. Ebrahimi, A. Fazel S.A., Photographic study of bubble departure diameter in saturated pool boiling to electrolyte solutions, CI & CEQ 2014, 20, 143. https://doi.org/10.2298/CICEQ120707120P

[99] M. Zlokarnik, Stirring: Theory and Practice, Wiley-VCH, Weinheim, Chichester, 2001, 76.

[100] A. Rosseburg, J. Fitschen, J. Wutz, T. Wucherpfennig, M. Schlüter, Hydrodynamic inhomogeneities in large scale stirred tanks – Influence on mixing time, Chemical Engineering Science 2018, 188, 208. https://doi.org/10.1016/j.ces.2018.05.008

[101] B.J. Michel, S.A. Miller, Power requirements of gas-liquid agitated systems, AIChE Journal 1962, 8, 262. https://doi.org/10.1002/aic.690080226

[102] P. M. Doran, Bioprocess Engineering Principles, Academic Press. Elsevier, Waltham, 2013, 204.

[103] Y.A. Çengel, J. M. Cimbala, Fluid Mechanics – Fundamentals and Applications, Mc.Graw-Hill, New York, 2006, 324.

[104] H.K. Larsson, Modelling of Mass Transfer Phenomena in Chemical and Biochemical Reactor Systems using Computational Fluid Dynamics, Danmarks Tekniske Universitet (DTU), 2015, 166.

[105] M.C. Mccray, P.G.A. Cizmas, Experimental investigation of the critical Reynolds number for bubbly two-phase flow, Incas Bulletin 2023, 15, 47. https://doi.org/10.13111/2066-8201.2023.15.3.4

[106] D. Wenzel, Rotating packed bed in liquid-liquid and liquid-solid separation, Editors: M. Skiborowski, A. Górak, Process Intensification, De Gruyter 2022, 43. https://doi.org/10.1515/9783110724998

[107] H.-S. Liu, C.-C. Lin, S.-C. Wu, H.-W. Hsu, Characteristics of a Rotating Packed Bed, Ind. Eng. Chem. Res. 1996, 35, 3590. https://doi.org/10.1021/ie960183r

[108] W. Liu, Y. Luo, Y.-B. Li, G.-W. Chu, Scale-Up of a Rotating Packed Bed Reactor with a Mesh-Pin Rotor: (II) Mass Transfer and Application, Ind. Eng. Chem. Res. 2020, 59, 5124. https://doi.org/10.1021/acs.iecr.9b06684

[109] M.P. Meissner, M. Nordblad, J.M. Woodley, Online Measurement of Oxygen-Dependent Enzyme Reaction Kinetics, ChemBioChem 2017, 19, 106. https://doi.org/10.1002/cbic.201700577

[110] Y. Chisti, U.J. Jauregui-Haza, Oxygen transfer and mixing in mechanically agitated airlift bioreactors, Biochemical Engineering Journal 2002, 10, 143. https://doi.org/10.1016/S1369-703X(01)00174-7

[111] R. Petříček, T. Moucha, J.F. Rejl, L. Valenz, J. Haidl, T. Čmelíková, Gas-liquid-solid volumetric mass transfer coefficient and impeller power consumptions for industrial vessel design, International Journal of Heat and Mass Transfer 2018, 121, 653. https://doi.org/10.1016/j.ijheatmasstransfer.2018.01.041

[112] P. Tufvesson, W. Fu, J.S. Jensen, J.M. Woodley, Process considerations for the scale-up and implementation of biocatalysis, Food and Bioproducts Processing 2010, 88, 3. https://doi.org/10.1016/j.fbp.2010.01.003

[113] R.A. Rocha, R.E. Speight, C. Scott, Engineering Enzyme Properties for Improved Biocatalytic Processes in Batch and Continuous Flow, Org. Process Res. Dev. 2022, 26, 1914. https://doi.org/10.1021/acs.oprd.1c00424

[114] M. Dias Gomes, J.M. Woodley, Considerations when Measuring Biocatalyst Performance, Molecules 2019, 24, 3573. https://doi.org/10.3390/molecules24193573

[115] P.K. Robinson, Enzymes: principles and biotechnological applications, Essays in Biochemistry 2015, 59, 1.

[116] L. Michaelis, M. L. Menten, Die Kinetik der Invertinwirkung, The Kinetics of Invertase Action (translated by R. S. Goody and K. A. Johnson), 1913

[117] L.A. Alves, J.B. Almeida e Silva, M. Giulietti, Solubility of d-Glucose in Water and Ethanol/Water Mixtures, J. Chem. Eng. Data 2007, 52, 2166. https://doi.org/10.1021/je700177n

[118] M. H. Brecht, Investigation of the process stability of immobilized glucose oxidase in a rotating bed reactor under fine bubble aeration, B.Sc. Thesis, 2023, TUHH

[119] F. Paradisi, L. Poppe, Continuous-flow biocatalysis with enzymes and cells, Flow Chemistry – Applications, Editors F. Darvas, G. Dormán, V. Hessel, S. V. Ley, De Gruyter, 2021, 277, 285. https://doi.org/10.1515/9783110693690-205

[120] J.M. Harris, C. Reyes, G.P. Lopez, Common causes of glucose oxidase instability in in vivo biosensing: a brief review, J Diabetes Sci Technol 2013, 7, 1030. https://doi.org/10.1177/193229681300700428

[121] R.M. Lindeque, J.M. Woodley, The Effect of Dissolved Oxygen on Kinetics during Continuous Biocatalytic Oxidations, Org. Process Res. Dev. 2020, 24, 2055. https://doi.org/10.1021/acs.oprd.0c00140

[122] R.H. Ringborg, A. Toftgaard Pedersen, J.M. Woodley, Automated Determination of Oxygen-Dependent Enzyme Kinetics in a Tube-in-Tube Flow Reactor, ChemCatChem 2017, 9, 3285. https://doi.org/10.1002/cctc.201700811

[123] H.P. Erickson, Size and Shape of Protein Molecules at the Nanometer Level Determined by Sedimentation, Gel Filtration, and Electron MicroscopyBiol Proced Online 2009, 11, 32. https://doi.org/10.1007/s12575-009-9008-x

[124] S. Cantone, V. Ferrario, L. Corici, C. Ebert, D. Fattor, P. Spizzo, L. Gardossi, Efficient immobilisation of industrial biocatalysts: criteria and constraints for the selection of organic polymeric carriers and immobilisation methods, Chem. Soc. Rev. 2013, 42, 6262. https://doi.org/10.1039/c3cs35464d

[125] T. Henzler, E. Steudle, Transport and metabolic degradation of hydrogen peroxide in Chara corallina: model calculations and measurements with the pressure probe suggest transport of H_2O_2 across water channels, Journal of Experimental Botany 2000, 51, 2053. https://doi.org/10.1093/jexbot/51.353.2053

[126] S. Arana-Peña, D. Carballares, R. Morellon-Sterlling, Á. Berenguer-Murcia, A.R. Alcántara, R.C. Rodrigues, R. Fernandez-Lafuente, Enzyme co-immobilization: Always the biocatalyst designers' choice…or not? Biotechnology Advances 2021, 51, 107584. https://doi.org/10.1016/j.biotechadv.2020.107584

[127] M. Aliveli, Investigation of diffusion limitations in a rotating bed reactor, Project Work, 2024, TUHH

[128] J.M. Bolivar, J.M. Woodley, R. Fernandez-Lafuente, Is enzyme immobilization a mature discipline? Some critical considerations to capitalize on the benefits of immobilization. Chem. Soc. Rev. 2022, 51, 6251. https://doi.org/10.1039/d2cs00083k

[129] M. Nouaimi-Bachmann, O. Skilewitsch, S. Senhaji-Dachtler, H. Bisswanger, Co-immobilization of different enzyme activities to non-woven polyester surfaces, Biotech & Bioengineering 2006, 96, 623. https://doi.org/10.1002/bit.21136

[130] Size of glucose ring molecule, reached on 2nd of May 2024. https://bionumbers.hms.harvard.edu/bionumber.aspx?id=110368

[131] Daniel Minoli, Nanotechnology Applications to Telecommunications and Networking, Wiley-Interscience, 2005, 1st Edition, 6. ISBN: 978-0-471-71639-6

[132] T. Henzler, E. Steudle, Transport and metabolic degradation of hydrogen peroxide in Chara corallina: model calculations and measurements with the pressure probe suggest transport of H_2O_2 across water channels, Journal of Experimental Botany 2000, 51, 2053. https://doi.org/10.1093/jexbot/51.353.2053

[133] A. Basso, S. Serban, Industrial applications of immobilized enzymes—A review, Molecular Catalysis 2019, 479, 110607. https://doi.org/10.1016/j.mcat.2019.110607

[134] W. Tischer, F. Wedekind, Immobilized Enzymes: Methods and Applications, Topics in Current Chemistry 1999, 95, 113. https://doi.org/10.1007/3-540-68116-7_4

[135] D. Pečar, Đ. Vasić-Rački and A. Vrsalović Presečkib, Immobilization of Glucose Oxidase on Eupergit C: Impact of Aeration, Kinetic and Operational Stability Studies of Free and Immobilized Enzyme, Chem.Biochem.Eng.Q. 2019, 32, 511. https://doi.org/10.15255/CABEQ.2018.1391

[136] A. Rekuć, B. Jastrzembska, J. Liesiene, J. Bryjak, Comparative studies on immobilized laccase behaviour in packed-bed and batch reactors, Journal of Molecular Catalysis B: Enzymatic 2009, 57, 216. https://doi.org/10.1016/j.molcatb.2008.09.007

[137] H.-Y. Kim, Analysis of variance (ANOVA) comparing means of more than two groups, Restor Dent Endod 2014, 39, 74. http://dx.doi.org/10.5395/rde.2014.39.1.74

[138] T.K. Kim, Understanding one-way ANOVA using conceptual figures, Korean J Anesthesiol 2017, 70, 22. https://doi.org/10.4097/kjae.2017.70.1.22

[139] S. Matthes, T. A. Merbach, J. Fitschen, M. Hoffmann, M. Schlüter, Influence of counterdiffusion effects on mass transfer coefficients in stirred tank reactors, Chemical Engineering Journal Advances 2021, 8, 100180. https://doi.org/10.1016/j.ceja.2021.100180

[140] D. Ohde, B. Thomas, S. Matthes, S. Tanaka, P. Bubenheim, K. Terasaka, M. Schlüter, A. Liese, Microbubble enhanced mass transfer efficiency of CO2 capture utilizing aqueous triethanolamine for enzymatic resorcinol carboxylation, RSC Adv. 2021, 11, 4087.

[141] Z. Perçin, P. Bubenheim, M. Schlüter, A. Liese, Process Intensification of Biocatalysts with a Fine-Bubble Aerator, Chemie Ingenieur Technik 2022, 94, 1213. https://doi.org/10.1002/cite.202255239

[142] P. Pietrek, M. Kraut, R. Dittmeyer, Towards a Novel Computer-Aided Optimization of Microreactors: Techno-Economic Evaluation of an Immobilized Enzyme System, Symmetry 2021, 13, 524. https://doi.org/10.3390/sym13030524

[143] P. Tufvesson, J. Lima-Ramos, M. Nordblad, J.M. Woodley, Guidelines and Cost Analysis for Catalyst Production in Biocatalytic Processes, Org. Process Res. Dev. 2010, 15, 266. https://doi.org/10.1021/op1002165

[144] D-(+)-Glucose, 25 kg, Carl Roth GmbH + Co. KG, Karlsruhe, Germany, https://www.carlroth.com/de/de/monosaccharide/d%28%2B%29-glucose/p/x997.5, reached on 7th of August 2024

[145] Sodium acetate, 1 kg, Carl Roth GmbH + Co. KG, Karlsruhe, Germany, https://www.carlroth.com/de/de/natriumsalze-na/natriumacetat/p/6773.2, reached on 11th of April 2024

[146] Acetic acid, 1 L, Carl Roth GmbH + Co. KG, Karlsruhe, Germany, https://www.carlroth.com/de/de/iodzahlbestimmung/essigsaeure/p/3738.1, reached on 7th of August 2024

[147] Sodium hydroxide, 1 kg, Carl Roth GmbH + Co. KG, Karlsruhe, Germany, https://www.carlroth.com/de/de/nicht-regenierbare-trocknungsmittel/natriumhydroxid/p/9356.1, reached on 11th of April 2024

[148] Ergun, S., Fluid flow through packed columns, Chemical Engineering Progress, 1952, 48, 89

[149] H. S. Fogler, Elements of Chemical Engineering, Pearson Education Inc, Westford, Massachusetts, 2010, 4th Edition, 196, ISBN. 0-13-127839-8.

[150] M.R. Serial, S. Benders, P. Rotzetter, D.L. Brummerloh, J.P. Metzger, S.P. Gross, J. Nussbaum, C.R. Müller, K.P. Pruessmann, A. Penn, Temperature distribution in a gas-solid fixed bed probed by rapid magnetic resonance imaging, Chemical Engineering Science 2023, 269, 118457. https://doi.org/10.1016/j.ces.2023.118457